POLITECNICO DI TORINO

Master's Degree in Ingegneria Aerospaziale

Master's Degree Thesis

Methodology and tool to support the conceptual design of a reusable VTVL TSTO vehicle

Supervisors

Prof. Roberta FUSARO

Prof. Nicole VIOLA

Ing. Giuseppe NARDUCCI

Candidate

Antonio GREGORIO

308044

December 2024

Summary

In recent years, the advent of reusable launch systems has revolutionised the space sector, demonstrating not only their operational feasibility but also a significant reduction in cost per mission. Although these advanced systems are now dominated by developments in the United States, Europe is beginning to actively invest in the research and development of similar technologies, with the aim of building its capacity to access space in a sustainable manner.
This thesis proposes an innovative design methodology, together with a supporting Python tool, for the rapid dimensioning of advanced expendable or reusable launch vehicles. The design tool developed is designed to be highly flexible, allowing rapid iteration from high level design and mission requirements. Within seconds, it will provide data on the size, mass, performance and mission profile of the selected launcher type.
In this study, we focus on the investigation of a Two Stage to Orbit (TSTO) vehicle with Vertical Take-Off and Landing (VTVL). This type of architecture allows the reuse of the first stage, increasing operational sustainability and drastically reducing long-term costs. To validate the effectiveness of the proposed tool and methodology, the thesis includes an application study and results comparison on the case of RETALT1, a future reusable TSTO launcher currently under development in Europe.
The use of the commercial software ASTOS allowed the validation of the mission analysis module by comparing the results of the developed methodology and replicating it within the software. The application of a tool such as ASTOS ensures that the results are robust and representative of the actual performance of the system.
Finally, the study concludes by analysing the results obtained and outlining potential future developments of both the methodology and the tool.

Acknowledgements

I would like to express my gratitude to Professor Roberta Fusaro, the supervisor of this thesis, for her valuable support. Her availability and advice have been a fundamental point of reference, as has her welcome in the research group, which has allowed me to grow both professionally and personally.

My thanks also go to PhD student Giuseppe Narducci, whose competent and efficient guidance played a crucial role in the development of this work.

Table of Contents

List of Tables

List of Figures

Acronymus

2BP

Two Body Problem

ACS

Attitude Control System

AoA

Angle of Attack

ASTRID

Aircraft on-board Systems sizing and TRade-off analysis in Initial Design

CFD

Computational Fluid Dynamics

DA

Direct Ascent

DL

Downrange Landing

DRL

Downrange barge

EL

Expandable Launchers

ELVs

Expendable Launch Vehicles

EPS

Electrical Power System

GTO

Geostationary Transfer Orbit

HLS

Human Landing System

HTA

Hohmann Transfer Ascent

LCH4

Liquid methane

LC3H8

Liquid propane

LEO

Low Earth Orbit

LH2

Liquid hydrogen

LOX

Liquid oxygen

LRE

Liquid Rocket Engine

LTO

Lower Transfer Orbit

MDA

Multidisciplinary Design Analysis

MDO

Multidisciplinary Design Optimisation

MECO

Main Engine Cut-Off

ML

Micro Launchers

MTOM

Maximum Take-Off Mass

PCPF

Planet-centred-Planet-fixed

RETALT

RETro propulsion Assisted Landing Technologies

RK4

Runge-Kutta fourth-order

RL

Reusable Launchers

RLV

Reusable Launch Vehicle

RP-1

Kerosene, Rocket Propellant-1

RBS

Reusable Booster System

RTLS

Return-to-launch-site

SSTO

Single Stage to Orbit

TPS

Thermal Protection System

TSTO

Two Stage to Orbit

TVC

Thrust Vectoring Control

VTHL

Vertical Take-off and Horizontal Landing

VTVL

Vertical Take-off and Landing

Chapter 1

Background and aim of the work

1.1 Reusable Launch Vehicles - RLV: Historical Background

Launch vehicle re-usability has been a topic of engineering discussion since the beginning of the space age. From the earliest days of expendable launch vehicles (ELVs), the primary objective has been to reduce the cost of access to orbit. This drive has become a fundamental driver for both government and private space initiatives worldwide, with a focus on increasing competitiveness in the launch market [1]. Among the various approaches, system reusability stands out as the most promising strategy for achieving significant cost reductions, especially when focused on the first stage. Although there is no evidence that a launcher can be completely reused, partial reuse can reduce production costs over its lifetime. This can be done through the re-use of both hardware and software, depending on factors like the number of launches, the number of units produced and the number of re-uses [2].

The success of SpaceX's partially reusable Falcon 9 and Falcon Heavy rockets has highlighted the need for reusable vehicles. As a result, the design focus for new space transportation systems has shifted from prioritizing high performance to achieving cost reductions. This shift is also influencing technology choices; for example, SpaceX chose not to use high-performance cryogenic liquid oxygen/hydrogen (LOX/LH2) in favor of RP-1 kerosene, which is easier to store. Building on this historical precedent, retro-propelled vertical takeoff and landing systems have emerged as the most promising solution for future reusable launch vehicles [2].

While this has been achieved in the United States, Europe is struggling to have

a reusable way to access space, and with the test launches of Ariane 6, it does not look like this will be achieved in the short term. Despite these problems, there are many past and active projects in the European context that have led to important advances in the study of these new technologies [3]. Europe's autonomous access to space is crucial for strategic independence. The European space strategy emphasizes the need for reliable and cost-effective launch systems, highlighting cost reduction and flexibility as crucial challenges to strengthen the competitiveness of European industry in the global market. A list of main project are reported below:

- **RETALT** (RETro Assisted propulsion assisted Landing Technologies) is a comprehensive study of two vertical take-off and landing (VTVL) reference vehicles, focusing particularly on the technologies required for the re-entry of the propulsion stage. The study examines two configurations: *RETALT1* (Figure 1.1a), similar to Falcon 9, designed for Two-Stage-to-Orbit (TSTO) with retro propulsion combined with aerodynamic control surfaces, and *RETALT2* (Figure 1.1b), similar to the *DC-X*, intended for Single-Stage-to-Orbit (SSTO)[4].

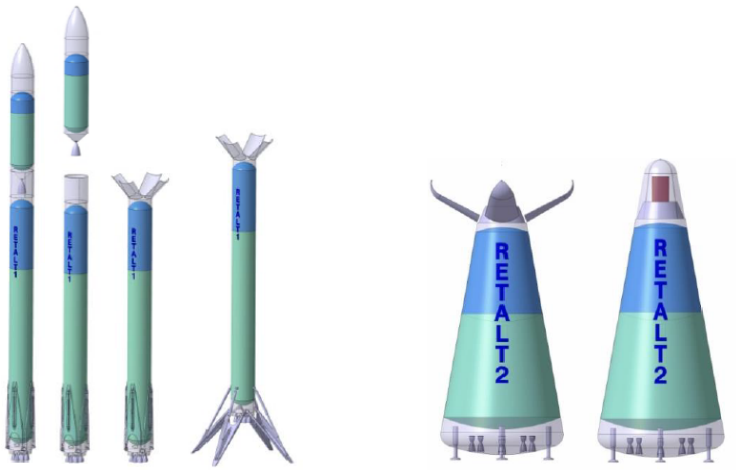

(a) RETALT1 Concept **(b)** RETALT2 Concept

Figure 1.1: RETALT1 and RETALT2 Concepts [4].

This project, launched in 2019 and completed in 2022, significantly expanded European expertise in this field. This type of launcher, particularly the first configuration, will be frequently referenced throughout this work and will also serve as a validation model.

- **ENTRAIN** (Europe's NexT Reusable ArIaNe) is a *'Deutsches Zentrum für Luft- und Raumfahrt'* DRL internal project focusing on the comparison of reusable VTVL and VTHL configurations on system level. The project aims

to analyse application scenarios and provide an insight into the possibilities of applying the technologies in future launchers [3].

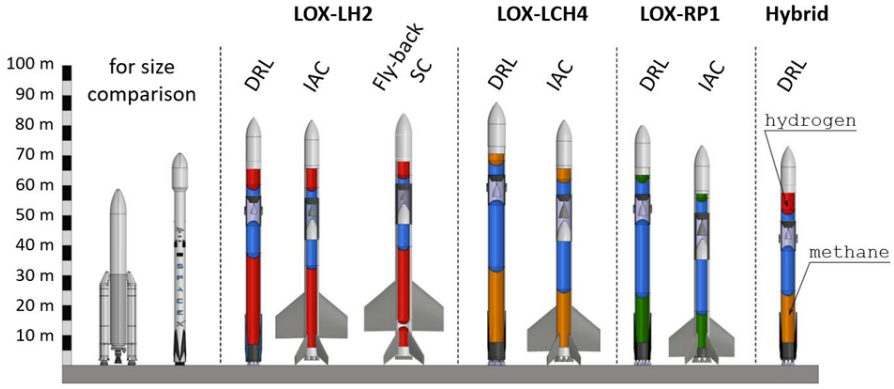

Figure 1.2: ENTRAIN RLV case study: VTVL and VTHL [5]

In Figure 1.2, the case studies under consideration are highlighted, showcasing how they compare to currently existing technologies. Aligned with the scope of this thesis, attention is directed instead to Figure 1.3, which focuses exclusively on the VTVL cases.

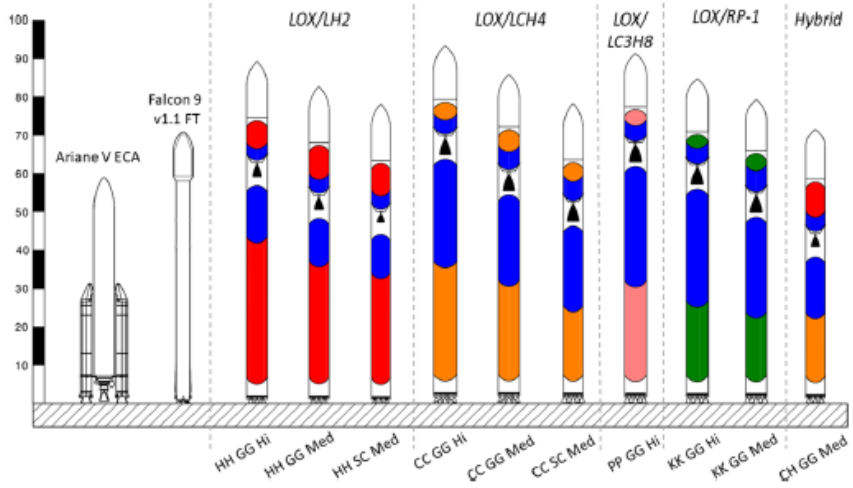

Figure 1.3: ENTRAIN RLV case study: VTVL [3]

This study evaluates ten different VTVL reusable launchers preliminary sized. In Figure 1.3, they are categorized using a nomenclature that provides information about the engine type and cycles. Specifically, 'Hi', 'Med' and 'Lo' refer to the magnitude of the first stage separation velocity, while 'GG' denotes Gas Generator, and 'SC' represents Staged Combustion. The results

highlight the impact of design choices on launcher size and mass, showing that methane stages have higher dry mass than hydrogen stages, and that hybrid configurations (hydrocarbon first stage and hydrogen upper stage) offer advantages in reducing overall mass, albeit with added complexity in engine and fuel handling [3].

- The **CALLISTO** (Cooperative Action Leading to Launcher Innovation for Stage Toss-back Operations) project is a joint effort by *JAXA*, *CNES*, and *DLR* to prove technologies and collect know-how for applications closer to full-scale launchers (Figure 1.4a). The initiative focuses on understanding and developing the design, optimization, and operational requirements for reusable launch systems [6].

- **THEMIS** is a European prototype of a low-cost reusable launch vehicle (Figure 1.4b). It is developed by *ESA* with *ArianeGroup* as prime contractor. It is powered by the future methane engine 'Prometheus', and Themis is designed for vertical take-off, landing and reusability. It incorporates technologies such as landing legs, grid stabilisers, lightweight fuel tanks and avionics. Themis is intended to be cheaper and more powerful than current European rockets, exceeding the performance achievable with the Vulcain. The project is currently in Phase A and is expected to be a 30 meters single-stage vehicle with a diameter of 3.5 meters. In addition, its development will benefit from the experience gained from the achievements of the CALLISTO project [7].

(a) CALLISTO Vehicle **(b)** THEMIS Concept

Figure 1.4: CALLISTO and THEMIS concepts [8, 9]

1.2 Multidisciplinary Design Optimization

During the initial design phases, public companies and private agencies would greatly benefit from a tool capable of predicting both the design of a given system and its mission profile. Such tools often aim to optimize outcomes by maximizing or minimizing specific variable. For example, achieving maximum payload or minimising costs. However, a common issue lies in the proprietary nature of existing software, which is typically unavailable to third-party users and not open-source.

Although recent European initiatives such as those mentioned above have broadened the knowledge base on complex problems such as RLV, there remains a significant gap in open source solutions for fast and reliable conceptual design simulations. As a result, engineers often have to develop their own proprietary software to run such simulations efficiently and quickly.

This thesis will address this challenge. Since a launcher is a complex system comprised of numerous subsystems, its design presents a multidisciplinary problem. Multidisciplinary Design Analysis (MDA) ensures integration between subsystems, while Multidisciplinary Design Optimization (MDO) exploits this coupling to achieve optimal solutions for mission. In these cases, MDO techniques aim to find compromises between the different disciplines with the goal of achieving a valid and concrete end result. These methods are commonly used in launch vehicle design, as highlighted in [10], [11], and [2]. In particular, MDO has been applied to Vertical Takeoff and Vertical Landing (VTVL) systems, as demonstrated in [3], where performance is derived from high-level requirements.
The design of RLV to be applied to different missions can be described as a multi-objective optimisation problem. A general multi-objective problem characterised by n objective functions and q constraints can be formulated in eq 1.1, 1.2 and 1.3 ([12]):

$$\text{Minimize}\,(f(\mathbf{z},\mathbf{x},\mathbf{y})) = [f_1(\mathbf{z},\mathbf{x},\mathbf{y}), f_2(\mathbf{z},\mathbf{x},\mathbf{y}), \ldots, f_n(\mathbf{z},\mathbf{x},\mathbf{y})] \tag{1.1}$$

$$\text{subject to} \quad g_i(\mathbf{z},\mathbf{x},\mathbf{y}) \leq 0, \quad i = 1, 2, \ldots, q \tag{1.2}$$

$$\mathbf{z}_{\min} \leq \mathbf{z} \leq \mathbf{z}_{\max} \tag{1.3}$$

Where:

- $\mathbf{z}$ is the design variables. These variables change all along the optimization process in order to find the optimal design point. The same variables can be used in one or several subsystems ([13]).
- $\mathbf{y}$ are the coupling variables. These variables are used to link the different subsystems and to evaluate the consistency of the design with respect to coupling ([13]).

- $\mathbf{x}$ are the state (or disciplinary) variables. These variables can be change during the multi-disciplinary analysis in order to find an equilibrium in the state equations (disciplinary equations). Unlike z, the state variables are not independent degrees of degrees of freedom, but depend on the design variables z, the coupling variables y, and the state equations ([13]).

- $\mathbf{f}(\mathbf{z})$ objective function. This function quantifies the quality of the design and has to be optimized by the MDO process.

- $g_i(\mathbf{z})$ is the i-th constraint function, forming the vector $\mathbf{g}(\mathbf{z})$ of size q .

A general MDO process is illustrated in Figure 1.5.

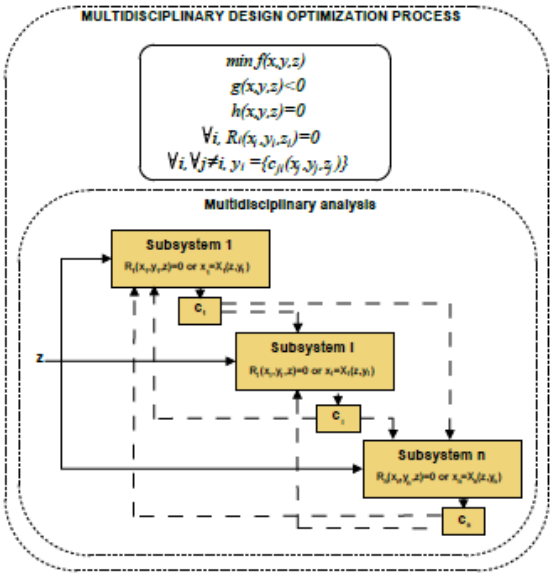

Figure 1.5: Typical MDO scheme [13]

Going into more detail, when dealing with RLV, it is crucial to identify the disciplines, variables, and constraints involved in the problem. The Launch Vehicle Design problem is generally decomposed into various physical disciplines: aerodynamics, propulsion, fuel systems (including tanks), mass estimation and sizing, as well as other subsystems, and trajectory for performance evaluation. The design variables $\mathbf{z}$, such as the masses, diameters, propulsion parameters (chamber pressures, mixture ratios, etc.), fairing shape, and others, are typically considered at the system level. The trajectory variables are usually treated as state variables $\mathbf{x}$. Typical coupling variables $\mathbf{y}$ can include dry mass, stage diameters, thrust-to-weight ratio, and others. The involved constraints in the launcher design problem include

various factors that must be satisfied. These constraints are typically composed of mission requirements, such as the desired orbit, payload mass, and Gross Lift-Off Weight (GLOW). Other constraints may include factors like the maximum chamber pressure, maximum angle of attack, maximum load factor, and minimum nozzle exit pressure. Additionally, coupling constraints may arise from the interactions between trajectory and weights and sizing, or between trajectory and aerodynamics, among others. As for the objective functions, common goals include maximizing the payload mass, minimizing fuel consumption, and reducing overall costs, among others [13].

1.3 Research Outline

The main objective of this research is to develop a tool that can quickly provide the conceptual design of reusable launch vehicles, with a focus on retro-propulsion for re-entry, recovery, and reuse of the first stage. A secondary objective is to evaluate and optimize the ascent and descent trajectories of a typical RLV. The starting point for the work was an analysis of the design methodologies already developed at the *Politecnico di Torino*. In particular, those present in the proprietary software ASTRID (Aircraft on-board Systems sizing and TRade-off analysis in Initial Design), which has been developed for almost a decade through research activities including master's and doctoral theses. This tool allows the conceptual and preliminary design of aircraft, the sizing and integration of subsystems for a wide range of aircraft, from conventional to innovative configurations, mainly in the subsonic and low supersonic speed range. ASTRID has been validated through its application to various case studies and has recently been included in the Multidisciplinary Optimisation Framework set up within the Horizon 2020 AGILE project (Aircraft 3rd Generation MDO for Innovative Collaboration of Heterogeneous Teams of Experts) and is currently being used in the follow-up H2020 AGILE 4.0. More recently, the rapid vehicle prototyping capability of ASTRID-H (shown in figure 1.6) has been validated in the H2020 STRATOFLY (Stratospheric Flying Opportunities for High-Speed Propulsion Concepts) project for supersonic and hypersonic civil aircraft [14]. The research team from *Politecnico di Torino* has worked on upgrading ASTRID-H capabilities to extend its applicability to space-related applications. In the past, two routines were introduced: one for Micro Launchers (ML) and another for the Human Landing System (HLS). The current effort aims to further extend the use cases by introducing a routine for Reusable or Expandable Launchers (RL or EL).
Given the overview of the state-of-the-art European launchers, the introduction to multidisciplinary analysis, and the context in which this thesis work is situated, the research question is:

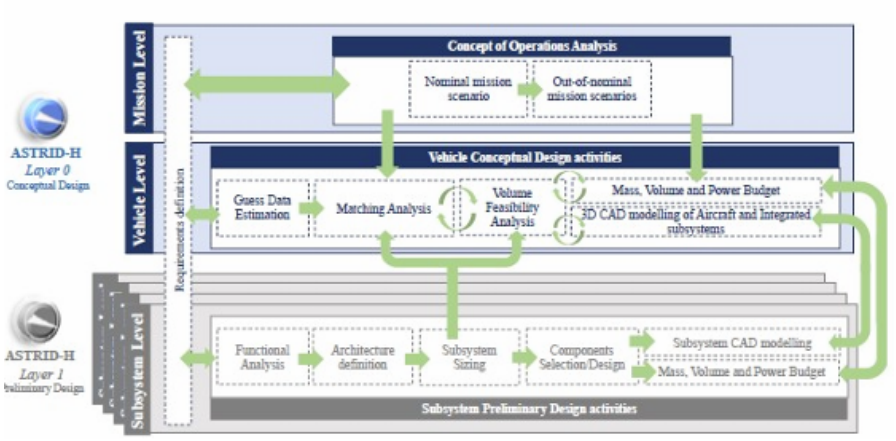

Figure 1.6: ASTRID-H layout

Is it possible to develop a methodology on which to base software for the rapid estimation of design parameters and performance of a reusable launch vehicle?

Can this work align with the state-of-the-art European technologies and be easily integrated into ASTRID-H?

To answer this question, the approach begins with detailed explanation of how the thesis work addresses this issue, followed by a definition of key requirements.

1.3.1 Thesis contents

In Chapter 2, the adopted approach to MDA is presented, starting with an overview of the methodology/software developed. Each module of the software will be explained in detail. Notably, the absence of a section involving statistical analysis of the transport vehicles in this introductory part is due to the fact that the statistical module is an integral part of the tool. Used only in the first iteration, this module plays a critical role as it significantly reduces the number of inputs required from an external user. The other modules related to mass and size estimation, as well as the trajectory, will be discussed in greater detail in the next chapter.

Chapter 3 follows, in which the tool is applied to a specific case study. The inputs are based on a typical mission conducted by the RETALT1, introduced in section 1.1. The results obtained will be compared in Chapter 4 for model validation and verification. For the design output, a direct 1:1 comparison will be made between the model and the considered vehicle, evaluating the percentage

differences. For the mission validation, the commercial software ASTOS will be used, where the same mission will be implemented to allow a comparison of losses and velocity consumption.

The final Chapter 5 will give space for reflections on the work in general, the results obtained and possible improvements and future applications of the tool.

1.3.2 Methodology and Tool Requirements

The list of requirements has been drawn up together with the thesis supervisors in order to create a reliable tool that is adaptable with integration into the ASTRID routine. All requirements (denoted as *REQ*) are listed in Table 1.1 and are categorized according to their relevance to the methodology (*MET*), trajectory (*TR*), and tool (*TL*) requirements, as shown in Table 1.2.

Requirement ID	Description
REQ-MET-10	The tool shall be able to model the thrust of liquid stages to within 15% accuracy.
REQ-MET-20	The tool shall be able to model the propellant mass of liquid stages to within 10% accuracy.
REQ-MET-30	The tool shall be able to model the inert mass of launch vehicle stages to within 10% accuracy.
REQ-MET-40	The tool shall be able to model the length of launch vehicle to within 10% accuracy.
REQ-MET-50	The tool shall be able to model the diameters of launch vehicle stages to within 10% accuracy.
REQ-MET-60	The tool shall be able to model the MTOM of launch vehicles to within 10% accuracy.
REQ-TR-10	The tool shall be able to evaluate launch mission consumption (ΔV) to within 10% accuracy.
REQ-TR-20	The tool shall be able to evaluate landing phase consumption (ΔV) to within 10% accuracy.

Table 1.1: Methodology Requirements

The source of some of these requirements is thesis work cited in [2].

Requirement ID	Description
REQ-TL-10	The tool shall be developed in Python.
REQ-TL-20	The tool shall model return-to-launch-site and downrange landing for reusable launch vehicles.
REQ-TL-30	The tool shall model as well as expendable launch vehicles.
REQ-TL-40	The tool shall be able to model a reusable launch vehicle in short time.
REQ-TL-50	The tool shall be able to simulate the ascent and descent of a reusable launch vehicle.
REQ-TL-60	The tool shall be able to output the physical launch vehicle parameters necessary for analysis and comparison purposes.
REQ-TL-70	The inputs and outputs of the tool shall be read from Excel files.
REQ-TL-80	The tool shall be stored databases in user-modifiable files.

Table 1.2: Tool Requirements

Chapter 2

Methodology and tool: Holistic Framework

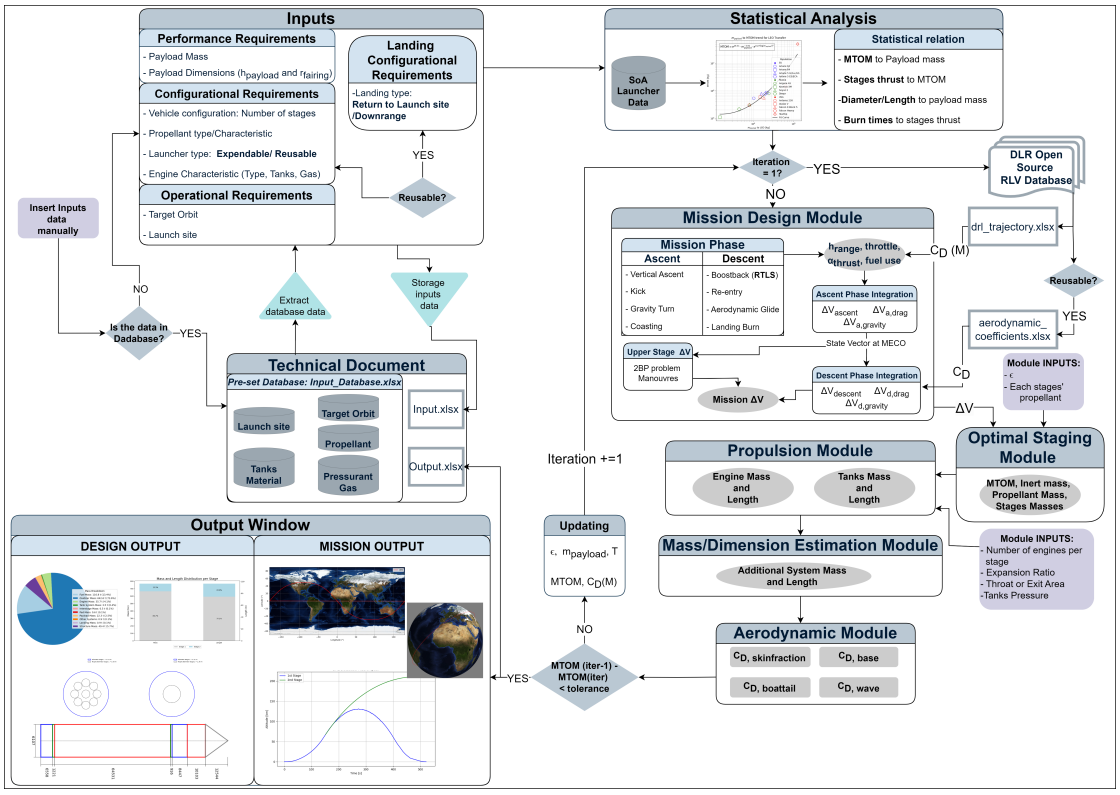

Figure 2.1: Expandable/Reusable Launcher Mission and Design Methodology: Logic scheme

This chapter describes the mission and vehicle design methodology and tool for expandable/reusable launchers (EL or RL). The methodology supports the design of these launcher types, given a reference mission and based on a set of high-level requirements. Figure 2.1 provides a logical overview of the RLV/ELVs launchers MDA produced for this work. The method described in this study starts with the definition of a set of inputs that describe the desired configuration of the launcher and the mission parameters. Subsequently, these inputs are subjected to a statistical analysis, which serves as an initial step useful to generate reasonable estimates and reducing the number of detailed inputs required from the user. The data now enters the mission routine, in which, by evaluating the possible trajectory of the launcher, it is possible to have an estimation of the velocity consumption to accomplish it. Subsequently, the analysis continues with a series of subsystem routines and mass and length estimation, including the aerodynamic and propulsion module. A final check is made on the MTOM by evaluating by how much the value of the previous iteration is shifted from that of the first, given a tolerance. Some of the parameters are updated and the cycle begins again. If the condition is met, the final objective of this methodology is to generate a comprehensive set of outputs, including budgetary information and schematic representations of design and trajectory data pertinent to the mission. The following sections will present a detailed account of the methodology in question.

2.1 Inputs

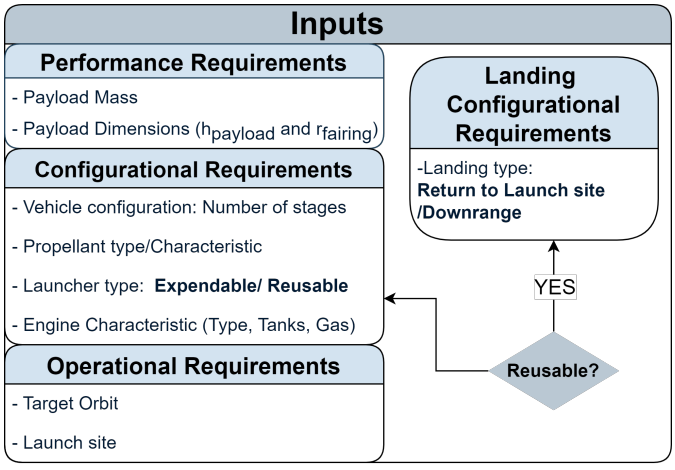

Figure 2.2: Methodology Input

As shown in Figure 2.2, there are several inputs for the methodology, coming from typical high-level requirements, namely: **Performance Requirements**, **Configurational Requirements** and **Operational Requirements**. The mass of the payload and its size are certainly among the most influential inputs. The number of stages, type of propellant and engine, and the type of launcher are critical for the most accurate mass estimation (including a landing system in the case of a reusable). Finally, operational requirements must be defined for an acceptable

mission analysis. The user manually enters input data; however, if they have a mission or specific propulsion system technologies in mind that align with existing options, they can utilize the pre-existing database (introduced in the next section). The routine is designed to support a wide range of missions or technologies, as long as the user provides all necessary data manually within feasibility limits. For clarity, consider these examples: if a chosen transfer orbit is not available in the database, the user can manually input the six orbital parameters. Similarly, if a preferred launch site is not listed, latitude and longitude can be specified as needed.

2.2 Technical Document

To support the methodology, databases were created, whose data were collected in a module called the Technical Document Module (Figure 2.3). In particular, the databases is stored in an Excel file '*Input_Database.xlsx*', while , to track the inputs used and outputs generated by the software, the '*Input.xlsx*' and '*Output.xlsx*' files are overwritten with the new data, each time the routine is used. This gives the end user quick access to all the information they need.

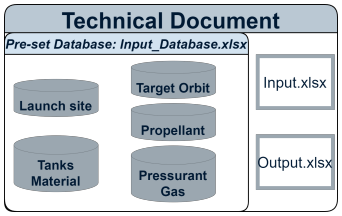

Figure 2.3: Technical Document Module

2.2.1 Database: Launch site

In compliance with the reference [15], the main recently used launch sites are listed in the database. The main characteristics of each are shown in the table 2.1 and the location in Figure 2.4.

Launch Site	Latitude (δ)	Longitude (α)	Earth Rotation Speed ($v_{\mathbf{rot}}$) [m/s]	Country
Guiana Space Centre (CSG)	5.24° N	52.77° O	465.3	France (EU)
Esrange Space Center	67.89° N	21.24° E	160.1	Sweden (EU)
Andøya Space	69.30° N	16.02° E	149.1	Norway (EU)
SaxaVord Spaceport	60.82° N	0.87° O	252.3	UK (EU)
Cape Canaveral	28.56° N	80.58° O	407.7	USA
Vandenberg Space Force Base	34.63° N	120.61° O	388.2	USA
Tanegashima Space Center	30.40° N	130.98° E	403.2	Japan
Plesetsk Cosmodrome	62.93° N	40.57° E	232.1	Russia
Baikonur Cosmodrome	45.97° N	63.31° E	318.6	Kazakhstan

Table 2.1: Database Launch Sites [15]

In the case of launching eastwards, in accordance with the direction of the Earth's rotation, there is a need to evaluate a gain in terms of ΔV due to this effect. For this reason there is a need to calculate v_{rot} with respect to the launch

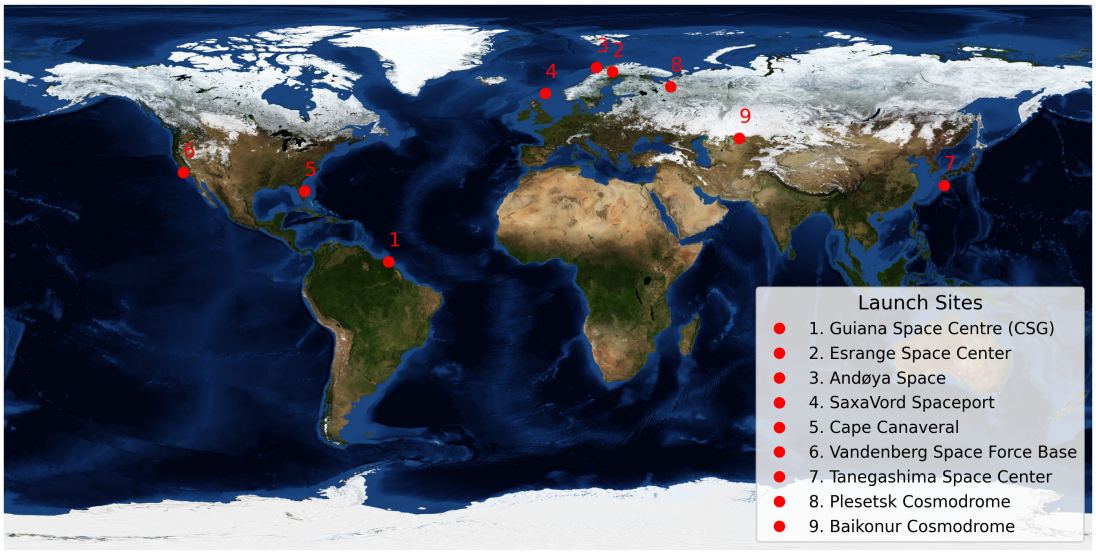

Figure 2.4: Launch Site Map

site. Starting to the distance from the centre of the Earth (R_e) at a given latitude δ is calculated using the formula:

$$R_e = \sqrt{\frac{(a^2\cos^2(\delta) + b^2\sin^2(\delta))}{(a\cos(\delta))^2 + (b\sin(\delta))^2}} \tag{2.1}$$

where:

- $a = 6378.137$ km is the equatorial radius of the Earth,
- $b = 6356.752$ km is the polar radius of the Earth,
- δ is the latitude of the launch site.

The rotational speed of the Earth at the surface (v_{rot}) for a given latitude is calculated in eq. 2.2:

$$v_{\text{rot}} = R_e \cdot \omega \cdot \cos(\delta) \tag{2.2}$$

where $\omega = 7.2921159 \times 10^{-5}$ rad/s is the angular velocity of the Earth. The total savings of ΔV will be counted in the Mission Design Module.

2.2.2 Database: Target Orbit

Depending on the objective of the mission, the payload that is transported by the launch vehicle is placed into a certain orbit. The only two orbits that were

considered in the database are the Geostationary Transfer Orbit (GTO) (orbital parameters [16]) and the Low Transfer Orbit (LTO). As reference values for the latter, the same as for RETALT1 (RETro propulsion Assisted Landing Technologies) were chosen [4] , the same launcher that will be used to validate the design section of the methodology. Orbit features are shown in Table 2.2.

Orbit Type	Acronym	Orbital Parameters
Lower Transfer Orbit [4]	LTO (BLUE)	a = 6718.0 [km] e = 0.0 i = 50.0 [°] RAAN = 0.0 [°] ω = 0.0 [°] ν = 0.0 [°]
Geostationary Transfer Orbit [16]	GTO (RED)	a = 24371.0 [km] e = 0.73 i = 7.0 [°] RAAN = 0.0 [°] ω = 180.0 [°] ν = 0.0 [°]

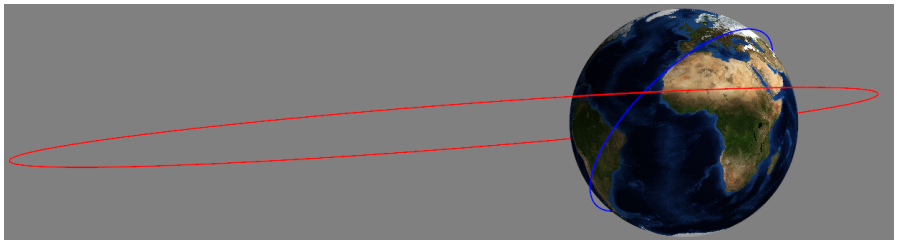

Table 2.2: Database Transfer Orbit: Red-GTO, Blue-LTO

For a better understanding of the data in Table 2.2 some theoretical hints on the orbital parameters are given here: a is the **semi-major axis** which defines the size of the conical orbit; e the **eccentricity** gives information about the shape of the orbit, the type of conic; i **inclination** is the angle between the orbital plane and the equatorial reference plane; Ω is the **Rigth Ascension of Ascending Node**, it is the angle between a fixed reference point (ram constellation in a geocentric reference system) and the ascending node, and gives me information about the orientation of the orbit in the reference plane. **Periapsis argument** ω is the angle between the ascending node and the periapsis of the orbit measured in the orbital plane. **True anomaly** ν indicates the position of the object on the orbit at a given time.

2.2.3 Database: Propellant

The propellants considered within the methodology are only liquids, given the tool's ability to adapt to both RLV and ELVs launchers. To better justify the choice one must take into account that retro-propulsion landings use liquid-propellant rocket engines, as these have the ability to re-ignite and throttle, essential during re-entry and landing. These conditions are extremely difficult to achieve with solid engines. For this reason, this work will only deal with liquid-type propellants. The performance of each type of propellant is derived from the Sutton [17] and, in particular, the performance of bi-propellants is shown in Figure 2.5. In Figure 2.5 is also shown the kind of storability, important in the Propulsion System Module (Section 2.6) for estimation of tanks' mass.

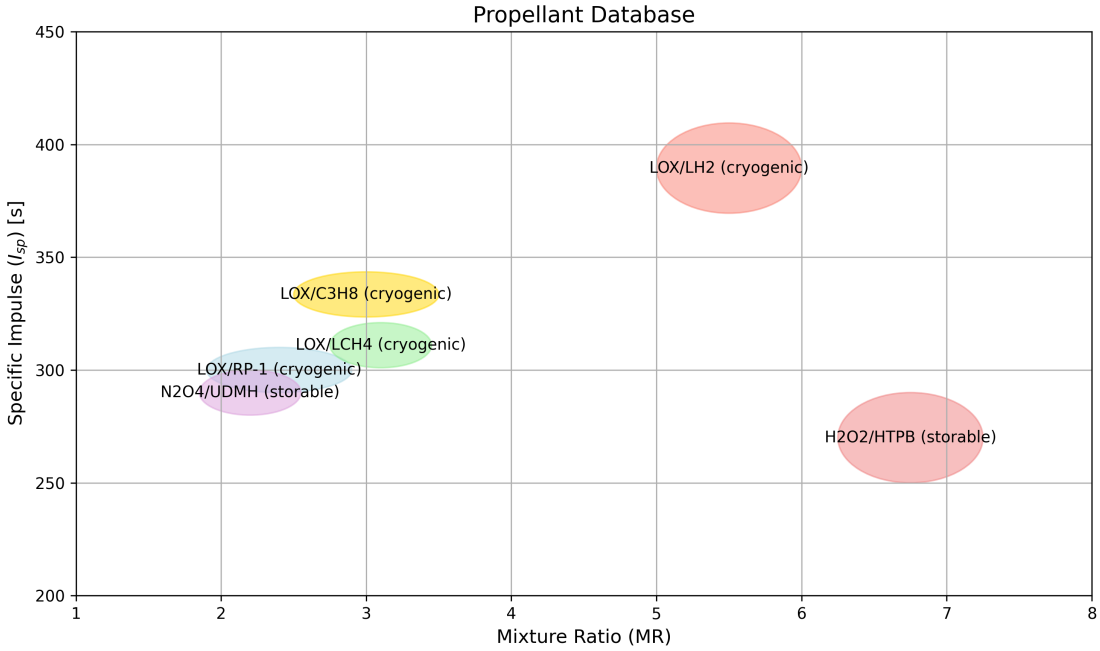

Figure 2.5: Database Propellant Characteristics: I_{sp} vs MR(Mixture ratio)

Here is a list of propellants in the database, including their acronyms and full names:

- **LOX/RP-1**: Liquid Oxygen / Refined Petroleum-1
- **LOX/LCH4**: Liquid Oxygen / Liquid Methane
- **LOX/LH2**: Liquid Oxygen / Liquid Hydrogen

- **LOX/C3H8**: Liquid Oxygen / Propane (C_3H_8)
- **H2O2/HTPB**: Hydrogen Peroxide / Hydroxyl-Terminated Polybutadiene
- **UDMH**: Unsymmetrical Dimethylhydrazine
- **N2O4/UDMH**: Nitrogen Tetroxide / Unsymmetrical Dimethylhydrazine
- **HTPB**: Hydroxyl-Terminated Polybutadiene

Finally, the mono-propellant **UDMH** (Asymmetric Dimethyl-hydrazine) is also included in the database.

2.2.4 Database: Tanks Material and Pressuring Gas

There is also a database containing typical characteristics of the materials used for fuel and oxidizer tanks, specifically alloys of steel, titanium, and carbon fiber. The primary material characteristics that influence design are shown in Figure 2.6. Additionally, for a pressure-regulated system, the use of a pressurizing gas

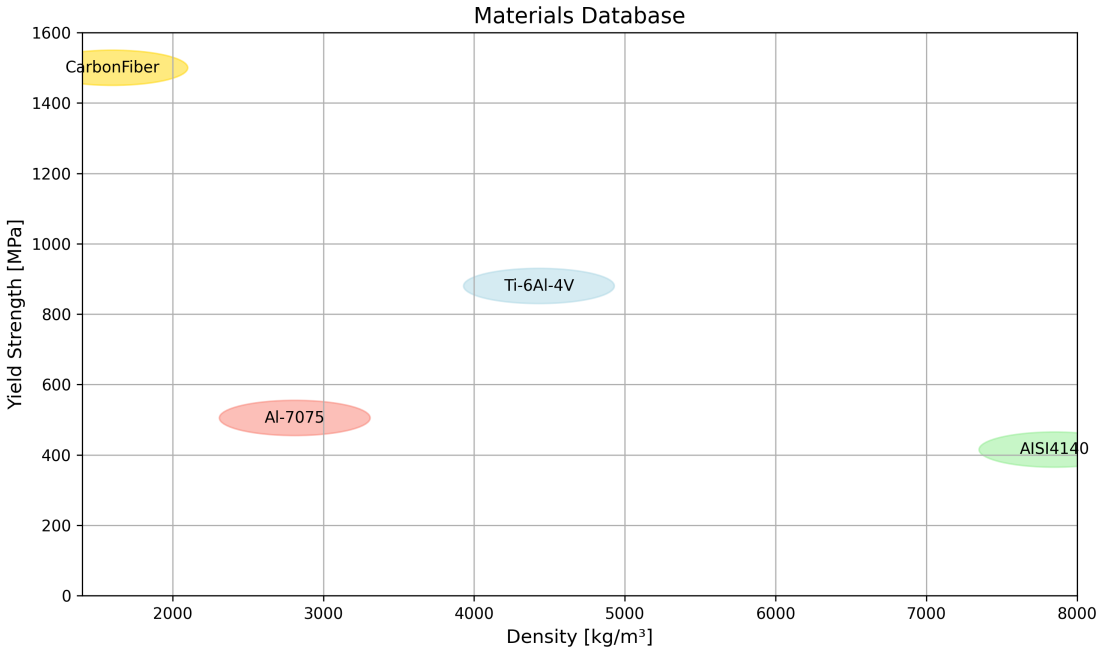

Figure 2.6: Database Tanks Material

is essential. All gases in the database are stored at a pressure of 286 bar and a temperature of 293 K. The two gases considered, along with their densities, are as follows:

- **He** (Helium), with a density of 5.24 $\frac{kg}{m^3}$;
- **GN2** (Gaseous Nitrogen), with a density of 43.3 $\frac{kg}{m^3}$.

This database was created to make the framework more complete. It is recognised that it is not an extremely precise dataset, it has been considered a good approximation for the conceptual design phases and a starting point for subsequent ones. However, it is recommended that users enter more specific data related to their own case study to ensure a more accurate and focused analysis.

2.3 Statistical analysis

Supporting the methodology is a statistical analysis of the most influential launchers of the past decades. Most launchers are expendable, except for those from SpaceX. They are categorized by geographical area: European launchers in blue, American in red, and Russian in green. This division highlights how national expertise varies by country, impacting launcher performance. For instance, factors such as launcher diameter may depend on the configuration of the launch pad and, consequently, on the infrastructure available at the launch site.
Within the statistical analysis module (Figure 2.7), the steps are simple: collect the data from the database mentioned above, analyse the data by looking for equations that correlate them and use these equations to get more realistic quantities for the first iteration of the cycle. All data within the Statistical Analysis are derived from 'The Annual Compendium of Commercial Space Transportation' reported in [18].

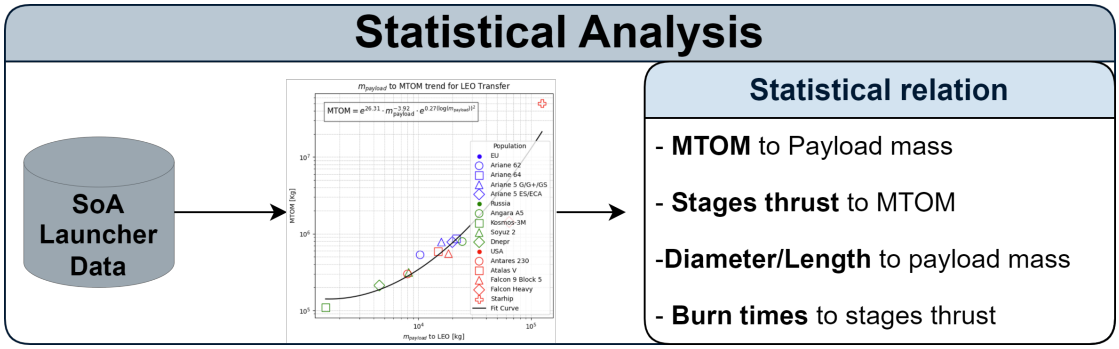

Figure 2.7: Statistical Analysis Module

In addition, a coefficient of determination, R^2, is shown in Statistical trend plot. It is a statistical measure that indicates how well data points fit a model. It quantifies the proportion of the variance in the dependent variable that can be explained by the independent variables. In practical terms:

- An R^2 value of 1 means a perfect fit, where the model explains all the variability of the data.
- An R^2 value of 0 means the model does not explain any of the variability.

R^2 is calculated as:

$$R^2 = 1 - \frac{\sum(y_i - \hat{y}_i)^2}{\sum(y_i - \bar{y})^2} \tag{2.3}$$

- y_i are the observed values;

- $\hat{y}_i$ are the predicted values from the model;
- $\bar{y}$ is the mean of the observed values.

The statistical trends used are now displayed. As presented in the Inputs section, one of the dimensioning quantities is the $m_{payload}$. It begins the relationship that links it to MTOM (maximum take-off mass).

In Figure 2.5 there is a very optimistic coefficients of determination, which allow

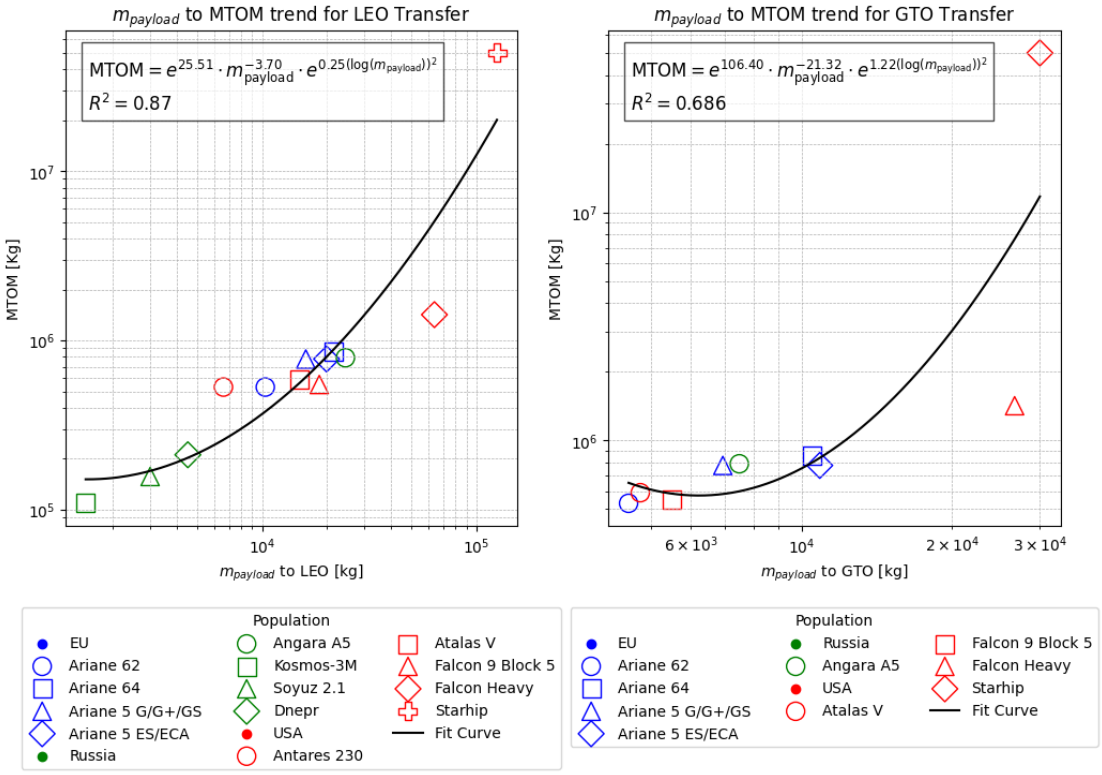

Figure 2.8: Statistical Relation: MTOM vs $m_{payload}$

to state that the least squares curve, especially for the LEO case ($R^2_{LEO} \simeq 0.87$), is a good approximation of the data. The process now proceed with the statistical analysis concerning the dimensions of the launcher, specifically evaluating the diameter and length. Before presenting the statistical trends, it is important to note that, to transport a certain mass into a target orbit, many current launchers often utilize parallel stages: the boosters. One of the objectives of this thesis work is to develop the conceptual design of a RLV TSTO vehicle without the presence of additional vectors. To this end, the following assumptions have been made:

- In the case of rocket in statistical population using two boosters, the total diameter of launcher increases by $D_{booster}/2$.

- In the case of using four boosters, the total diameter of launcher in statistical population increases by $D_{booster}$.

To clarify this with an example, considering the Ariane 6 as a launcher, there are two different configuration types: Ariane 62 and Ariane 64, where the final digit indicates the number of boosters. Since the diameter of the first stage is $D_{stage1} = 5.4\,\text{m}$ and that of its booster, the P120C, is $D_{booster} = 3.1\,\text{m}$, the results are:

$$D_{Ariane62} = D_{stage1} + \frac{D_{booster}}{2} \simeq 7\,\text{m} \tag{2.4}$$

$$D_{Ariane64} = D_{stage1} + D_{booster} \simeq 8.5\,\text{m} \tag{2.5}$$

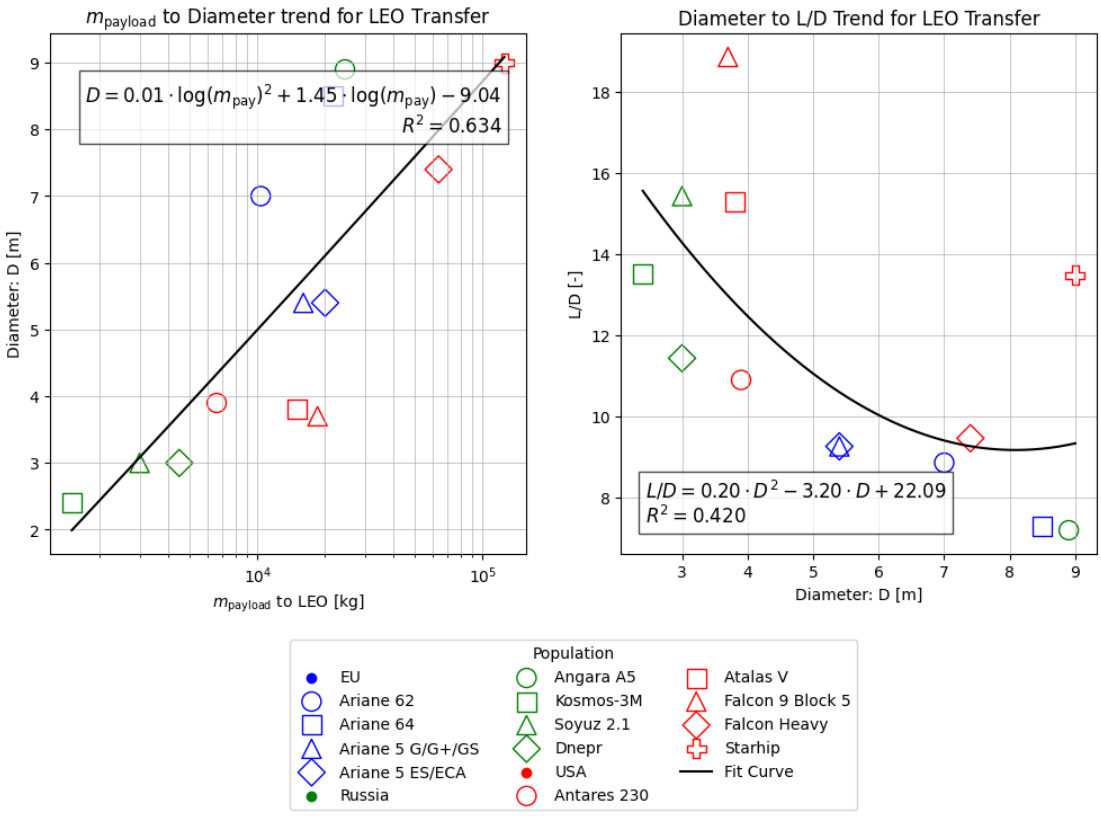

Figure 2.9: Statistical Relation: *Diameter* vs $m_{payload}$ and $\frac{L}{D}$ vs *Diameter*

Figure 2.9 shows that the relationship between mass and payload yields realistic results given the coefficient of determination, while for $\frac{L}{D}$, there is a much larger spread of data points. Therefore, a correction will be necessary, which will be

presented in the next section, validating the statistical analysis.

Below is an evaluation of the thrust of each stage with respect to the MTOM using parabolic regression to replicate the thrust-to-weight ratio, $\frac{T}{W}$, which will also be referred to in the later stages of the methodology. As anticipated for the diameter case, here too there is a need to emulate the presence of the boosters in order to have a realistic statistical trend. To this end, the following assumptions were made:

- In the case of using two boosters, the thrust T_1 of the first stage of the launchers in the statistical population increases by $\frac{T_{1,\text{booster}}}{2}$.
- In the case of using four boosters, the thrust T_1 of the first stage of the launchers in the statistical population increases by $T_{1,\text{booster}}$.

Consider the example of Ariane 6 with its Ariane 62 and Ariane 64 configurations. Since the thrust of the first stage is $T_{\text{stage1}} = 1370\,\text{kN}$ and that of its booster, the P120C, is $T_{\text{booster}} = 9000\,\text{kN}$:

$$T_{1,\text{Ariane62}} = T_{\text{stage1}} + \frac{T_{\text{booster}}}{2} \simeq 6000\,\text{kN}, \tag{2.6}$$

$$T_{1,\text{Ariane64}} = T_{\text{stage1}} + T_{\text{booster}} \simeq 10000\,\text{kN}. \tag{2.7}$$

From Figure 2.10, it is evident that there is no true correlation among the data for T_2, given the very low values of the coefficient of determination. For the analysis to be valid, a validation process is necessary. Therefore, corrections need to be made to the previously introduced module.

It should be noted that the statistical analysis is conducted only in the first iteration of the cycle. It does not impact the final result of the methodology but serves solely to reduce computational costs.

2.3.1 Statistical Analysis Validation: RETALT1 Case

The typical RETALT1 mission in a (LTO) at an altitude of $340\,km$ is used to validate the statistical analysis. The payload capacity considered for the mission is $m_{payload} = 20000\,kg$ ([16]). Table 2.3 shows the results considering the previously introduced capacity for both the RETALT and the statistical case.

An obvious problem with the statistical analysis is the underestimation of mass and thrust. Possible reasons for this behaviour include the fact that only two of the cases in the statistical population use reusable technologies. As can be seen in the statistical trends of thrust (T) against MTOM (Figure 2.10), the thrust at the same mass $\frac{T}{W}$ for the two Reusable cases (Falcon 9 and Falcon Heavy) present has much higher values.

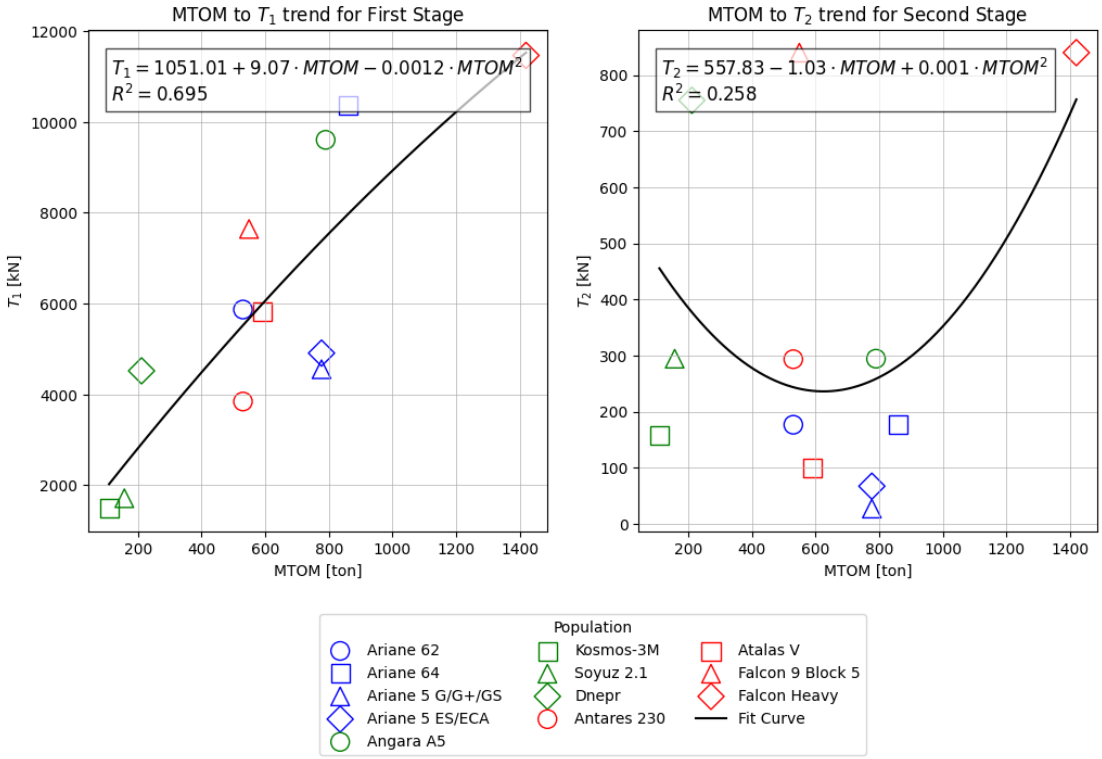

Figure 2.10: Statistical Relation: T_1 vs MTOM and T_2 vs MTOM

RETALT1 [16]	**Statistical Analysis**
$MTOM_{RETALT} = 887.5\,\text{ton}$	$MTOM_{LEO} = e^{25.51} \cdot m_{payload}^{-3.70} = 651.39\,\text{ton}$
$D_{RETALT} = 6.00\,\text{m}$	$D = 0.01 \cdot \log(m_{payload})^2 + 1.45 \cdot \log(m_{payload}) - 9.04 = 6.30\,\text{m}$
$L_{RETALT} = 103.0\,\text{m}$	$\frac{L}{D} \cdot D = (0.2 \cdot D^2 - 3.2 \cdot D + 22.09) \cdot D = 62.17\,\text{m}$
$T_{1,RETALT} = 10581\,\text{kN}$	$T_1[\text{kN}] = 1051.01 + 9.07 \cdot MTOM - 0.0012 \cdot MTOM^2 = 6449.94\,\text{kN}$
$T_{2,RETALT} = 830\,\text{kN}$	$T_2[\text{kN}] = 557.83 - 1.03 \cdot MTOM + 0.001 \cdot MTOM^2 = 311.20\,\text{kN}$

Table 2.3: RETALT1 data and Statistical Analysis Result given $m_{payload}$

Figure 2.11a shows, through a radar graph, how the results obtained from the statistical analysis deviate from those of RETALT. The percentage difference is significant for the thrust, indicating that a model correction is necessary. Therefore, an adjustment was made directly to the thrust-to-weight ratio, $\frac{T}{W}$, using eq. :

$$\frac{T_1}{W}* = 1.5 \quad \text{(first stage)} \tag{2.8}$$

$$\frac{T_i}{W}* = 2 \quad \text{(upper stages, i} > 1) \tag{2.9}$$

This adjustment yields realistic thrust values and thus provides optimal starting

inputs for the methodology. It was decided not to apply corrections to the lengths and masses, as these will be estimated in greater detail in subsequent steps. In

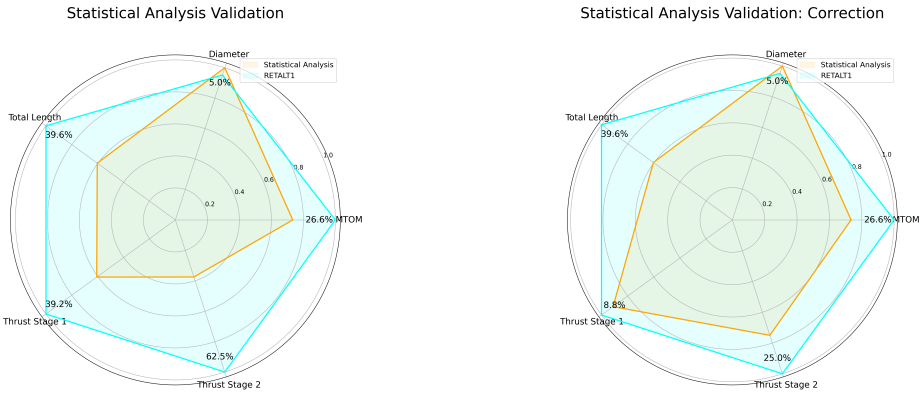

(a) **(b)**

Figure 2.11: Comparison of Statistical Validation Results: a.Validation, b. Corrected validation

Figure 2.11b, one can observe how the percentage differences have now reached acceptable values. This is the validation of the first statistical module and the starting point for the next stage.

2.4 Mission Design Module

Starting with an analysis of a typical launcher mission profile, including both ascent and landing phases, we now enter the core of the methodology itself. The trajectories primarily serve as a tool for determining the final sizing of the launchers. The mission is divided into segments of duration dt, which are then integrated sequentially. For each mission phase, a specific altitude range, throttle setting, thrust angle, and fuel usage percentage are defined. These parameters are passed to a function, 'Ascent Phase Integration', that integrates the equations of motion, evaluating ΔV consumption along with gravity and drag losses. In the case of a reusable launcher, the state vector at MECO (Main Engine Cut Off) is used as the initial condition for integration to determine the required ΔV for landing in 'Descent Phase Integration'. Starting from MECO, the ΔV consumption of the upper stages is also assessed to achieve the desired reference orbit. This is done by analysing changes in orbital parameters using the two-body problem framework. To ensure accurate functioning, an aerodynamic model is necessary to provide the drag coefficient C_D at each mission phase, as the aerodynamic module has not yet been addressed. For this purpose, there is a database provided by the German Aerospace Centre (DLR) for the configurations RLV [19], which will be detailed later. The logical flow of the process is illustrated in Figure 2.12.

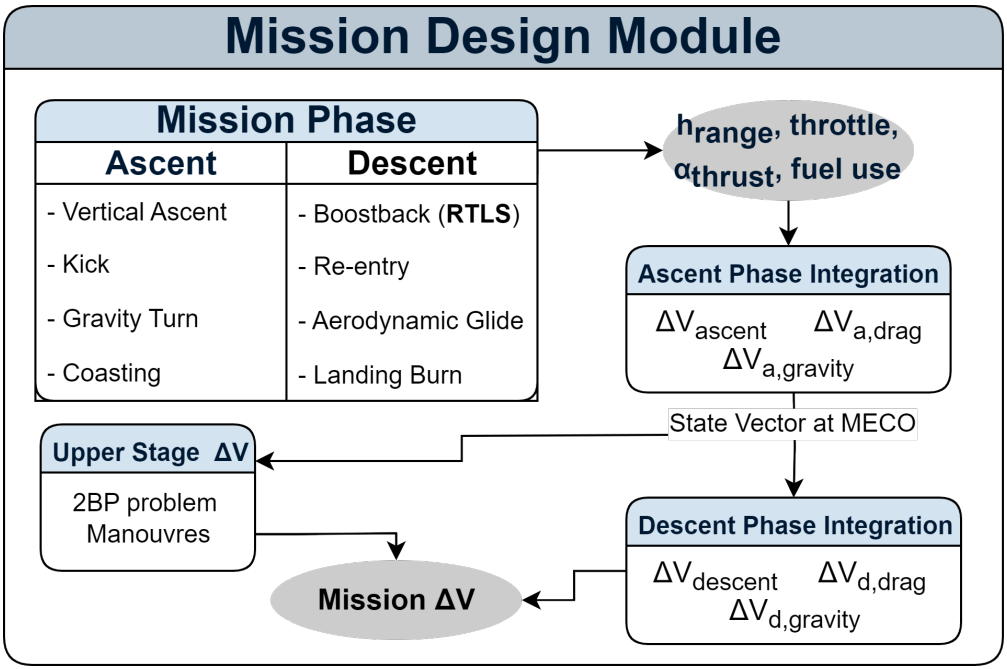

Figure 2.12: Mission Design Module

2.4.1 Mission Phases

To define the main phases of a typical rocket mission, refer to Figure 2.12. In particular the mission is divided into distinct phases for ascent and descent, with each phase characterized by specific parameters such as height range, throttle setting, thrust (or pitch) angle, and fuel usage.The task of a MDO is to determine the value of these quantities for each phase in order to reach the optimal value of the function to be maximised or minimised. Each phase is configured to simulate realistic mission dynamics, and in this work the strategy includes setting a target function (maximum height) and optimising mission duration. For multi-parameter optimisation, please refer to the analysis performed in ASTOS in section 4.2. As indicated in section 5, one of the future goals will be to incorporate a multi-parameter optimisation model into the tool. According to the thesis principal topic RLV typically use one of two trajectory types: downrange landing (DL) or return to launch site (RTLS) presented in Figure 2.12. In first one, the first stage follows a natural arc after stage separation and lands away from the launch site. In RTLS, the first stage performs a boost-back burn to return and land near the launchpad. Figure 2.12 also lists flip over manoeuvres and attitude correction manoeuvres, since the design of the Attitude Control System (or also of the Guidance, Navigation & Control system) is beyond the scope of this paper, only the effects these have on pitch angle will be considered. Given the possibility of validating the model in the

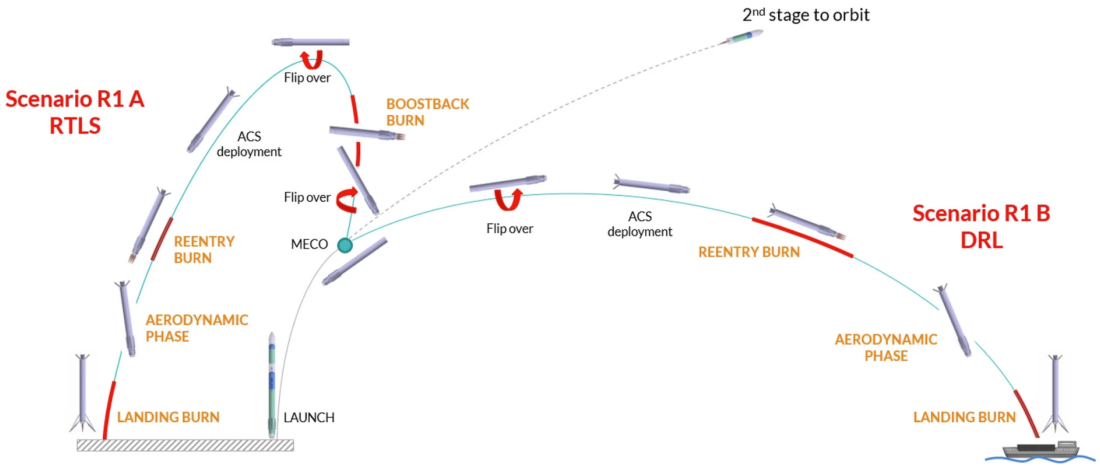

Figure 2.13: Typical Mission Profile [20]

ASTOS environment, the mission will be divided, at least for the ascent, into as many phases as indicated in the manual for 'Conventional Launcher' [21].

1. **Lift off:** This phase initiates the launch with full throttle, providing maximum thrust to overcome gravitational forces and increase altitude quickly. The

pitch angle remains vertical (90°) as the vehicle ascends. Engine fuel usage is set on maximum value, reflecting the high energy requirement to lift off and clear dense atmospheric layers. The purpose of this phase is to gain initial altitude and speed while stabilizing the vehicle's trajectory.

2. **Pitch Over:** This is a very short phase in which the throttle is maintained at a high level. The pitch angle, on the other hand, decreases at a rate of about $-1.5\,\frac{°}{s}$ allowing a smooth transition from vertical to horizontal flight. This phase continues to increase momentum and altitude, preparing the rocket for the next phase.

3. **Costant pitch:** Like the previous one, it is also very short. The only difference is that the pitch angle is kept constant, the launcher is now ready for one of the longest phases, the gravity turn.

4. **Gravity Turn:** During the gravitational turn, the throttle is further reduced to 80% and the thrust angle is strongly influenced by the effect of gravity. Here you will find the "Q-max", the time when the dynamic pressure reaches its highest level and therefore the maximum resistance. Using a typical Falcon 9 mission as a reference [22], when the vehicle reaches an altitude between $70000\,m$ and $100000\,m$, first stage release altitude, allowing the upper stages to deliver the payload to the established target orbit.

5. **Main Engine Cut Off (MECO):** Rather than a stage, the MECO marks the moment when the engines are switched off, the first stage is re-launched and the upper stages of the vehicle are in a condition to continue the ascent.

6. **Coasting Phase with Fairing:** In this phase, the vehicle continues to climb thanks to the previous thrust, without applying throttle, and the pitch angle continues to decrease. The duration of this phase is usually about ten seconds and, at the end, the payload will be exposed to the atmosphere due to the jettison of the fairing. In fact, this action avoids pushing the fairing with a considerable mass, with a consequent consumption of propellant, since one is now in those layers of the atmosphere that no longer represent a harmful environment for the payload. Furthermore, for the Expandable class, this point marks the beginning of the uncontrolled descent phase, while for the Reusable class, it is a controlled phase, explained in more detail later.

7. **Orbit Insertion:** The upper stages are now involved in the orbit insertion phase, the accelerator and thrust angle are precisely adjusted to position the vehicle in the target orbit. A calculated increase in ΔV allows sufficient energy to be acquired to reach the target orbit. The purpose of this phase is to achieve orbital velocity and altitude, ensuring that the vehicle's trajectory

and velocity match the desired orbital parameters. This phase completes the ascent part of the mission, stabilising the vehicle for mission objectives or payload deployment.

As mentioned earlier, since guidance is not the primary objective of this research, it is assumed that the on-board attitude control system and cold gas thrusters can reorient the first stage to the desired attitude before performing recovery maneuvers. The reorientation involves pitching the first stage so that the thrust vector is opposite to the velocity vector before reigniting the main engines. A simplified approach is to decelerate the rocket to zero (or near zero) velocity at the intended landing altitude. Outside of boostback, the first stage maintains an angle of attack AoA of 180°, ensuring that the thrust vector directly opposes the velocity vector[2]. Additional assumptions for the reusable landing trajectory are as follows:

1. The pitch angle during the boostback manoeuvre is set to 190°, a value shown to replicate typical boostback trajectories.

2. The duration of the boostback manoeuvre ranges from 20 to 60 seconds [2], but in the working case a maximum altitude has been set.

3. The re-entry burn starts at altitudes between $80\,km$ and $50\,km$ and ends between $55\,km$ and $30\,km$, depending on landing conditions.

4. The landing burn begins below an altitude of $15\,km$ [2].

In the case of RTLS, two propulsion maneuvers are considered between the MECO phase and the aerodynamic phase: a boostback burn is necessary to aim at the correct landing site, and a second maneuver (re-entry) could be necessary to slow down the vehicle and keep the incoming aerodynamic loads under control. The main objective of the boostback burn is to change the velocity direction and correctly point to the desired landing site: the launch pad or a nearby alternative landing pad [23].

The various steps for landing are now reported in detail:

1. **Boostback Burn:** For reusable vehicles (RLV), only in the case of a 'return landing to the launch site' (RTLS), the boostback burn phase controls re-entry, with the throttle not set to maximum and with the use of not all engines (in the case studies presented in Chapter 3 only 3 of the total 9 engines are used in this phase). The thrust angle varies between values ranging from 90° to 180° and causes the vehicle to slow down and orient itself for re-entry. This phase is crucial for trajectory adjustment to ensure that the vehicle can safely return for landing. Figure 2.14 shows how the velocity vector must change direction to prepare for this type of manoeuvre.

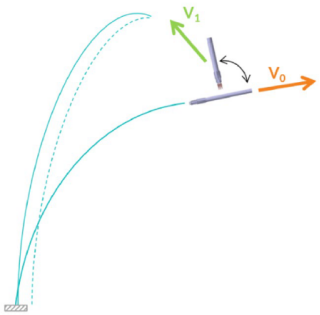

Figure 2.14: Boostback Burn Velocity turn[23]

2. **Re-entry Burn:** The objective of the re-entry burn is to reduce the velocity of the vehicle using the propulsion system and thus keep the aero-thermo-mechanical loads under control during the subsequent aerodynamic phase. In addition, the control of the thrust vector attitude would allow the control of the trajectory, contributing to the compensation of the trajectory dispersions accumulated during the high-altitude aerodynamic flight due to uncertainties or errors with respect to the reference conditions. The performance during the re-entry burn depends on the start point of the burn, its duration and the initial conditions at the start of the burn. Preliminary analysis has shown that the start of the re-entry burn cannot be tuned too much, and that initiation of the re-entry burn at 70 km altitude is [23]. After this phase, the vehicle is now ready to enter the aerodynamic glide phase.

3. **Aerodynamic Glide:** This phase relies on aerodynamic forces to guide the vehicle's descent without the use of propulsion. The vehicle decelerates to a target height without fuel consumption. The main objective is to slow the vehicle down to the desired initial conditions for the landing phase, keeping thermomechanical loads within structural limits and contributing to trajectory control. In particular, aerodynamic drag reduces the speed of the vehicle from hypersonic to supersonic, and finally subsonic, depending on the conditions under which the landing phase is initiated. During this phase, it is crucial to limit the aero-thermo-mechanical loads within the maximum values tolerated by the vehicle structure and the thermal protection system (TPS). In addition, the phase must compensate for residual trajectory losses accumulated during re-entry and aerodynamic flight, often caused by uncertainties. Control of the aerodynamic attitude angle, i.e. the orientation of the vehicle with respect to the velocity vector, plays a crucial role in determining aerodynamic performance and deceleration success. This phase ends when a new point of maximum dynamic pressure (Q-max) is reached, characterised by much greater loads than the initial re-entry [23].

4. **Landing Burn:** In the landing phase, the throttle is set to maximum but, in this case, one or a few engines are used to bring the speed down to approximately zero. In the case considered in Chapter 3 the engine used, for example, will only be the middle one.

2.4.2 DLR Reusable Launcher Database

The German Aerospace Center (DLR) has made available, in open-source mode, a database for a typical mission of a reusable launcher. Given the premises outlined in Chapter 1 regarding the importance of establishing a European research network on this technology, it was decided to make it an integral part of the tool presented in Figure 2.1. The database is essential for the first iteration of the methodology, as it allows to obtain, based on the tabulated trajectory values, a profile of the aerodynamic drag coefficient from the outset 2.15. The structure of the database and how the data were used will be presented later.

The Database, denoted *RFZ*, can be broken down into three subcategories for ascent, re-entry and landing [24].The scenario describes the landing case of type DL for a LEO flight, performing computational study for aerodynamic glide phase.

Before introducing the trajectory described by the launcher treated in the *RFZ* model, it is useful to give an overview of the characteristics. The RFZ model, based on SpaceX's Falcon 9, is a simplified version designed for CFD (Computational Fluid Dynamics) analysis that represents the launch, re-entry, and landing configurations in Figure 2.16. The vehicle is 70 m tall with a stage 1 diameter of 3.66 m [24]. The model includes nine nozzles: one central nozzle slightly protruding, and eight peripheral nozzles arranged in a circular layout as model analyzed in Chapter 3.

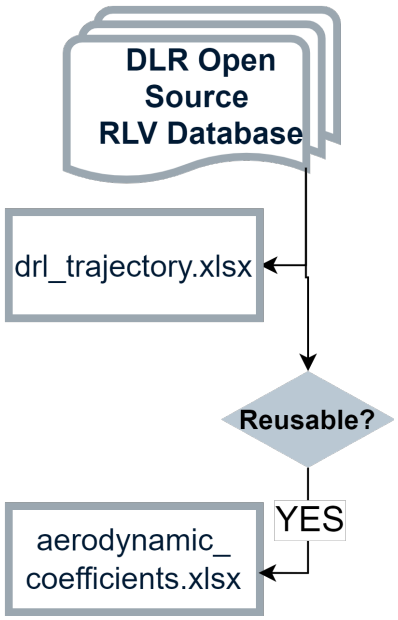

Figure 2.15: Database connection in tool

To gain a more detailed understanding of the systems enabling controlled reentry, attention is focused on the grid fins of the *RFZ* model. With a hexagonal profile and a thickness-to-chord ratio of 10%, these fins span 3 m with a chord length of 2 m and are designed to withstand thermal and aerodynamic loads [24].

Equally important is analyzing the rocket's behavior during various mission phases. For this purpose, Figure 2.17 illustrates the main results obtained from the

Figure 2.16: RFZ model layout: launch configuration, re-entry configuration and landing configuration [24]

tabulated trajectory data. Of particular interest to the methodology are the graphs

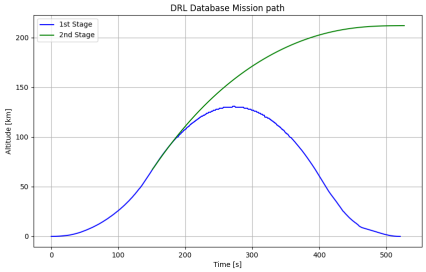

(a) Mission Path: Height

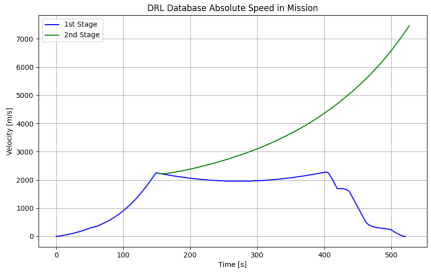

(b) Mission Path: Speed

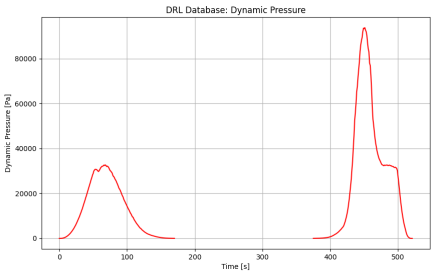

(c) Dynamic Pressure

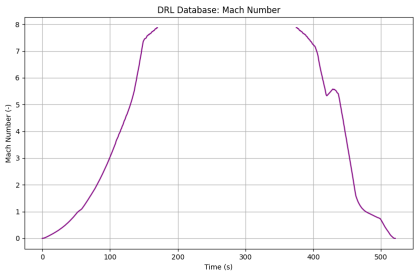

(d) Mach Number

Figure 2.17: RFZ Model Trajectory Data: (a) Mission Path, (b) Mission velocity, (c) Dynamic Pressure, (d) Mach Number

2.17c and 2.17d, which, for an initial iteration, allow the evaluation of resistance coefficient profiles C_D useful for the integration of the equation of motion.
Drag coefficients are primarily functions of the vehicle configuration, flight Mach number, and angle of attack. At low flight speeds, Mach number effects may be

neglected, and the drag coefficient is only functions of the angle of attack. Values for these coefficients reach a maximum near a Mach number of unity. Vehicle's flight regime in the neighborhood of Mach 1, called the transonic flight region. Here strong unsteady aerodynamic forces often develop, which are noticeable in the steep rise and subsequent decrease of the coefficients [17]. After this brief introduction, for the estimation of C_D, during the ascent phase, the values of resistance coefficients as a function of Mach proposed by Castellini [10] were used for the first iteration. For 'Boostback Burn', 'Re-entry Burn' and 'Landing' the C_D were estimated with values considering the function $C_D(M)$ proposed by Castellini in [10] and the number of mach in the Figure 2.17d. During the Aerodynamic Glide phase the C_D can have values between $[1.65, 1.81]$ depending on the AoA ([170,190]°) and the vane deflection ([0,10]°) [24]. The value used for this stage in the methodology is equivalent to the average value of 1.7. Table 2.4 shows the values of C_D used for the first iteration.

All the contributions necessary for the integration of the equations of motion

Parameter	Value
C_D (ascent)	Peak $\simeq 0.7$ (AoA= 0)
C_D (boostback)	$\simeq 0.3$
C_D (re-entry burn)	$\simeq 0.3$
C_D (aerodynamic glide)	1.7
C_D (landing)	0.4

Table 2.4: Drag Coefficient (C_D) values for various flight phases: First iteration

are now available, explained in detail below. The main objective of the model is to estimate the *DeltaV* required for the ascent and descent, taking into account atmospheric and gravity losses for the first case.

2.4.3 Ascent phase: First Stage

The flight to the planned orbit is now to be simulated, considering mission requirements such as the semi-major axis of the final orbit, eccentricity, inclination, perigee argument and longitude of the ascending node. The objective of this research is not the fine-tuning of the final orbit, but rather the accuracy of the first three orbital parameters (note that 2BP is used to reach the orbit). This section describes the method used to model the trajectory of the launch vehicle to the intended orbit, with a focus on the ascent trajectory. Two main types of ascent trajectories are commonly used: Direct Ascent (DA) and Hohmann Transfer Ascent (HTA). In DA, the trajectory is designed such that the summit point coincides with the target orbit before the final stage is accelerated to the required velocity. In HTA, the vehicle

reaches a parking orbit at about 200 km altitude, then the upper stage engines are reignited to achieve the desired orbit [2]. For this study, the DL approach is chosen as the best option for the developed tool (2-DOF), while for validation in ASTOS (3-DOF) in Section 4.2, given the possibility of optimising the trajectory, the HTA solution brings reality closer. The equations characterising the motion of a launcher will now be introduced, presenting the forces involved. The drag D acts in a direction opposite to the flight path and is due to resistance to the body's motion by the surrounding fluid. Gravitational attraction is applied to any flying spacecraft by all the massive bodies in the system. The forces of gravity pull the vehicle in the direction of the centre of mass of the attracting body. In the immediate vicinity of the Earth, the attraction of the other planets and celestial bodies can be neglected [17] (this case of study). The thrust generated by the launch vehicle allows it to overcome Earth's gravitational attraction, while the centripetal force, resulting from its curved trajectory, maintains its path along an orbital arc. The reference system used for this trajectory analysis has its origin at the Earth's center, with a radial axis directed towards the launcher's center and a tangential axis aligned with the direction of travel. This radial-tangential system is crucial for tracking the launcher's position. A simplified illustration for the ascent phase can be found in Figure 2.18.

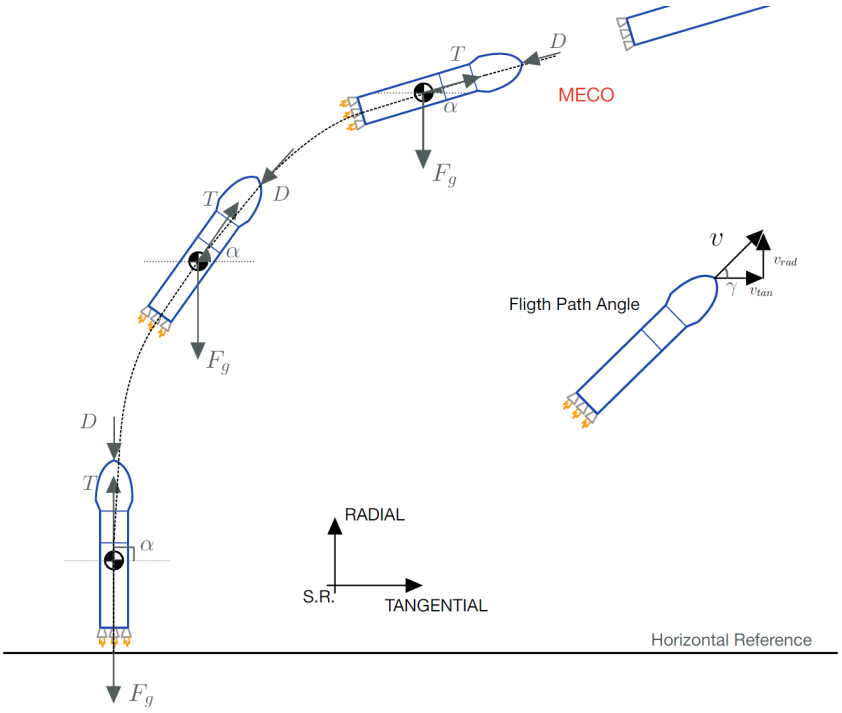

Figure 2.18: Mission Force Diagram: Ascent

The balance of forces along the tangential axis is given by the eq. 2.10 and2.11:

$$\uparrow \ddot{r_{rad}} = \frac{v_{tan}^2}{r} + \frac{\delta T sin(\alpha)}{MTOM} - \frac{\mu}{r^2} - \frac{1}{2}\frac{\rho C_D A}{MTOM}\sqrt{v_{rad}^2 + v_{tan}^2}v_{rad} \tag{2.10}$$

$$\rightarrow \ddot{r_{tan}} = \frac{v_{tan}v_{rad}}{r} + \frac{\delta T cos(\alpha)}{MTOM} - \frac{1}{2}\frac{\rho C_D A}{MTOM}\sqrt{v_{rad}^2 + v_{tan}^2}v_{tan} \tag{2.11}$$

Given the assumptions made in the 2.4.1 section, the values of throttle, pitch angle and fuel fraction are in the following ranges:

$$\begin{cases} \text{Throttle: } \delta = [0,1] \\ \text{Thrust Angle: } \alpha = \left[-\frac{\pi}{2}, \frac{\pi}{2}\right] \\ \text{Fuel Fraction: } f_f = [0,1] \end{cases}$$

. The objective function is to achieve the desired phase height while minimising the mission time within the constraint given below:

$$h_{reach} - h_{phase,final} \simeq 0 \tag{2.12}$$

Once the constraint and the objective function are set, the trajectory is divided in different mission phases (presented in Section 2.4.1). During the coast phase and other phase without burn, motion equations remain the same, but the throttle δ is set to 0. The equations of motion which must be integrated, in line with Figure 2.18 and Equation 2.11, are the following:

$$dr = v_{rad} \quad \left[\frac{m}{s}\right] \tag{2.13}$$

$$d\theta = \frac{v_{tan}}{r} \quad \left[\frac{1}{s}\right] \tag{2.14}$$

$$\begin{aligned} d(v_{rad}) = \frac{v_{tan}^2}{r} + \frac{\delta T}{MTOM}\sin(\alpha) - \frac{\mu}{r^2} \\ - \frac{1}{2}\frac{\rho C_D}{MTOM}\sqrt{v_{rad}^2 + v_{tan}^2}\, A\, v_{rad} \quad \left[\frac{m}{s^2}\right] \end{aligned} \tag{2.15}$$

$$\begin{aligned} d(v_{tan}) = \frac{v_{tan}v_{rad}}{r} + \frac{\delta T}{MTOM}\cos(\alpha) - \frac{\mu}{MTOM \cdot r^2} \\ - \frac{1}{2}\frac{\rho C_D}{MTOM}\sqrt{v_{rad}^2 + v_{tan}^2}\, A\, v_{tan} \quad \left[\frac{m}{s^2}\right] \end{aligned} \tag{2.16}$$

$$d(MTOM) = -\frac{\delta T}{f_f g_0 I_{sp}} \quad \left[\frac{kg}{s}\right] \tag{2.17}$$

$$d(\Delta V) = I_{sp} g_0 \log\left(\frac{MTOM}{MTOM + dMTOM}\right) \tag{2.18}$$

$$d(\Delta V_{drag}) = \frac{\text{Drag}}{MTOM} \quad \left[\frac{m}{s}\right] \tag{2.19}$$

$$d(\Delta V_{gravity}) = \frac{g_0}{(r/R_{earth})^2} \sin(\gamma) \quad \left[\frac{m}{s^2}\right] \tag{2.20}$$

Where:

- r is the distance between the launcher and the centre of the main body (Earth);
- θ is the angle of the launcher with respect to a surface reference point (starting point);
- v_{rad} is the radial component of the velocity;
- v_{tan} is the tangential component of the velocity;
- μ is the standard gravitational parameter of the Earth;
- $MTOM$ is the total mass of the system;
- T is the thrust provided by the engines;
- g_0 is the standard acceleration of gravity at sea level;
- C_D is the drag coefficient;
- ρ following atmospheric model described in Appendix A;
- A is the cross-sectional area;
- $\gamma = \arccos\left(\frac{v_{\text{tan}}}{\sqrt{v_{\text{tan}}^2 + v_{\text{rad}}^2}}\right)$ is the trajectory angle;
- f_f is the fraction of fuel.

ΔV_{drag}, $\Delta V_{gravuty}$ are estimated in Equations 2.19 and 2.20 , while ΔV shall be estimated in Equation 2.18. It is the Tsiolkovsky equation, which describes the motion of vehicles that generate thrust by expelling part of their mass at high speed and thus accelerate due to conservation of momentum. For the integration, the fourth-order Runge-Kutta method (RK4) was used, which is discussed in detail

in Appendix C. In addition to constraints, for integration to be successful, initial conditions, a state vector, must be defined:

$$\text{state}_{\text{initial}} = \Big[\text{Launch site height}, \quad 0, \quad 0, \quad 0, \quad \text{MTOM}_0, \quad 0, \quad 0, \quad 0, \quad 0\Big] \tag{2.21}$$

The final state vector of the phase under analysis will be that of the initial conditions for the next phase. Consider, for example, the phase MECO. The final state vector will be the initial conditions for both the orbit insertion phase and the coasting phase.

2.4.4 Ascent phase: Upper Stage, 2BP equation

After the jettison of the first stage, the upper stages are ready to be used for orbit insertion. Choose the target orbit, the mission's ΔV budget, from MECO phase to orbit, can be calculated. The ΔV budget is the sum of all flight velocity increments needed to accomplish the mission objective and it is a convenient way to describe the magnitude of the energy requirement for this phase of the space mission.
The total energy required (Equation 2.22) to put an object from MECO into orbit consists of its kinetic energy in orbit as well as the potential energy that is needed to move the object in earth's gravitational field from its position to its orbital altitude:

$$\Delta E_{tot} = \Delta E_{kin} + \Delta E_{pot} \tag{2.22}$$

Hence the vis-viva (Equation 2.23), which is useful for assessing consumption due to energy changes:

$$E_{tot} = -\frac{1}{2a} = \frac{v^2}{2} - \frac{\mu}{r} \tag{2.23}$$

The velocity increment of total ΔV depends on various orbital parameters and adjustments required for orbit insertion, including:

- **Alignment of Apogee and Perigee**: For an efficient orbital transfer, the altitude at MECO (Main Engine Cut-Off) and that of the perigee of the transfer orbit should ideally coincide. The velocity increment required for insertion can be calculated as:

$$v_f = \sqrt{\frac{\mu}{r_0}\left(2 - \frac{1}{r_0 + r_f}\right)} \tag{2.24}$$

$$\Delta V = |v_f - v_0| \tag{2.25}$$

- **Inclination** i: The inclination of an orbit, i, is the angle between the equatorial plane and the orbital plane. It is determined by the launch azimuth, which is the direction of flight at orbit insertion. A direct eastward launch results in the lowest possible inclination equal to the launch site latitude. Otherwise, inclination will increase and cannot be less than the launch latitude, as the orbital plane must intersect the Earth's center. Consequently, inclination changes require ΔV adjustments, which can be calculated as:

$$\Delta V_i = 2v_0 \sin\left(\frac{\Delta i}{2}\right) \tag{2.26}$$

At this point a total estimate of the ΔV needed to carry a payload mass from the Earth's surface to the transfer orbit is reached. To this value, however, must be added, in the reusable case, the consumption in terms of ΔV required for the Landing phase.

2.4.5 Landing phase: First Stage

To better explain how the landing takes place, it is worth explaining the typical flight profile of the Falcon 9. After launch and upon separation of the second stage, the cold-gas thrusters tip the first stage so that its tail is in line with the velocity vector. Then, the engine reignites in a boostback burns to bring the vehicle's trajectory back towards the landing site. At this point, the grids are opened to stabilise and control the stage during the re-entry phase. The engine is switched on again to slow down the first stage, before the grid fins are used to steer the lift produced by the stage. Before landing, the landing legs are deployed and the first stage is switched on one last time to ensure a precise landing [25]. SpaceX has demonstrated a soft landing both on a drone ship in the ocean (DL) and return to the launch site(RTLS). The latter scenario, as presented below, requires an additional burn to change the trajectory of the first stage, resulting in higher propellant consumption. In fact, reusing a first stage reduces the payload capability of the launch vehicle, decreasing by 20% for a downrange landing (DL) compared to 40% for a return-to-launch-site (RTLS) landing for a LEO payload [2]. Regarding the forces at work, what was introduced in the section 2.4.3 is valid, what changes is how they act on the equilibrium. The two landing cases are presented in: DL in Figure 2.19 and RTLS in Figure 2.20. Deployed fins show that you have entered a phase of aerodynamic control, with higher C_D. In particular for the case DL the

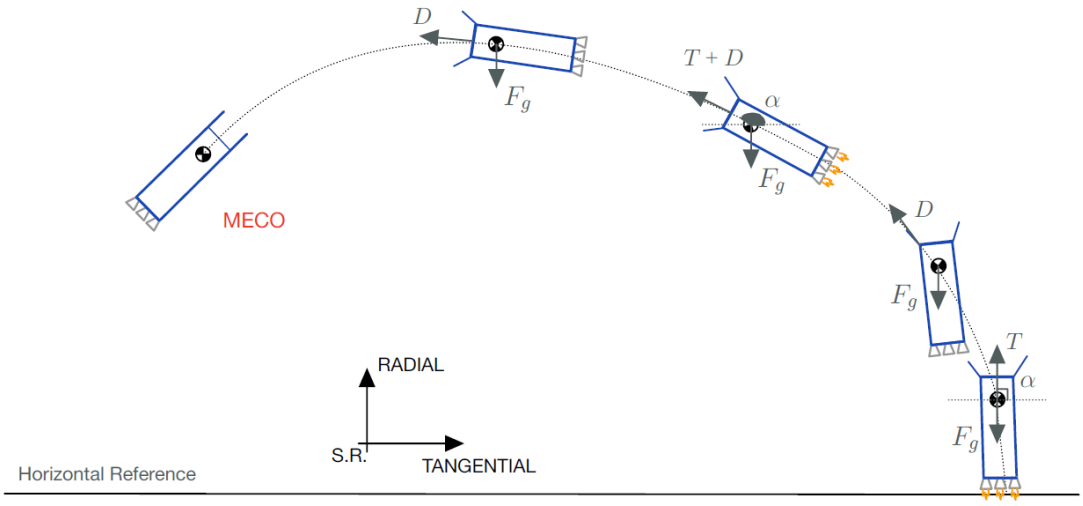

Figure 2.19: Mission Force Diagram: Descent- Downrange Landing

equilibrium of forces will be:

$$\uparrow \ddot{r_{rad}} = \frac{v_{tan}^2}{r} + \frac{\delta T sin(\alpha)}{m_{stage1}} - \frac{\mu}{r^2} + \frac{1}{2}\frac{\rho C_D A}{m_{stage1}}\sqrt{v_{rad}^2 + v_{tan}^2}v_{rad} \tag{2.27}$$

$$\rightarrow \ddot{r_{tan}} = \frac{v_{tan}v_{rad}}{r} + \frac{\delta T cos(\alpha)}{m_{stage1}} + \frac{1}{2}\frac{\rho C_D A}{m_{stage1}}\sqrt{v_{rad}^2 + v_{tan}^2}v_{tan} \tag{2.28}$$

In the case of RTLS, a difference must be made between the specific phases; in the case of 'Boostback Burn', the contribution of the drag is negative, whereas, for the rest of the phases, it is positive. Obviously, having an extra burn, this type of landing will be more expensive in terms of ΔV than the previous one.

While ΔV shall be estimated. ΔV_{drag} and $\Delta V_{gravity}$ are now forces that help the vehicle in its descent, not forces to be overcome, their contribution is then not part of the consumption. Even in this case, given the assumptions made in the 2.4.1 section, the values of throttle, pitch angle and fuel fraction are in the following ranges:

$$\begin{cases} \text{Throttle: } \delta = [0,1] \\ \text{Thrust Angle: } \alpha = \left[-\frac{\pi}{2}, \frac{\pi}{2}\right] \\ \text{Fuel Fraction: } f_f = [0,1] \end{cases}$$

The objective function is to achieve the desired phase height while minimising the mission time within the constraint given below:

$$h_{reach} \simeq 0 \tag{2.29}$$

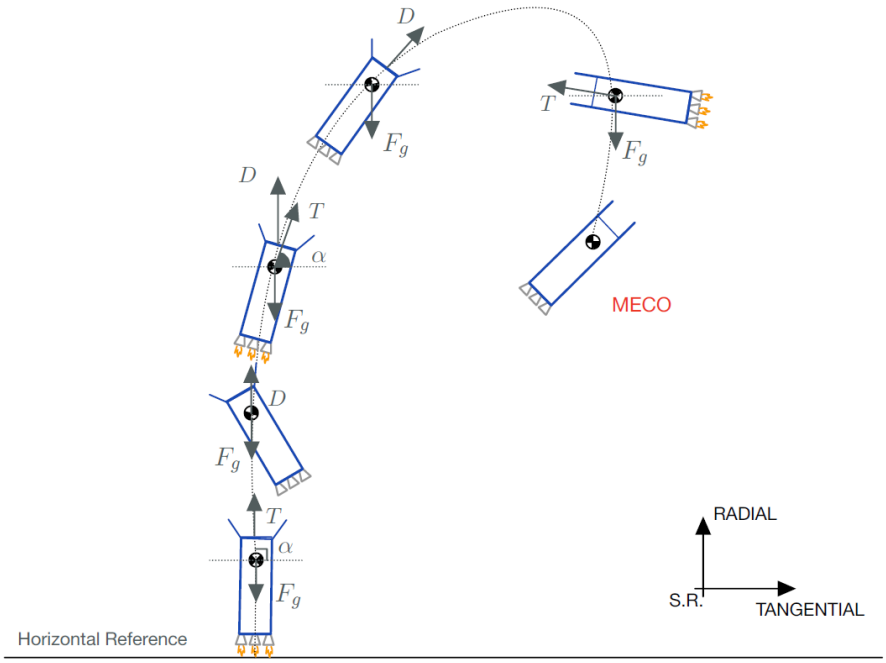

Figure 2.20: Mission Force Diagram: Descent- Return to Launch Site Landing

Once the constraint and the objective function are set, the trajectory is divided in different mission phases (presented in Section 2.4.1). The equations of motion which must be integrated (RK4 in Appendix C), in line with Figure 2.19 and in part, for reasons previously explained, in line with Figure 2.20, are the following:

$$dr = v_{rad} \quad \left[\frac{m}{s}\right] \tag{2.30}$$

$$d\theta = \frac{v_{tan}}{r} \quad \left[\frac{m}{s}\right] \tag{2.31}$$

$$d(v_{rad}) = \frac{v_{tan}^2}{r} + \frac{\delta T}{m_{stage1}}\sin(\alpha) - \frac{\mu}{m_{stage1}r^2} + \frac{1}{2}\frac{\rho C_D}{m_{stage1}}\sqrt{v_{rad}^2 + v_{tan}^2}Av_{rad} \quad \left[\frac{m}{s^2}\right] \tag{2.32}$$

$$d(v_{tan}) = \frac{v_{tan}v_{rad}}{r} + \frac{\delta T}{m_{stage1}}\cos(\alpha) - \frac{\mu}{m_{stage1}r^2} + \frac{1}{2}\frac{\rho C_D}{m_{stage1}}\sqrt{v_{rad}^2 + v_{tan}^2}Av_{tan} \quad \left[\frac{m}{s^2}\right] \tag{2.33}$$

$$d(m_{stage1}) = -\frac{\delta T}{f_f g_0 I_{sp}} \quad \left[\frac{kg}{s}\right] \tag{2.34}$$

$$d(\Delta V) = I_{sp} g_0 \log\left(\frac{m_{stage1}}{m_{stage1} + dm_{stage1}}\right) \tag{2.35}$$

$$d(\Delta V_{drag}) = \frac{Drag}{m_{stage1} M} \quad \left[\frac{m}{s}\right] \tag{2.36}$$

$$d(\Delta V_{gravity}) = \frac{g_0}{(r/R_{earth})^2} \sin(\gamma) \quad \left[\frac{m}{s^2}\right] \tag{2.37}$$

Where m_{stage1} means the mass of the first stage net of the propellant consumed for ascent.
Knowing the total ΔV necessary to accomplish the mission, one now has the basis to move into the Optimal staging module.

2.5 Optimal Staging Module [26]

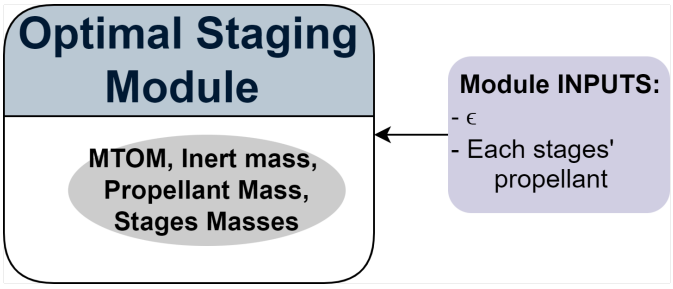

Figure 2.21: Optimal Staging Module

When there is a large amount of propellant, as is typically the case in missions involving chemical propulsion, very large tanks are required. These tanks have a significant weight, and part of the propulsive effort must therefore accelerate not only the payload but also the tank itself. Since this is an unnecessary mass, it is considered to divide the mission into stages. According to the Tsiolkovsky equation, it can be seen that the performance of the rocket (ΔV) is influenced by two factors, the specific impulse (I_{sp}) of the engines and the ratio of the initial mass before launch (m_0) to the final mass(m_f). Since the engine performance is limited by the type of propellant and the engine cycle the parameter to be maximised is then the ratio $\frac{m_0}{m_f}$.

$$\frac{m_0}{m_f} = \frac{m_e + m_p + m_{pay}}{m_e + m_{pay}} \tag{2.38}$$

where m_e is empty or structure mass, m_p propellant mass and m_{pay} payload mass. The objective is to optimize the payload fraction λ:

$$\lambda = \frac{m_{pay}}{m_0} \tag{2.39}$$

Objective is optimize λ assigned ΔV. Now, the structural ratio, are introduced:

$$\epsilon = \frac{m_e}{m_e + m_p} \tag{2.40}$$

This ratio is an index of technological level, a measure of the efficiency of a rocket design: the smaller it is, the better it is. In m_s, all structural masses are considered, which includes everything that is neither payload nor propellant.
Before delving into the staging optimization process, it is beneficial to clarify the inputs for the methodology illustrated in Figure 2.21. For the first iteration, a value that will be updated throughout the cycles is the structural ratio for liquid propellants (the only type considered in this work), which can range from 0.08 to 0.12[27]. Another important input is the type of propellant for each stage, which can be selected from the database (Section 2.2.3) or chosen by the user. The two

most commonly used types of staging are serial staging and parallel staging. Figure 2.22 shows a representation of serial staging, i.e., stacking several flares on top of each other. When the tanks of the lower stage are empty, it is deploy and the next stage is ignited. The advantages of serial staging are that the engines can be adapted to the environment in which they operate, optimising the performance in which they are used [11].

After this brief presentation, the algorithm is based on the search for the minimum

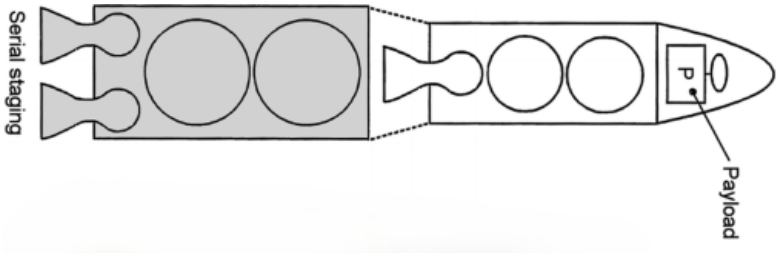

Figure 2.22: Rocket's Serial Staging scheme [28]

mass for a n-stage vehicle carrying a given payload mass (m_{pay}) to a specified velocity (ΔV). Let now introduce the step mass ($m_{0,stage,i}$) of the i-th stage. The step mass can be defined as the propellant mass ($m_{p,stage,i}$) of the stage plus the empty mass ($m_{e,stage,i}$) of the same stage, neglecting the other stages. This allows to estimate the empty mass, the propellant mass and the total mass ($MTOM$) as described here:

$$m_{0,stage,i} = m_{e,stage,i} m_{p,stage,i} \tag{2.41}$$

$$m_{e,stage,i} = \epsilon_{stage,i}(m_{e,stage,i} m_{p,stage,i}) = \epsilon_{stage,i}(m_{0,stage,i}) \tag{2.42}$$

$$MTOM = m_0 = \sum m_{0,stage,i} + m_{pay} \tag{2.43}$$

Hereafter, the algorithm for a 2-stage launcher is reported. Please, remember that this algorithm is valid for a vehicle with an arbitrary number of stages. For a 2-stage launcher, the total mass can be expressed also as $m_0 = m_{0,stage,1} + m_{0,stage,2} + m_{pay}$. This can also be written as:

$$\frac{1}{\lambda} = \frac{m_{0,stage,1} + m_{0,stage,2} + m_{pay}}{m_{0,stage,2} + m_{pay}} \frac{m_{0,stage,2} + m_{pay}}{m_{pay}} \tag{2.44}$$

The mass ratios $n_{stage,i}$ can be expressed below and step masses $m_{0,stage,i}$ are:

$$n_{stage,1} = \frac{m_{0,stage,1} + m_{0,stage,2} + m_{pay}}{\epsilon_{stage,i} m_{0,stage,1} + m_{0,stage,2} + m_{pay}} \quad n_{stage,2} = \frac{m_{0,stage,2} + m_{pay}}{\epsilon_{stage,i} m_{0,stage,2} + m_{pay}} \tag{2.45}$$

$$m_{0,stage,1} = \frac{n_{stage,1} - 1}{1 - n_{stage,1}\epsilon_{stage,1}}(m_{0,stage,2} + m_{pay}) \quad m_{0,stage,1} = \frac{n_{stage,2} - 1}{1 - n_{stage,2}\epsilon_{stage,2}} m_{pay} \tag{2.46}$$

A substitution of the equations 2.46 into 2.44 yields the following function:

$$\frac{m_0}{m_{pay}} = \frac{(1-\epsilon_{stage,1})n_{stage,1}}{1-n_{stage,1}\epsilon_{stage,1}} \frac{(1-\epsilon_{stage,2})n_{stage,2}}{1-n_{stage,2}\epsilon_{stage,2}} \tag{2.47}$$

Applying the natural logarithm to both sides:

$$\ln\left(\frac{m_0}{m_{pay}}\right) = [\ln(1-\epsilon_{stage,1}) + \ln(n_{stage,1}) - \ln(1-\epsilon_{stage,1}n_{stage,1})] \tag{2.48}$$

$$+ [\ln(1-\epsilon_{stage,2}) + \ln(n_{stage,2}) - \ln(1-\epsilon_{stage,2}n_{stage,2})] \tag{2.49}$$

Derive the function, since the objective way is to minimise m_0.

$$\frac{d}{dm_0}\left(\ln\left(\frac{m_0}{m_{pay}}\right)\right) = \frac{1}{m_0} > 0 \tag{2.50}$$

The veolity of each stages can be expressed as:

$$\Delta V = v_{bostage\ 1} + v_{bostage\ 2} = c_{stage\ 1}\ln(n_{stage\ 1}) + c_{stage\ 2}\ln(n_{stage\ 2}) \tag{2.51}$$

$$\Rightarrow \Delta V - c_{stage\ 1}\ln(n_{stage\ 1}) - c_{stage\ 2}\ln(n_{stage\ 2}) = 0 \tag{2.52}$$

Introducing the Lagrange multiplier η, it's now possible to find the payload ratios $\lambda_{stage\ 1}$ and $\lambda_{stage\ 2}$ which guarantee h, to be stationary and maximise $\ln\frac{m_0}{m_{pay}}$ and hence minimise m_0 for the desired ΔV. By respecting the constraints in eq. 2.54, the stationarity of h is assured.

$$\begin{aligned} h = &[\ln(1-\epsilon_{stage\ 1}) + \ln(n_{stage\ 1}) - \ln(1-\epsilon_{stage\ 1}n_{stage\ 1})] \\ &+ [\ln(1-\epsilon_{stage\ 2}) + \ln(n_{stage\ 2}) - \ln(1-\epsilon_{stage\ 2}n_{stage\ 2})] \\ &+\eta\left(\Delta V - c_{stage\ 1}\ln(n_{stage\ 1}) - c_{stage\ 2}\ln(n_{stage\ 2})\right) \end{aligned} \tag{2.53}$$

$$\begin{cases} \frac{\delta h}{\delta n_{stage\ 1}} = \frac{1}{n_{stage\ 1}} + \frac{\epsilon_{stage\ 1}}{1-\epsilon_{stage\ 1}n_{stage\ 1}} - \eta\frac{c_{stage\ 1}}{n_{stage\ 1}} = 0 \\ \frac{\delta h}{\delta n_{stage\ 2}} = \frac{1}{n_{stage\ 2}} + \frac{\epsilon_{stage\ 2}}{1-\epsilon_{stage\ 2}n_{stage\ 2}} - \eta\frac{c_{stage\ 2}}{n_{stage\ 2}} = 0 \\ \frac{\delta h}{\delta \eta} = \Delta V - c_{stage\ 1}\ln(n_{stage\ 1}) - c_{stage\ 2}\ln(n_{stage\ 2}) = 0 \end{cases} \tag{2.54}$$

The equations from eq. 2.55, 2.56 eq. 2.57 held to the estimation of the step masses in eq. 2.58:

$$\begin{aligned} n_{stage\ 1} &= c_{stage\ 1}\eta - 1c_{stage\ 1}\epsilon_{stage\ 1}\eta \\ n_{stage\ 2} &= c_{stage\ 2}\eta - 1c_{stage\ 2}\epsilon_{stage\ 2}\eta \\ v_{bo} &= c_{stage\ 1}\ln(n_{stage\ 1}) + c_{stage\ 2}\ln(n_{stage\ 2}) \end{aligned} \tag{2.55}$$

$$h = \sum \left[\ln(1-\epsilon_{stage\ i}) + \ln(n_{stage\ i}) - \ln(1-\epsilon_{stage\ i})\right] \\ -\eta\left(\Delta V - \sum_{i=1}^{N} c_{stage\ i} \ln(n_{stage\ i})\right) \tag{2.56}$$

$$\begin{cases} \sum c_{stage\ i} \ln c_{stage\ i}\eta - 1 c_{stage\ i}\epsilon_{stage\ i}\eta = \Delta V \\ n_{stage\ i} = \frac{c_{stage\ i}\eta - 1}{c_{stage\ i}\epsilon_{stage\ i}\eta} \quad i = 1, 2, 3, \ldots, N \end{cases} \tag{2.57}$$

$$\begin{cases} m_{0\ stage\ N} = (n_{stage\ N} - 1)\left(1 - n_{stage\ N}\epsilon_{stage\ N}\right) m_{pay} \\ m_{0\ stage\ N-1} = (n_{stage\ N-1} - 1)\left(1 - n_{stage\ N-1}\epsilon_{stage\ N-1}\right)\left(m_{pay} + m_{0\ stage\ N}\right) \\ \ldots \\ m_{0\ stage\ 1} = (n_{stage\ 1} - 1)\left(1 - n_{stage\ 1}\epsilon_{stage\ 1}\right) \\ \left(m_{pay} + m_{0\ stage\ N} + m_{0\ stage\ N-1} + \ldots + m_{0\ stage\ 2}\right) \end{cases} \tag{2.58}$$

For the solution, the numerical Newton-Raphson method is applied. Once the step masses have been found, the empty mass and the propellant mass of each stage can be estimated as Equation 2.61.

$$\begin{cases} m_{e,stage\ i} = \epsilon_{stage\ i} m_{0,stage\ i} \\ m_{p,stage\ i} = m_{0,stage\ i} - m_{e,stage\ i} \end{cases} \tag{2.59}$$

To minimise the function h, thus guaranteeing the minimum initial mass, evaluate its second derivative:

$$\frac{d^2 h}{dn_{stage\ i} dn_{stage\ j}} = 0 \quad \text{for } i, j = 1, \ldots, N \quad (i \neq j). \tag{2.60}$$

2.6 Propulsion System Module

The thrust estimation for each stage, during the first iteration, is directly derived from the statistical model. This estimate will then be refined in subsequent iterations. Starting from the second iteration, the thrust will be adjusted using the regression formula shown below [27]:

$$T_{\text{stage,1}} = \left(24 + 0.0128 m_{0,\text{stage 1}} + 4.35 \cdot 10^{-8} m_{0\text{stage 1}}^2\right) \cdot 10^3 \tag{2.61}$$

$$T_{\text{stage } i} = \left(\frac{T}{W}\right)_{stage,i} m_{0,stage,i} g_0 \tag{2.62}$$

If the statistical model fails to provide a realistic thrust value, the approach outlined in Appendix B can be used, incorporating additional necessary input parameters. Once the type of propellant has been defined, choosing it from those indicated in section 2.2.3 (or choosing by user) and, having established the total mass with the optimal staging, in the case of a bi-propellant system, the oxidizer and fuel masses can be estimated using:

$$m_{F,\,\text{stage}\,i} = \frac{m_{P,\,\text{stage}\,i}}{1 + MR} \tag{2.63}$$

$$m_{OX,\,\text{stage}\,i} = m_{P,\,\text{stage}\,i} - m_{F,\,\text{stage}\,i} \tag{2.64}$$

With $m_{F,stage,i}$ is fuel mass and $m_{OX,stage,i}$ oxidizer one. As mentioned earlier, the only type of technology considered in this work is liquid technology. In relation to this, a distinction can be made between: *Turbopump cycle* and *Pressure-Fed cycle*. Since it is possible to select the motorcycle as an input, it is worth introducing the 3 main types (Figure 2.23):

- In the cycle **Gas generator** a part of the fuel, usually rich in fuel, representing $1 - 4\%$ of the total propellant mass flow is fed to the gas generator and burnt to produce the hot gas required to drive the turbine [11]. The remainder of the propellant is injected into the combustor, the oxidizer directly and the fuel after passing through cooling channels in the nozzle to minimise the internal wall temperature (regenerative cooling). This cycle is called an open cycle because the exhaust gases leaving the turbine are not injected into the combustion chamber. They can be discharged through one or two separate small nozzles with a low area ratio, or sucked into the main flow through openings in the divergent section of the nozzle further downstream of the nozzle throat to provide film cooling of the nozzle walls. Both methods provide a small amount of additional thrust. Due to the relatively low system

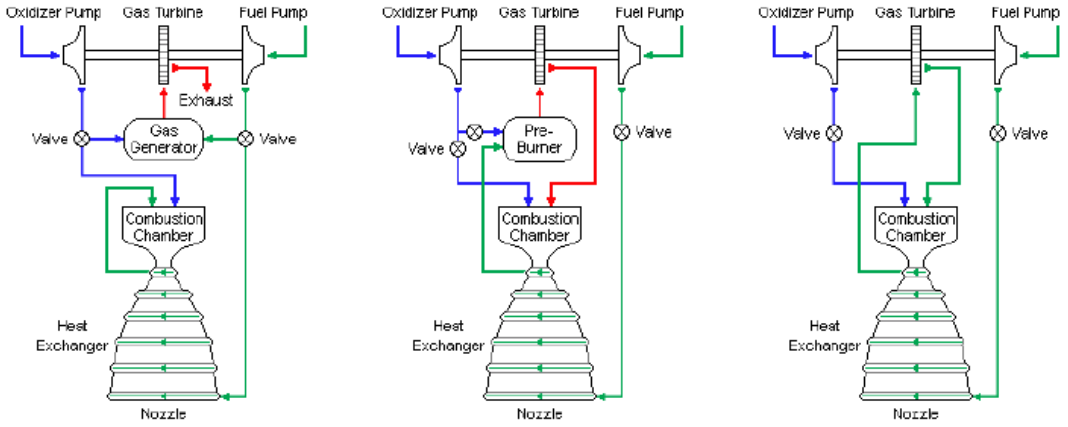

Figure 2.23: Engine cycles: Gas generator, Staged combustion and Expander [29]

pressures, the gas generator cycle is a relatively simple cycle that provides motion [17]. As part of the propellants is not available for combustion I_{sp} is lower for this type of cycle than closer one. This type of engine cycle is very common in Europe, the *Vulcains* of the Ariane, for example, make use of it.

- **Staged Combustion cycle**, is a closed cycle. The entire fuel mass flow is fed through the cooling channels in the nozzle before being burned with part of the oxidizer in a high-pressure pre-burner powering the turbopumps. The turbine exhaust gases and the remainder of the oxidizer are then injected into the combustion chamber [17].
- In the **Expander Cycle**, he entire fuel mass flow is also generally used as a coolant for the engine nozzle. Picking up energy while cooling down the nozzle walls, the fuel changes to the gaseous phase and expands in the turbine before being injected into the combustion chamber with the oxidizer. Being a closed engine cycle, the expander cycle has the advantages of high I_{sp}, simple design and low engine mass [17].

A comparison of motor cycles highlights their applications and aids the selection process for this work. In particular, the expander cycle is limited in its delivery of high thrust, making it suitable only for smaller upper stages. Since the upper stage of a vehicle TSTO with a reusable first stage is typically larger than that of expendable vehicles, the expander cycle cannot provide adequate thrust and is excluded from the optimisation process of this study [11]. The choice between the gas generator and the staged combustion cycle involves an evaluation of performance, reliability, reusability, cost and existing skills. Although the staged combustion cycle offers superior performance, its complexity, higher costs and lower reliability

due to the greater number of moving parts make it less favourable. Consequently, gas engines were chosen for the study case analysed in chapter 3.

Another classification, is on the type of propellant storability, with a choice between: *cryogenic propellant*, *cryo storable propellant* and *storable propellant*. The storability of the propellant on board is important to estimate the mass of e.g. the tanks that will house fuel and oxidiser, which will have different characteristics depending on the type of technology.

Finally, before entering the propulsion system module, in Figure 2.24, it is important to define inputs, concerning mainly thrusters, in particular: number of engines, Expansion ratio ($\epsilon = \frac{A_e}{A_t}$), Throat or Exit Area and Propellant tanks (p_{tank}).

For the liquid rocket engine LRE, the lengths:

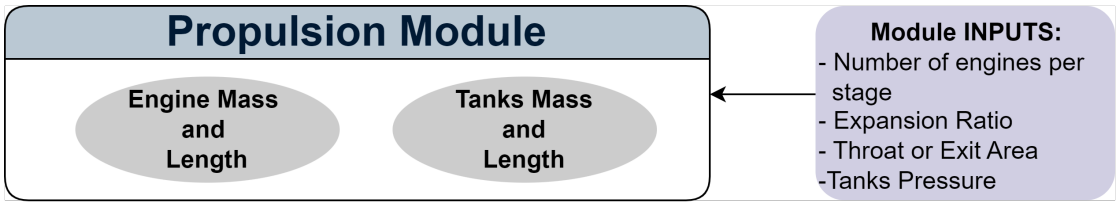

Figure 2.24: Propulsion system Module

$$L_{LRE} = L_{engine} + L_{tanks} \tag{2.65}$$

2.6.1 Propulsion module: Engine masses and lengths

In function of the available inputs, the lengths and the masses may be evaluated in different ways. In case the geometrical characteristics of the engine are unknown, it's possible to estimate the length of the engine by using following equations:

$$L_{engine} = \begin{cases} 0.88 \cdot T^{0.255} \cdot n_{engine}^{-0.4} \cdot \left(\frac{A_e}{A_t}\right)^{0.055} & \text{for Turbopump cycle} \\ 1.4921 \cdot \ln(T) - 13.179 & \text{for Pressure-fed cycle} \end{cases} \tag{2.66}$$

whit thrust T in Newton $[N]$. Following method proposed in [10], the engine length can be esitmated:

$$L_{engine} = L_{feed} + L_{Conv} + L_{Div} \quad [m] \tag{2.67}$$

Where:

- $L_{Conv} = \frac{D_{case} - D_{throat}}{2\tan(\zeta)}$ $[m]$, whit ζ is the convergent half angle (set as 45°, which is a value from literature, usually $30° < \phi < 60°$).

- $L_{\text{Div}} = K\frac{D_{\text{exit}} - D_{\text{throat}}}{2\tan(\xi)}$ [m], where K is a constant ($K = 0.8$ for a bell nozzle (default), $K = 1$ for a cone nozzle), and ξ is the divergent half-angle (set to 15°, which is a commonly used value in literature, usually $12° < \xi < 18°$).

The combustion chamber length is estimated following the procedure described in [10]:

$$L^*_{cc} = \begin{cases} 0.89 & \text{for cryogenic propellant} \\ 1.15 & \text{for cryo-storable propellant} \\ 0.74 & \text{for storable propellant} \end{cases} \tag{2.68}$$

$$A_{cc} = \frac{\pi}{4} D^2_{cc} \quad [m^2] \tag{2.69}$$

$$V_{cc} = A_{throat} \cdot L^*_{cc} \quad [m^3] \tag{2.70}$$

$$L_{feed} = K_{ft} \cdot (L_{cc} + L_{Conv}) \quad [m] \tag{2.71}$$

Where:

- L^*_{cc}: combustion chamber characteristic length;
- A_{cc}: combustion chamber area and D_{cc} diameter
- V_{cc}: combustion chamber volume;
- A_{throat}: throat area;
- L_{feed}: length of the feed system;
- K_{ft}: assumes different values based on engine cycle (0.6 for pressure-fed, 1 for turbopump).

To determine the mass of each engine now, as anticipated, a breakdown is made by type of technology, and then statistical approaches used in [10] and [27].

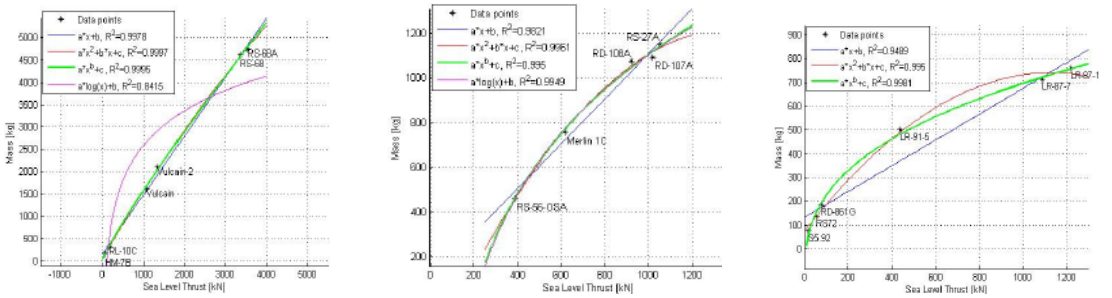

(a) Gas Generator: Cryogenic **(b)** Gas Generator: Cryo-storable **(c)** Gas Generator: Storable

Figure 2.25: Mass engine estimation trends: Gas Generator [10]

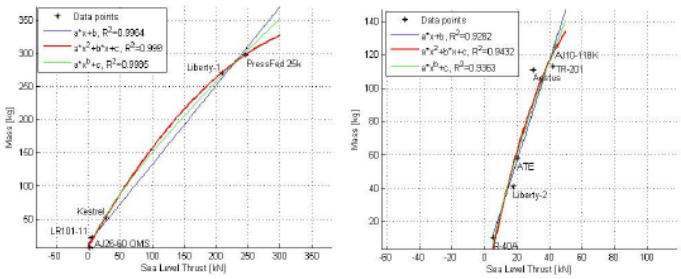

(a) Pressure-Fed: Cryo-storable **(b)** Pressure-Fed: Storable

Figure 2.26: Mass engine estimation trends: Pressure Fed [10]

The mass estimation equations are given below: $m_{\text{engine}}\,(\text{Turbo-pump}) =$

$$\begin{cases} 7.54354 \cdot 10^{-3}\, T^{0.885635} + 20.2881 & \text{cryogenic} \quad (T \leq 200 \cdot 10^3) \\ 1.9101 \cdot 10^{-3}\, T & \text{cryogenic} \quad (T > 200 \cdot 10^3) \\ 3.75407 \cdot 10^3\, T^{0.0705627} - 8.8479 \cdot 10^3 & \text{cryo-storable} \quad (T \geq 450 \cdot 10^3) \\ -0.0003 \left(\frac{T}{1000}\right)^2 + 1.3807 \left(\frac{T}{1000}\right) & \text{cryo-storable} \quad (T < 450 \cdot 10^3) \\ 6.37913\, T^{0.353665} - 148.832 & \text{storable} \quad (T \geq 200 \cdot 10^3) \\ -0.0021 \left(\frac{T}{1000}\right)^2 + 2.0264 \left(\frac{T}{1000}\right) & \text{storable} \quad (T < 200 \cdot 10^3) \end{cases} \tag{2.72}$$

For the lower thrust values, which are not between the trends in Figure 2.25, statistical trends analysed in [27] were used, as shown below.

$m_{\text{engine}}\,(\text{Pressure-Fed}) =$

$$\begin{cases} -2.13325 \cdot 10^{-9}\, T^2 + 1.7087 \cdot 10^{-3}\, T + 6.38629 & \text{cryo-storable} \ (T \geq 300 \cdot 10^3) \\ -0.0005 \left(\frac{T}{1000}\right)^2 + 1.244 \left(\frac{T}{1000}\right) + 18.336 & \text{cryo-storable} \quad (T < 300 \cdot 10^3) \\ -3.36532 \cdot 10^{-8}\, T^2 + 4.74402 \cdot 10^{-3}\, T - 19.3920 & \text{storable} \quad (T < 55 \cdot 10^3) \\ 25.56 \log\left(\frac{T}{1000}\right) + 29.824 & \text{storable} \quad (T \geq 55 \cdot 10^3) \end{cases} \tag{2.73}$$

The total mass of the engine can be evaluated as in:

$$m_{\text{engine}}^{\text{TOT}} = n_{\text{engine}} \cdot m_{\text{engine}} \quad [\text{kg}] \tag{2.74}$$

(2.75)

Finally, Thrust Vectoring Control TVC were used to estimate the mass of the system (from [27]):

$$m_{\text{TVC}} = \begin{cases} m_{\text{engine}} \cdot 0.26 & iter = 1 \\ 0.1078 \cdot T \cdot 0.001 + 43.702 & iter > 1 \end{cases} \tag{2.76}$$

2.6.2 Propulsion module: Engine masses and lengths

To achieve a pressurized system, a high-pressure pressurizing gas is used, as already mentioned in the 'Database' section 2.2.4. The mass of gas and tank where it is stored can be estimated with:

$$m_{\text{press}} = 1.1 p_{\text{tank}} \cdot 10^5 \left(V_F + V_{ox}\right) \frac{R}{T_{\text{press}}} \cdot \frac{\gamma}{1 - \frac{p_{\text{tank}}}{p_{\text{press}}}} \quad [\text{kg}] \tag{2.77}$$

$$m_{\text{press tank}} = 4\pi \left(D_{\text{press}}\right)^2 \tau_{\text{press}} \rho_{\text{tank}} \quad [\text{kg}] \tag{2.78}$$

$$m_{\text{press sys}} = m_{\text{press}} + m_{\text{press tank}} \quad [\text{kg}] \tag{2.79}$$

The pressurizing system mass is estimated considering equations in [27]

$$m_{press} = 1.1 \frac{p_{tank} \cdot 10^5 \left(V_F + V_{OX}\right)}{\frac{R}{T_{press}}} \cdot \frac{\gamma}{1 - \frac{p_{tank}}{p_{press}}} \quad [\text{kg}] \tag{2.80}$$

$$m_{press,tank} = 4\pi \left(D_{press}\right)^2 \tau_{press} \rho_{tank} \quad [\text{kg}] \tag{2.81}$$

$$m_{press,sys} = m_{press} + m_{press,tank} \quad [\text{kg}] \tag{2.82}$$

Where:

- T_{press} is pressure temperature.
- $R = 2077\,[\frac{J}{KgK}]$ is the specific gas constant and $\gamma = 1.667$ the specific heat ratio.
- $\tau_{press} = SF \frac{p_{tank} \frac{Dpress}{2}}{2\sigma}$ is the thickness of the pressurizing tank in meters.
- ρ_{tank} is the density of the tank $[\frac{kg}{m^3}]$.
- SF is the safety factor set to 2.
- σ is the tank material strength yield.
- p_{tank} is the tank pressure in $[bar]$ and p_{press} is the initial pressure in the pressurization gas tank.
- D_{press} is the diameter of the tank, dimensioned as a sphere $[m]$.

For what concern the tank lengths and masses, they can be evaluated following equations, where, ullage Volume (V_{ullage}) is set on 5% of tank volume.

$$L_{\text{tank}} = \begin{cases} \left(\frac{m_{OX}}{\rho_{OX}} + \frac{m_F}{\rho_F} + \frac{\pi}{6}\right) \frac{(1+V_{ullage})4}{\pi D_{rocket}^2} & \text{if bi-propellant} \\ \frac{m_{mono}}{\rho_{mono}} \frac{(1+V_{ullage})4}{\pi D_{rocket}^2} & \text{if mono-propellant} \end{cases} [m] \tag{2.83}$$

The mass of the tanks that will contain the propellant is now estimated. For the bi-propellant type:

$$m_{tank}(bi-prop) = m_{tank,OX} + m_{tank,F} \tag{2.84}$$

$$\begin{cases} m_{tank,OX} = 1.2 \frac{\frac{\rho_{tank,OX}\pi}{6}(D_{rocket}^3 - (D_{rocket}-2\tau_{tank})^3)}{\pi(D_{rocket}-2\tau_{tank})^2} \\ +1.5\left(\left(\frac{D_{rocket}}{2}\right)^2 - \left(\frac{D_{rocket}}{2} - \tau_{tank}\right)^2\right) L_{tank,OX,cyl} \\ m_{tank,F} = 1.2 \frac{\frac{\rho_{tank,F}\pi}{6}(D_{rocket}^3 - (D_{rocket}-2\tau_{tank})^3)}{\pi(D_{rocket}-2\tau_{tank})^2} \\ +1.5\left(\left(\frac{D_{rocket}}{2}\right)^2 - \left(\frac{D_{rocket}}{2} - \tau_{tank}\right)^2\right) L_{tank,F,cyl} \end{cases} \tag{2.85}$$

For mono-propellant type:

$$m_{tank} = 1.2 \frac{\frac{\rho_{tank}\pi}{6}(D_{rocket}^3 - (D_{rocket} - 2\tau_{tank})^3)}{\pi(D_{rocket} - 2\tau_{tank})^2} \tag{2.86}$$

$$+1.5\left(\left(\frac{D_{rocket}}{2}\right)^2 - \left(\frac{D_{rocket}}{2} - \tau_{tank}\right)^2\right) L_{tank,cyl} \tag{2.87}$$

With $L_{tank,cyl}$ is the length of the cylindrical part of the tank in meters, and, in case $L_{tank,cyl} < 0$, the tank is considered spherical. Therefore, its mass is estimated following equation:

$$m_{tank} = 1.2 \frac{\rho_{tank}\pi}{6}(D_{rocket}^3 - (D_{rocket} - 2\tau_{tank})^3)\,[kg] \tag{2.88}$$

In this case:

- $D_{tank} = \left(6 + \frac{(1+V_{ullage})V_{tank}}{\pi}\right)^{\frac{1}{3}}$ is the tank diameter in meters.
- $\tau_{tank} = 0.5SF\frac{2p_{tank}D_{rocket}}{2\sigma}$ is the tank thickness meters.

In bi-propellant liquid case, if the tanks are not spherical, there is the possibility to estimate the inter-tank length and mass, according to:

$$L_{\text{intertank}} = 0.3 \cdot r_{\text{rocket}}[m] \tag{2.89}$$

$$m_{\text{intertank}} = \begin{cases} 5.4015 \cdot 2\pi r_{\text{rocket}} L_{\text{intertank}} \left(3.2808(2r_{\text{rocket}})\right)^{0.5169} & \text{for lower stage} \\ 3.8664 \cdot 2\pi r_{\text{rocket}} L_{\text{intertank}} \left(3.2808(2r_{\text{rocket}})\right)^{0.6025} & \text{for upper stages} \end{cases} \tag{2.90}$$

Where:

- $L_{\text{intertank}}$ is the intertank length [m],
- $m_{\text{intertank}}$ is the intertank mass [kg],
- r_{rocket} is the rocket radius [m].

The thermal protection system is a function of the storability of the propellant. In the case of a storable propellant, a zero thermal insulation mass is assumed, otherwise it's evaluated as in:

$$m_{\text{TPS,OX/F}} = k_{ins} \cdot S_{tank,OX/F}[kg] \tag{2.91}$$

Where:

- $k_{ins} = \begin{cases} 0.9765 & \text{for Oxidizer} \\ 1.2695 & \text{for cryogenic Fuel} \end{cases}$ is the insulation parameter [kg/m^2],

This model is validated by Castellini [10] and in [27] with a comparison with ARIANE 5 data. Ended the Propulsion module permit to enter in the next one to the estimation of auxiliary system and lengths.

2.7 Mass & Dimension Estimation Module

The next step is proceed from the propulsion module to the mass and length estimation module, considering all the subsystems that are part of a launcher and that have not been dealt with so far. The module is very simply and shown in Figure 2.27. All the subsystems considered in estimating the total mass of the

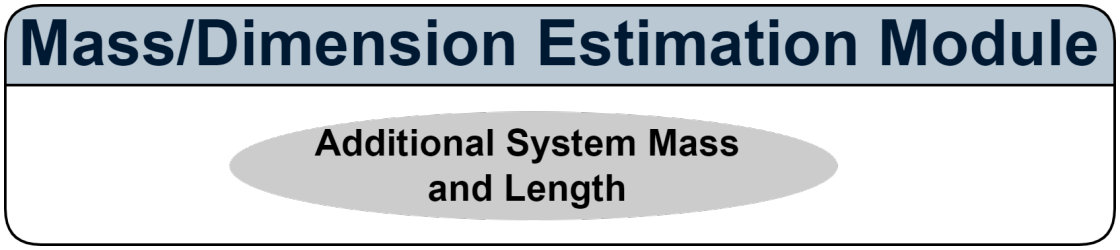

Figure 2.27: Mass/Dimension Estimation Module

rocket are listed below.

2.7.1 Mass and Dimension: Interstages

The interstage structure connects the first stage with the upper stage and the upper stage with the payload bay (or other stage).The interstage lengths and masses can be calculated by using

$$L_{\text{interstage stage } i} = \begin{cases} 0.2D_{\text{rocket stage } i} & \text{if } D_{\text{rocket stage } i} = D_{\text{rocket stage } i+1} \\ \frac{0.5|D_{\text{rocket stage } i} - D_{\text{rocket stage } i+1}|}{\tan(16.4)} & \text{if } D_{\text{rocket stage } i} > D_{\text{rocket stage } i+1} \\ \frac{0.5|D_{\text{rocket stage } i} - D_{\text{rocket stage } i+1}|}{\tan(12.4)} & \text{if } D_{\text{rocket stage } i} < D_{\text{rocket stage } i+1} \end{cases} \tag{2.92}$$

$$m_{\text{interstage stage } i} = \begin{cases} k_{sm} 7.7165 S_{\text{interstage stage } i} (3.2808 \cdot 2r_{\text{rocket}})^{0.4856} & \text{for lower stages} \\ k_{sm} 5.5234 S_{\text{interstage stage } i} (3.2808 \cdot 2r_{\text{rocket}})^{0.5210} & \text{for upper stages} \\ k_{sm} 25.763 S_{\text{pad}} (3.2808 \cdot 2r_{\text{rocket}}) r_{\text{rocket}})^{0.5210} & \text{for pad interfaces} \end{cases} \tag{2.93}$$

In particular:

- k_{sm} is a corrective factor form the structural material, (set as 0.7 for composite structure);
- $S_{\text{interstage}_i} = 2\pi \left(\frac{R_{rocket,i} + R_{rocket,i+1}}{2} \right) L_{interstage,i}$ is the interstage surface.
- S_{pad} is a pad interface, wich is the interface between the launch pad and the launcher itself (it is consider only for the first stage).

2.7.2 Fairing

The fairing protects the payload from the aerodynamic and thermal loads during the ascent, as well as from the environmental conditions on the launch pad. It is designed to maximise the aerodynamic performance of the launch vehicle while safely containing the payload. The fairing is jettisoned shortly after stage separation to maximise the launch vehicle's vehicle performance and maximise payload capacity. The fairing is sized as [27]:

$$L_{\text{fairing}} = 0.5 \cdot (\frac{L}{R})_{\text{ogive}} D_{pay} + L_{pay} + 0.15 D_{pay} \quad [\text{m}] \tag{2.94}$$

Where:

- $D_{pay} = \frac{r_{fairing}}{1.12}$ is the payload allocation diameter;
- $\left(\frac{L}{D}\right)_{ogive}$ is the nose ratio with value between [2.23,2.37].
- $r_{fairing}$ is the fairing radius.
- L_{pay} is the payload allocation length.

In order to evaluate the mass of the fairing, it is necessary to estimate the radius ogive nose:

$$m_{\text{fairing}} = 4.95 S_{\text{nose}}^{1.15} \quad [\text{kg}] \tag{2.95}$$

- $S_{nose} = 2\pi a_{ogive} \left(\left(\left(\frac{r_{rocket}}{2} - a_{ogive} \right) asin \left(\frac{L_{fairing}}{a_{ogive}} \right) + L_{fairing} \right) \right)$ is the fairing surface.
- $a_{ogive} = \frac{\left(\left(\frac{r_{rocket}}{2} \right)^2 + L_{fairing}^2 \right)}{r_rocket}$ is extension of ogive nose.

2.7.3 Avionics, EPS and Thrust Frame

The other components of the structural mass are the avionics mass, the electrical power system (EPS) and the thrust frame mass as in [10]. The first two systems follow the estimates in [27].

$$m_{\text{avionics}} = K_{rl}(1 - TRF_{\text{avionics}})(246.76 + 1.3183 S_{\text{total}}) \quad [\text{kg}] \tag{2.96}$$

Where:

- $K_{rl} = 1$ is the redundancy factor (0.7 if no redundancy, 1 for critical components and 1.3 for full redundancy).

- $TRF_{\text{avionics}} = 0.75$ is the Technology Reduction Factor.
- S_{total} is the total Launcher's surface (Approximate to cylindrical surface).

$$m_{\text{EPS}} = K_{rl} 0.405 m_{\text{avionics}} (1 - TRF_{\text{EPS}}) \quad [\text{kg}] \tag{2.97}$$

- $TRF_{\text{EPS}} = 0.18$ is the EPS Technology Reduction Factor.

Finally the Thrust Frame:

$$m_{\text{Thrust Frame}} = 2.55T \cdot 10^{-4} \quad [\text{kg}] \tag{2.98}$$

2.7.4 Landing system

VTVL Stages shall include hardware that safe and reliable return to Earth, including a powered landing. While the engines are responsible for deceleration and control during the propulsion phases, additional control are required to control the vehicle's trajectory during the non-propulsive descent phases within the atmosphere. These control surfaces also allow the stage to fly at small angles of attack. The lift and drag forces. The lift and drag forces generated in this way reduce the thermal loads on the stage, allowing the re-entry burn to be shorter. In addition to the control surfaces, the landing legs are essential to the recovery hardware mentioned above, a thermal protection system for the baseplate is required to protect the engine compartment from the heat of re-entry [3]. Only if the launcher is of the 'Reusable' type is its mass considered to be 10% of the weight of the corresponding stage. In particular

$$m_{landing} = 0.1 \cdot m_{stage,i} \tag{2.99}$$

2.7.5 Total Length

The total length of the rocket is estimated as in:

$$L_{\text{total}} = \sum_{i=1}^{n} L_{\text{stage},i} + L_{\text{fairing}} \tag{2.100}$$

with:

$$L_{stage,i} = L_{engine_{stage,i}} + L_{tank_{stage,i}} + L_{interstage_{stage,i}} \tag{2.101}$$

2.7.6 Total Mass

The total mass of a multi-stage rocket system can be defined by adding up the masses of the various stages. Each stage includes critical components such as engines, the TVC system, tanks, avionics, the EPS system, thrust frames and interstage structures, as appropriate. The mass of each stage is calculated as follows.

For the **first stage** $i = 0$, it is necessary to add a component for the launch pad structure is included:

$$\begin{aligned} m_{\text{stages},0} = {} & m_{\text{engine},0} + m_{\text{TVC},0} + m_{\text{tank},0} + m_{\text{pad}} \\ & + m_{\text{avionics},0} + m_{\text{eps},0} + m_{\text{thrust\_frame},0} + m_{\text{interstage},0} \end{aligned} \tag{2.102}$$

For **intermediate stages** ($1 < i < n_{\text{stages}} - 1$), the interstage structure mass is included, while the pad component is excluded:

$$\begin{aligned} m_{\text{stages},i} = {} & m_{\text{engine},i} + m_{\text{TVC},i} + m_{\text{tank},i} + m_{\text{avionics},i} \\ & + m_{\text{eps},i} + m_{\text{thrust\_frame},i} + m_{\text{interstage},i} \end{aligned} \tag{2.103}$$

For the **final stage** ($i = n_{\text{stages}}$), no interstage structure is needed to connect to a subsequent stage:

$$\begin{aligned} m_{\text{stages},i} = {} & m_{\text{engine},i} + m_{\text{TVC},i} + m_{\text{tank},i} + m_{\text{avionics},i} \\ & + m_{\text{eps},i} + m_{\text{thrust\_frame},i} \end{aligned} \tag{2.104}$$

Summing the masses of all stages provides the total mass of the rocket, which offers a flexible structure for configuring multiple stages and calculating mass based on stage-specific components and conditions. Due to the inherently higher uncertainty in mass estimation for RLVs compared to ELVs, all first stage structures and subsystems were assigned a mass margin of 14%. The mass margin for the main engines for both stages was set at 12%. All other elements of the second stage were assigned a mass margin of 10%. [3].

2.8 Aerodynamic Module

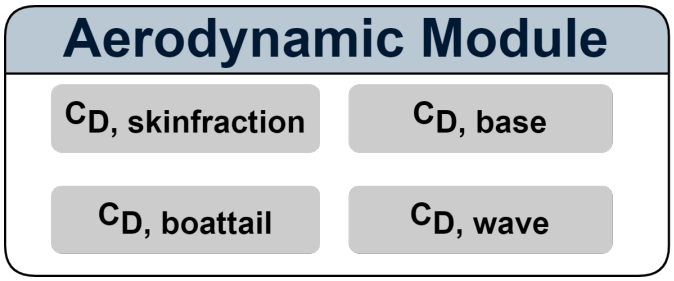

Figure 2.28: Aerodynamic Module

Before starting to describe the module, it is important to establish that the aerodynamic drag coincides with the zero angle of attack condition. Eddy drag is the only drag that will be considered in this study. It occurs at AoA = 0 of the rockets. The AoA refers to the angle of incidence between any component of lift (wing, fin, body, etc.) and its velocity vector. Induced drag is the drag associated with the generation of lift, which will be neglected in this work. When calculating the drag coefficient for the launcher of interest, it is very important to first separate the drag into component parts [30].The Aerodynamic Module is able to estimate the drag coefficient of a selected launcher as the sum of the friction (Viscous Effects), base (Increased pressure resistance due to blunt force during shutdown flight), wave (Pressure Drag increment due to compression or shock waves) e boat-tail drag coefficients following a typical build-up approach in [30].

$$C_{D,total} = C_{D,friction} + C_{D,base} + C_{D,wave} + C_{D,boattail} \tag{2.105}$$

Most of the equations presented in this chapter are empirically based (based on physical data) came from [31]. In particular, the aerodynamic coefficients in this study were estimated using empirical methods similar to those in Missile DATCOM [32].

2.8.1 Friction Drag Coefficient: $C_{D,friction}$

The skin friction drag is caused by the friction between the vicious airflow and the launcher. For the case of interest of this study, dealing with the size of the launcher and the high speeds occurring during the launcher ascent and descent, it is safe to assume that the turbulent flow regime will be dominant for the most part. The laminar and transitional regime will appear only in the first seconds of flight[31]. The friction drag coefficient $C_{D,friction}$ of body is defined as [31]:

$$C_{D,friction} = C_f(final)\left[1 + \frac{60}{\left(\frac{L}{D}\right)^3} + 0.0025\left(\frac{L}{D}\right)\right]\frac{4S_b}{\pi D^2} \tag{2.106}$$

with S_b wet surface e D maximum diameter. The Compressible skin friction coefficient C_f is given by can be modeled as a function of Reynolds number (R_n^*), the surface roughness (K), Mach Number (M) and launcher length (L). The skin friction coefficient can be estimated using:

$$C_f = \begin{cases} C_f = C_f^* \left(1 + 0.00798M - 0.1813M^2 + 0.0362M^3 - 0.00933M^4 + 0.000549M^5\right) \\ \text{if } C_f > C_f(\text{term}) \\ C_f(term) = \frac{C_f^*(\text{term})}{(1+0.2044M^2)} \\ \text{if } C_f < C_f(\text{term}) \end{cases} \tag{2.107}$$

where:

$$C_f^* = 0.037036 {R_n^*}^{-0.155079} \tag{2.108}$$

is the In-compressible skin friction coefficient, depending on Compressible Reynolds Number (R_n^*). While:

$$C_f^*(\text{term}) = \frac{1}{[1.89 + 1.62\log(\frac{L}{K})]^{2.5}} \tag{2.109}$$

is the In-compressible skin friction coefficient with roughness K.

$$K = \begin{cases} 0.0, & \text{for smooth surface} \\ 0.00002 \text{ to } 0.00008, & \text{for polished metal or wood} \\ 0.00016, & \text{for natural sheet metal} \\ 0.00025, & \text{for smooth matte paint, carefully applied} \\ 0.0004 \text{ to } 0.0012, & \text{for standard camouflage paint} \end{cases} \tag{2.110}$$

2.8.2 Base Drag: $C_{D,base}$

Base Drag is a contributor to Pressure Drag, and is attributed to the blunt aft end of the rocket. Base Drag can be a significant contributor to the rocket's overall drag during power-off flight (after engine burnout)[31]. Basic drag can be described as a change in the momentum of mass. Imagine a laminar air stream travelling over a smooth, gradually shaped body, when it suddenly encounters a blunt end, where the velocity drops to zero. The mass momentum (mass x velocity) changes abruptly, generating a force that acts in the opposite direction to the direction of flight. Most likely the boundary layer is not laminar but turbulent and the momentum thickness is well developed. The change in mass momentum at the blunt end is less severe with a fully developed boundary layer. The resulting drag

is also lower. The boundary layer is developed due to the presence of viscosity. Remember that viscosity is the cause of skin friction resistance. In general, when friction resistance increases, the tendency is for the basic resistance to decrease [31]. Base drag is difficult to predict.
The base drag $C_{D,base}$ for $M < 0.6$ is:

$$C_{D,\text{base}}(M < 0.6) = K_{\text{base}} \frac{\left(\frac{D_{\text{base}}}{D}\right)^n}{\sqrt{C_{D,\text{friction}}}} \tag{2.111}$$

where K_{base} is a constant of proportionality, D_b base diameter of rocket aft end, D rocket maximum diameter, $C_{D,friction}$ total skin-friction drag-coefficient and n exponent. In particular:

$$K_{base} = 0.0274 \tan^{-1}\left(\frac{L_0}{D} + 0.0116\right) \tag{2.112}$$

$$n = 3.6542 \left(\frac{L_0}{D}\right)^{-0.2733} \tag{2.113}$$

with L_0 the length between maximum diameter and the beginning of ogive. For a better comprehension, please refer to the image 2.29

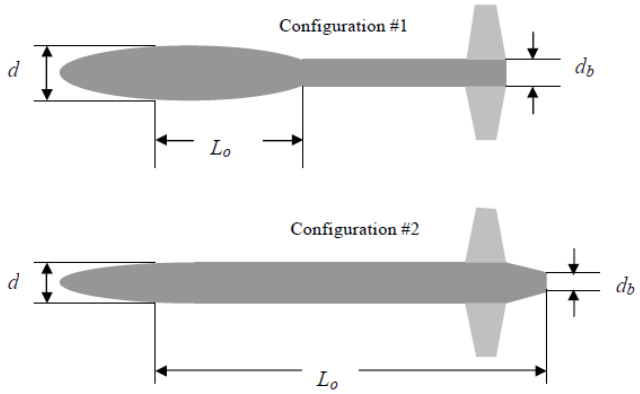

Figure 2.29: Aerodynamic shape useful $C_{D,base}$ estimation ([31])

The base drag $C_{D,base}$ for $M > 0.6$ is:

$$C_{D,base}(M \geq 0.6) = C_{D,base}(M = 0.6) f_{base} \tag{2.114}$$

where:

$$f_{base} = \begin{cases} 1 + 215.8(M - 0.6)^6 & \text{for } 0.6 < M < 1 \\ 1.0881(M-1)^3 - 3.738(M-1)^2 + 1.4618(M-1) + 1.883917 & \text{for } 1 \leq M < 2 \\ 297(M-2)^3 - 0.7937(M-2)^2 - 0.1115(M-2) + 1.64006 & \text{for } M \geq 2 \end{cases} \tag{2.115}$$

comes from tests on sounding rockets [31].

2.8.3 Wave Drag: $C_{D,wave}$

The wave drag can be calculated by summing transonic and supersonic wave drag contributions. Define M_D as transonic drag divergence Mach number and M_F as Final Mach number of transonic region, with L_{nose}, length of rocket nose, and, L_e. Effective length of rocket.

$$M_D = -0.0156\left(\frac{L_{nose}}{D}\right)^2 + 0.136\left(\frac{L_{nose}}{D}\right) + 0.6817 \tag{2.116}$$

$$M_F = a\left(\frac{L_e}{D}\right)^b + 1.0275 \tag{2.117}$$

where:

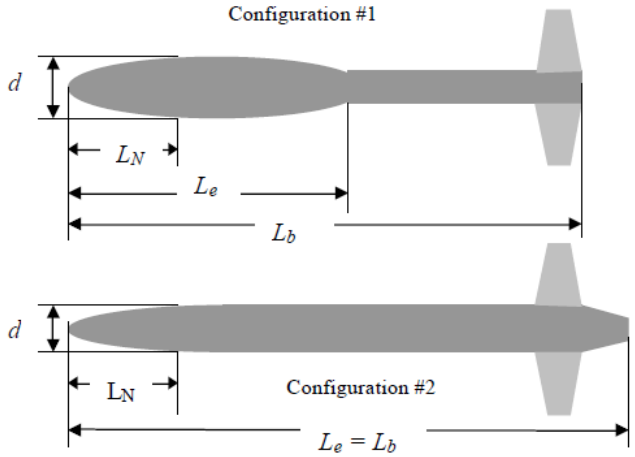

Figure 2.30: Aerodynamic shape useful $C_{D,wave}$ estimation ([31])

$$L_e = \text{Effective length of the rocket} \tag{2.118}$$

$$a = \begin{cases} 2.4 & \text{if } \frac{L_{nose}}{L_e} < 0.2 \\ -321.94\left(\frac{L_{nose}}{L_e}\right)^2 + 264.07\frac{L_{nose}}{L_e} - 36.648 & \text{if } \frac{L_{nose}}{L_e} \geq 0.2 \end{cases} \tag{2.119}$$

$$b = \begin{cases} -1.05 & \text{if } \frac{L_{nose}}{L_e} < 0.2 \\ -19.634\left(\frac{L_{nose}}{L_e}\right)^2 + 18.369\frac{L_{nose}}{L_e} + 1.7434 & \text{if } \frac{L_{nose}}{L_e} \geq 0.2 \end{cases} \tag{2.120}$$

The transonic drag increment $\Delta C_{D_{MAX}}$ is:

$$\Delta C_{D_{MAX}} = \begin{cases} c\left(\frac{L_e}{D}\right)^2 g, & \text{for } \frac{L_e}{D} \geq 6 \\ c(6)^g, & \text{for } \frac{L_e}{D} < 6 \end{cases} \tag{2.121}$$

where:

$$c = 50.676\left(\frac{L_{nose}}{L_{total}}\right)^2 - 51.734\frac{L_{nose}}{L_{total}} + 15.642 \tag{2.122}$$

$$g = -2.2538\left(\frac{L_{nose}}{L_{total}}\right)^2 + 1.3108\frac{L_{nose}}{L_{total}} - 1.7344 \tag{2.123}$$

The transonic and supersonic drag increments are defined as:

$$\Delta C_{D,transonic} = \begin{cases} \Delta C_{D_{MAX}} F, & \text{if } M_D \leq M \leq M_F \\ 0, & \text{if } M < M_D \text{ or } M > M_F \end{cases} \tag{2.124}$$

$$\Delta C_{D,supersonic} = \begin{cases} \Delta C_{D_{MAX}} F, & \text{if } M \geq M_F \\ 0, & \text{if } M < M_F \end{cases} \tag{2.125}$$

where:

$$F = -8.3474x^5 + 24.543x^4 - 24.946x^3 + 8.3321x^2 + 1.1195x \tag{2.126}$$

$$x = \frac{M - M_D}{M_F - M_D} \tag{2.127}$$

2.8.4 Boattail Drag: $C_{D,boattail}$

In the wave drag is often included the drag generated by boattail, defined from the base drag $C_{D,base}$.

$$C_{D,boattail} = \beta\frac{A_{fore}}{A_{aft}}C_{D,base}\begin{cases} 1, & \text{if } \sigma \leq 1 \\ \frac{3-\sigma^2}{2}, & \text{if } 1 < \sigma \leq 3 \\ 0, & \text{if } \sigma > 3 \end{cases} \tag{2.128}$$

where:

$$\beta = \begin{cases} 0, & \text{if } M \leq 0.8 \\ 1, & \text{if } M > 0.8 \end{cases} \tag{2.129}$$

$$\sigma = \frac{l_{boattail}}{d_{fore} - d_{aft}} \tag{2.130}$$

Here, A_{fore} and A_{aft} represent the areas of the fore and aft ends of the boattail, respectively, M is the Mach number, and $l_{boattail}$ is the boattail length. σ is length to height ratio [30].

2.8.5 Landing Drag: $C_{D,landing}$

For the descent phase for the evaluation of C_D it would be necessary to evaluate what effect the grids or fins used to control the descent have and which AoA to adopt for each phase. Given the difficulty of estimating such models, it was decided to use values of C_D found in the literature for the descent phase only, even for iterations above the first. In this case, reference was made to the ENTRAIN project also cited in Chapter 1. The idea was to use the data of the $C_D(M)$ presented in Figure 2.31 which allowed, thanks to the methods of integration of the equations of motion, to have good estimates of the ΔV for the landing. It is also a curve that presents a peak of $C_D \simeq 1.6$, a value comparable with that of the RFZ Datbase used for the first iteration and introduced in section 2.4.3.

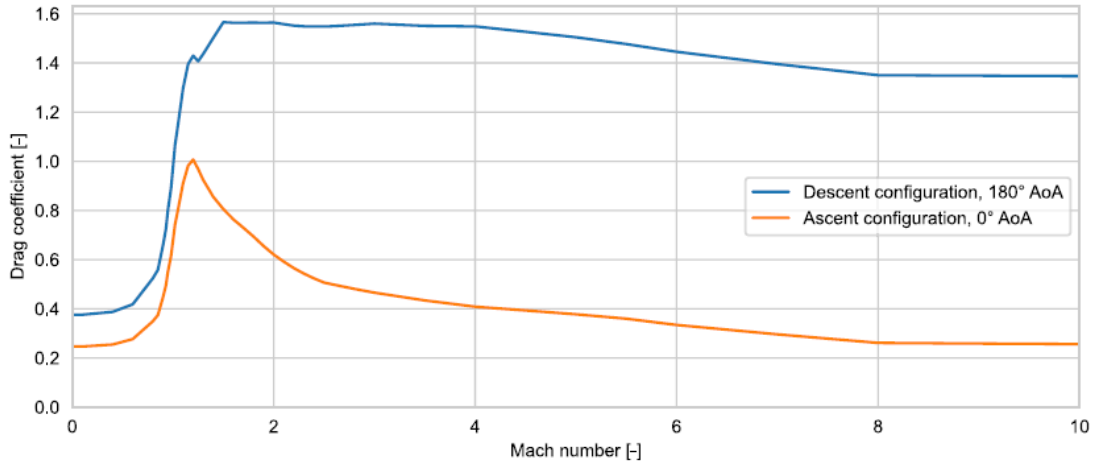

Figure 2.31: ENTRAIN mission: C_D versus Mach profile [3]

2.9 Output Window

Once an optimal MTOM value is reached, the tool proceeds to the final module: the Output Window (Figure 2.32). This section of the code provides the user with a direct view of the results obtained and facilitates the generation of reports for the study under examination.

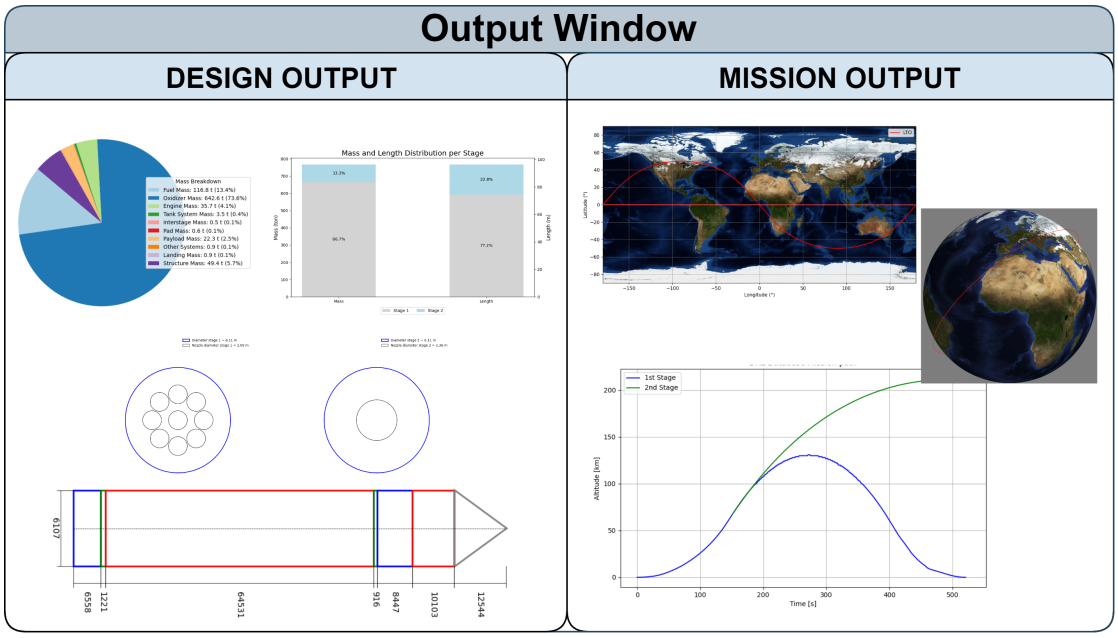

Figure 2.32: Tool's Output Window

Given the methodology's ability to analyze both mission and design phases, this chapter presents the outputs obtained for each category.

Before presenting the images that are part of the Output window, a recommendation is necessary: the images presented in the following sections are for illustrative purposes only, they do not refer to any case studies.

2.9.1 Design Output

Among the design outputs, Figures 2.33 to 2.35 respectively present: the launcher sketch, a system mass budget, and the mass and length distribution per stage.

The logic adopted for the placement of nozzles at the base of each stage is as follows:

- A single engine is always positioned at the center of the stage, ensuring that it remains aligned with the body x-axis, even when used individually (as in the landing burn introduced in section 2.4.1).

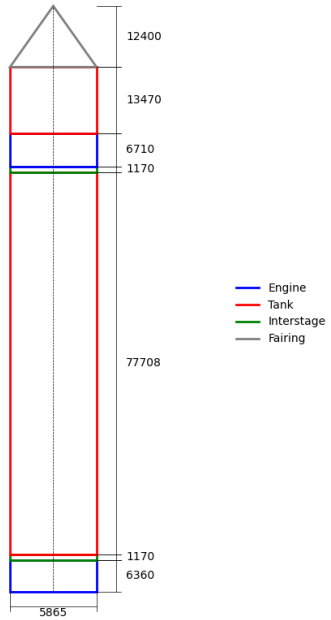

Figure 2.33: Sample: Launcher sketch

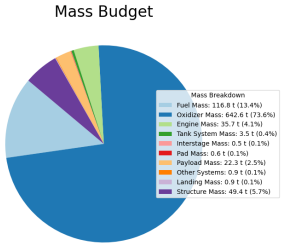

Figure 2.34: Sample: Mass budget

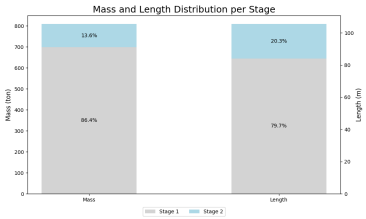

Figure 2.35: Sample: Stage distribution

- For two engines, they are placed symmetrically along a horizontal axis relative to the stage center, with a defined offset distance.

- For three engines, they are arranged along a circle, equidistant from each other, using regular angles of 0°, 120°, and 240°. If there is an overlap between the nozzles' exit areas, the radius of the circle is increased.

- For four or more engines configuration provides that one engine is always positioned at the center (core engine). The remaining engines are distributed along a circle around the center. The angles for the external engines are calculated by dividing the 360° evenly. If the engines overlap, the radius of the circle is progressively increased.

In Figure 2.36, various possible configurations, up to 10 nozzles, are presented.

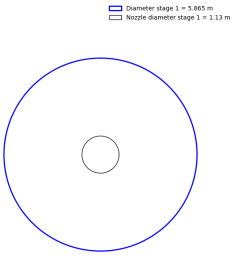

(a) 1 Engine

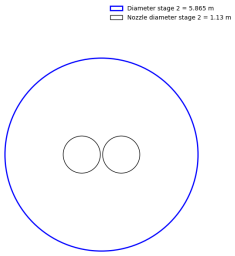

(b) 2 Engine

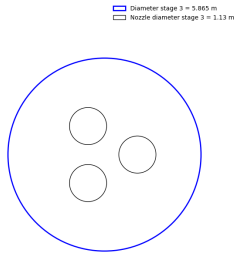

(c) 3 Engine

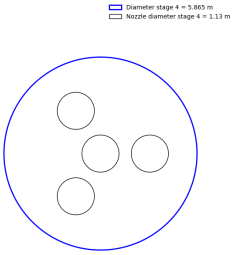

(d) 4 Engine

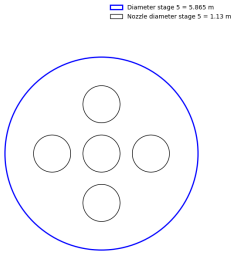

(e) 5 Engine

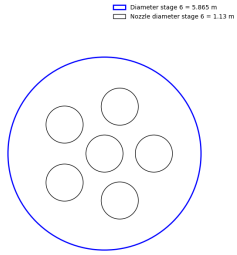

(f) 6 Engine

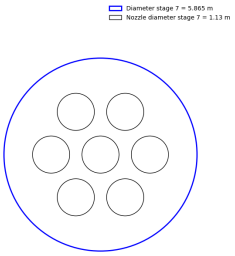

(g) 7 Engine

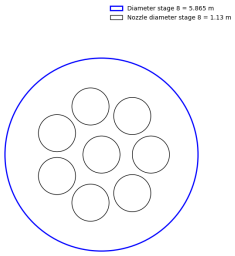

(h) 8 Engine

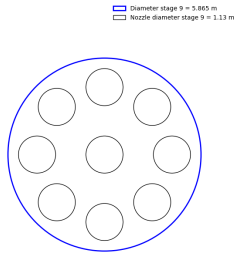

(i) 9 Engine

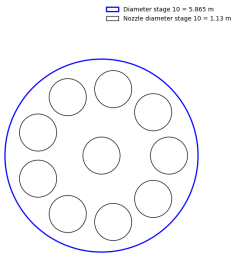

(j) 10 Engine

Figure 2.36: Nozzle configurations

2.9.2 Mission Output

Finally, for the mission outputs, the goal is to provide the user with an overview of the selected target orbit. This includes a 3D view, shown in Figure 2.37 (generated using the interactive Python library 'mayavi'), as well as a 2D ground track representation of the same orbit in Figure 2.38.

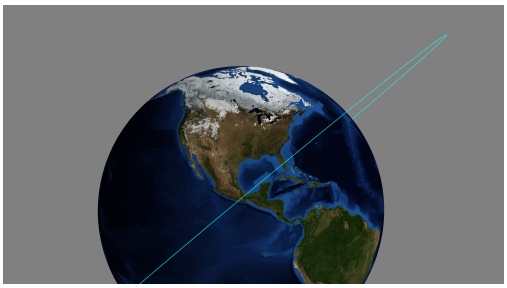

Figure 2.37: Sample: 3D orbit

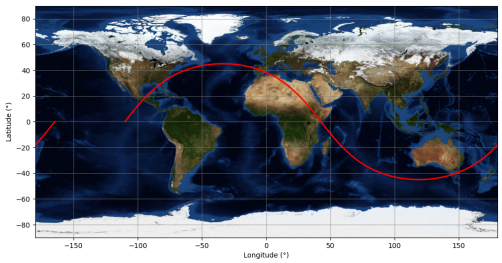

Figure 2.38: Sample: 2D orbit-Groundtrack

The graph of a typical mission profile for a VTVL TSTO is shown in Figure 2.38.

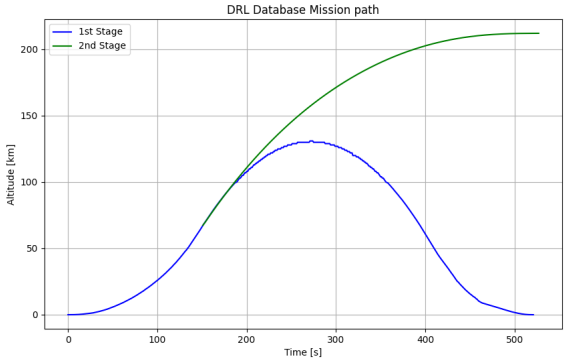

Figure 2.39: Sample: Mission path

In the following chapters, the methodology will be applied to a case study, and the results will be validated.

Chapter 3

Reusable VTVL TSTO: Thesis Case study

In this chapter it has been assumed, as the main objective of the thesis, that the chosen launcher is a reusable vehicle TSTO. This type of launcher, described below, has the same general layout as the RETALT1 mentioned in Chapter 1, with: the same propellant combination and the same engines for both stages, with one difference: the nozzle of the second stage has a higher expansion ratio. The reason for this choice lies in the need to validate the work performed, which will be discussed in detail in the next Chapter 4. Selected inputs and results obtained using the implemented software will be shown next.

3.1 VTVL TSTO: Inputs

For the case study that is the subject of this work, the following requirements were taken into account (Figure 2.2), properly divided by category.

- **Performance Requirements**, related to the rocket's main task of enabling a payload to be carried into orbit:
  - Payload mass of 20000 kg.
  - Payload size, height of 8 m and fairing radius equal to that of the launcher one (derived from the statistical analysis module in Section 2.3).
- **Configuration Requirements**, concern the type of launcher and type of engines used:
  - Number of stages equal to 2, in line with thesis objectives.

  - The type of bi-propellant is '*liquid oxygen and hydrogen*'('LOX/LH2') for both stages, the characteristics of which can be found in the Technical Documentation Database (Section 2.2). Using the same combination of propellant and engines in both stages results in component cost benefits. Using the same type of engine for the first and second stages results in a higher production rate, which reduces development and production costs per unit [3]. This type of decision, like the decision not to use boosters, is very common in the design of new generation launchers.
  - For the type of launcher technology, the choice is '*Reusable*' respect to '*Expendable*'.
  - For engine and tank characteristics, the choice is '*Turbopump cycle*' for the engine, '*Helium*' as pressuring gas, and '*Al-7075*' as the tank material. All these properties can be found in the pre-implemented databases in Section 2.2.

- **Operational Requirements** instead provide information on the launch site and target orbit into which the payload is to be released. In particular, these types of requirements are needed for the Mission Design Module in Section 2.4.
  - '*LTO*' as the orbit, with orbital parameters defined in Table 2.2.
  - '*Cape Canaveral*' as the launch site, with details available in Table 2.1.

Since the nature of the technology involves the reusability of the first stage, it is also important to define the **Landing Configuration Requirements**. For the case study, the landing type is defined as '*Downrange landing* (DL)'. In particular, before proceeding with the analysis of the results, it is necessary to define additional inputs, especially those related to the two modules, as shown in Figure 2.1. For the '*Optimal Staging*' (Section 2.5) module, a structural ratio ϵ of 0.1 will be defined for each of the two stages. This is an approximate value that will later be updated iteratively.

While, for the '*Propulsion module*' (Section 2.6), the following inputs need to be defined:

- Number of engines: 9 for the first stage and 1 for the second;
- Expansion ratio: 15 for the first stage and 70 for the second;
- Throat area: $0.06228\,\mathrm{m}^2$ for the first and second stage;
- Tanks storage pressure: 55 bar. This is a guess value that fits well with the type of rocket analysed.

The process by which these inputs are processed was discussed in detail in Chapter 2; the results, rather than the steps that led to them, will be analysed below.

3.2 VTVL TSTO: Reference mission

Before introducing the results obtained for the mission analysis, it is useful to introduce the constraints used for each stage introduced in section 2.4.2. The approach was to set a maximum height for each stage, the final pitch angle and the throttle in order to optimise the duration of each. The mission requirements for RETALT1 are to transport a payload of 20 $tons$ to a LEO of approximately 340 km [4]. As anticipated in section 2.4.3, the approach used is that of a 2-degree-

Mission Phase	Final Altitude [km]	Final Pitch Angle [°]	Throttle
Lift-Off	1.6	90	1.00
Pitch-Over	1.85	80	1.00
Constant Pitch	6	80	1.00
First Stage Burn	70	46	[0.7, 0.85]
Coasting with Fairing	120	-	0
Re-Entry Burn	70	150	0.45
Uncontrolled Descent	60	-	0.00
Aerodynamic Glide	2	-	0.00
Landing Burn	0	90	1.00

Table 3.1: Mission phases definition

of-freedom mission analysis, and in particular, for a subdivision into phases to exist, one must define for each the maximum height value that can be reached, the final pitch angle, and the permissible throttle range. In particular, columns 2, 3 and 4 of the table 3.1. Furthermore, as noted in column 1, the phases, at least for ascent, are similar to those used for conventional launchers mentioned in reference [21]. For the descent, the reference phases are those shown in 2.13. Moreover, the type of ascent is of the direct type and not Hohmann's. The choice of the maximum value, especially for the height, involved a great deal of cross-cutting work, which led to the definition of these values both from a comparison of the projects analyzed in Chapter 1 and from others. Having defined the final and path conditions of each phase, the analysis of the results obtained is illustrated below.

3.3 VTVL TSTO: Results

The aim of this section will be to analyse the results obtained from the use of the tool by dividing them into results relating to mission and design. As is well known, one of the most dimensioning parameters for launcher design is related to the consumption to carry out a given mission, which in the case under consideration, will have an even greater contribution given the reusability of the vehicle.

The table 3.2 summarises what the consumption is for this mission. There is a special row for the upper stage since the estimate was made with 2BP. In particular,

	Required ΔV [m/s]	ΔV Drag [m/s]	ΔV Gravity [m/s]	Total ΔV [m/s]
Ascent	4894.66	620.75	1222.36	6740.76
Ascent Upper Stage	-	-	-	2432.76
Descent	1646.45	-	-	1646.45

Table 3.2: Tool results: Mission ΔV values

the contribution for the ascent is the descent is:

$$\Delta V_{ascent} \simeq 9173 \, \frac{m}{s} \qquad \Delta V_{descent} \simeq 1646 \, \frac{m}{s} \tag{3.1}$$

These values are validated in Chapter 4 using the ASTOS software.

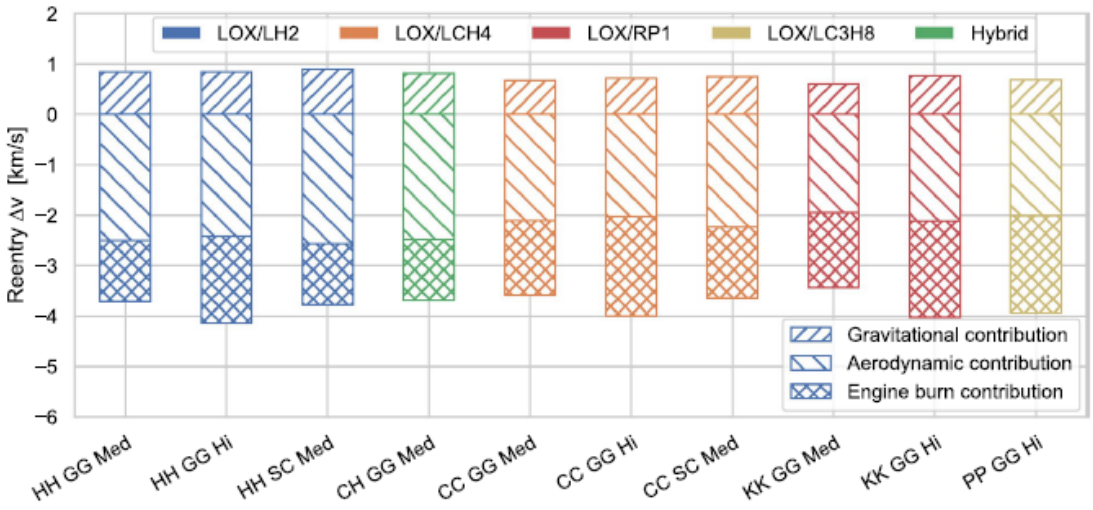

Figure 3.1: Re-entry velocity changes integrated of descent trajectory [3]

In Figure 3.1 in particular the second column in blue ('LOX/LH2'), for the engine burn contribution, there is a value of ΔV for re-entry of about 1.5, confirming the reliability of the mission module of the tool.

The total value of approximately 10.5 $\frac{km}{s}$ certainly allows for effective results. During the development of the tool, however, it was noticed that values already higher than 11.5 $\frac{km}{s}$, led to unfeasible vehicles. In that case, the use of boosters could mitigate the unfeasibility. The results obtained are the result of an interaction between the 'Mission Design Module' (Section 2.4) and the 'Aerodynamic Module' (Section 2.8), which made it possible, during the cycle, to have an increasingly precise estimate of the drag coefficient C_D. The output generated for the ascent

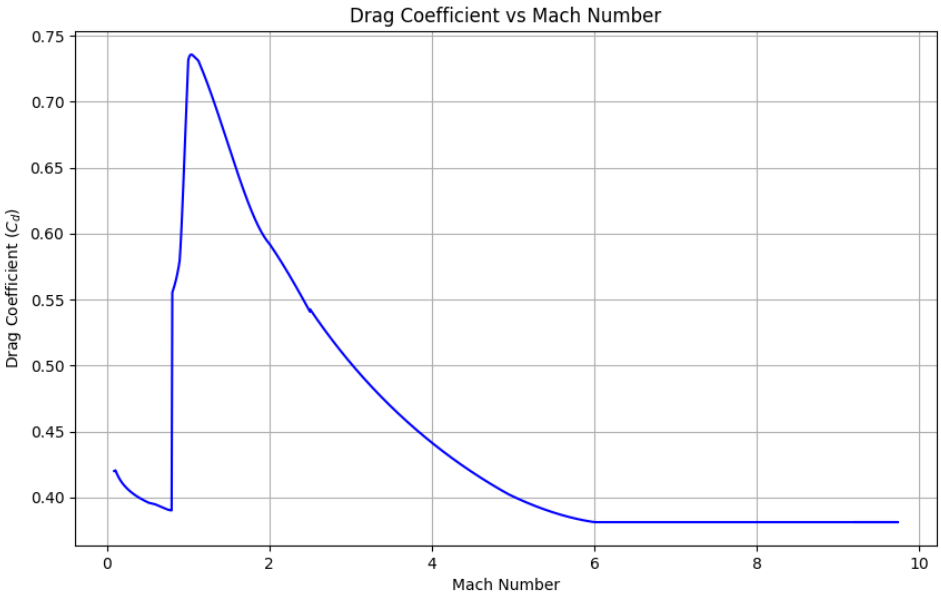

Figure 3.2: Drag Coefficient Extrapolation

phase (profile versus Mach) is presented in Figure 2.7. The peak of $C_D \simeq 0.75$ confirms an aerodynamically efficient output. It is important to note that the values of C_D arise from conditions of zero angle of attack (AoA). The remaining modules, in detail, that of 'Optimal staging' (Section 2.5), 'Propulsive' (Section 2.6) and 'Mass/Length Estimation' (Section 2.7) produced results that have been reported in Table 3.3. Let the results now be analysed in relation to the outputs generated by the tool, shown in Figure 3.3 to Figure 3.7. The mass of each stage, excluding payload and fairing, is distributed for about 77% for the former and about 23% for the latter, as shown in Figure 3.2, while the length distribution per stage (including interstage and engine), between 70% and 30%, again in Figure 3.6. The masses of the subsystems and fuel/oxidant shown in Table 3.3 are distributed in a pie chart (Figure 3.7) in the form of a 'mass budget'. For the distribution of lengths, the tool generates a dimensioned plan view, shown in Figure 3.3, for visual evaluation of the design. Finally, figures 3.4 and 3.5 show the base view of each stage, focusing on the thruster arrangement and the diameter of each stage. The main results obtained include a diameter of $6.11\,m$, a total length of $113.16\,m$ and a maximum take-off mass (MTOM) of $860186\,kg$.

Parameter	Stage 1	Stage 2
Stage mass, m_{TOT} [kg]	644847	195337
Structure mass, m_{Inert} [kg]	64485	19534
Fuel mass, m_{Fuel} [kg]	89287	27047
Oxidizer mass, $m_{Oxidizer}$ [kg]	491077	148757
Engine mass, m_{Engine} [kg]	25878	1254
TVC mass, m_{TVC} [kg]	6728	326
Engine length, L_{engine} [m]	6.56	8.45
Tank length, L_{tank} [m]	63.64	20.75
Fuel tank length, $L_{fuel,tank}$ [m]	42.92	13.00
Oxidizer tank length, $L_{oxidizer,tank}$ [m]	17.56	5.32
Oxidizer Volume, $V_{tank,OX}$ [m^3]	430.01	130.26
Fuel Volume, $V_{tank,F}$ [m^3]	1257.56	380.94
Pressuring system mass, $m_{press,sys}$ [kg]	2867	2672
Pressuring system length, $L_{press,sys}$ [m]	2.25	1.51
Tank mass, m_{tank} [kg]	750	712
Inter-tank length, $L_{intertank}$ [m]	0.92	
Inter-tank mass, $m_{intertank}$ [kg]	414	447
TPS mass, m_{TPS} [kg]	1248	458
Inter-stage mass, $L_{interstage}$ [m]	1.22	
Inter-stage length, $m_{interstage}$ [kg]	543	
Launcher Pad mass, m_{pad} [kg]	687	
Fairing mass, $m_{fairing}$ [kg]	1148	
Fairing length, $L_{fairing}$ [m]	12.54	
Avionics mass, $m_{avionics}$ [kg]	456	198
EPS mass, m_{EPS} [kg]	152	66
Landing system mass, $m_{landing}$ [kg]	4225	
Stages length, L_{stages} [m]	70.20	24.2
Diameter, D [m]	6.11	
Total length, L_{total} [m]	113.16	
MTOM [kg]	860186	
Update Vacuum thrust, T_{update} [kN]	10058	1430

Table 3.3: Tool results: Design

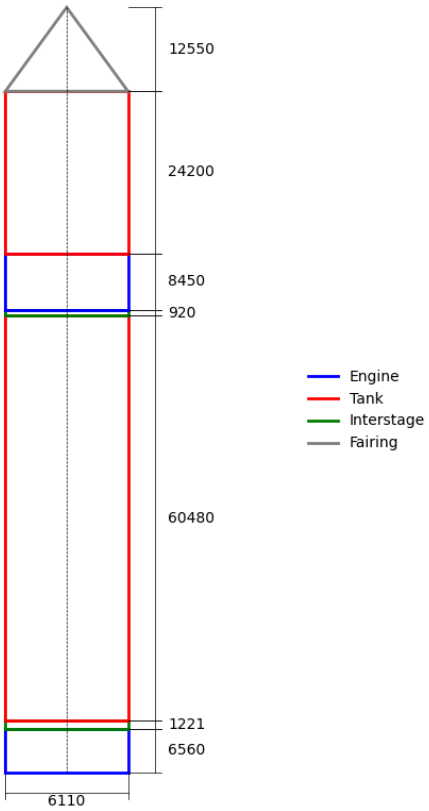

Figure 3.3: Rocket Plant view

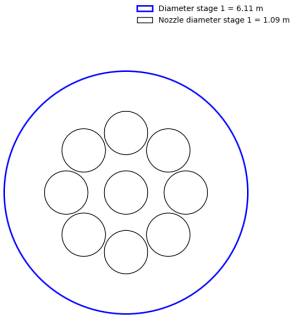

Figure 3.4: Engines Disposition Stage 1

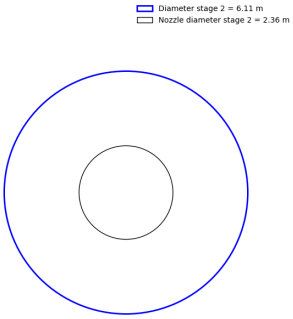

Figure 3.5: Engine Disposition Stage 2

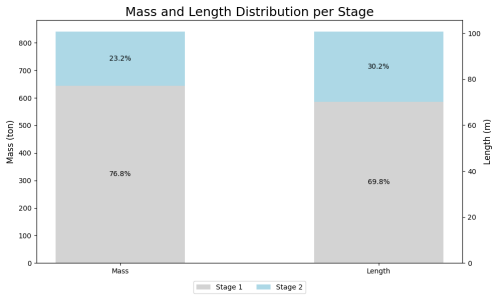

Figure 3.6: Mass-Length Distribution

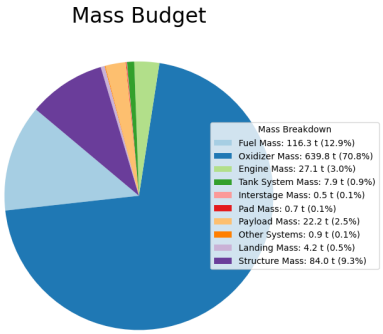

Figure 3.7: Mass budget

Initially, the tool also provided for the production of mission-related outputs, but, due to the problem of a scattered amount of data, due to the integration with Runge-Kutta (Appendix C) they do not adequately represent the mission, but, of course, describe its characteristics well. For this reason, they have not been reported in this work. Despite this graphical issue, the ASTOS software was used to produce a graphical output of the mission characteristics, which allowed to produce a large number of plots, which, in addition to validating the 'Mission Design Module', made it possible to analyse the mission well. How the mission was analysed was discussed in Chapter 4, and also represents an important validation from the design side.

Chapter 4

Methodology Validation

This chapter brings this thesis to a close. However, the validation of the case study analysed in chapter 3 through the methodology outlined in chapter 2 remains crucial to ensure the correctness of the approach adopted.

Next, comparisons between the case study and the RETALT1 prototype will be made, a mission analysis will be performed using the ASTOS software, and chapter will finish with a comparison of the consumption to accomplish it.

The reasons why the vehicle used is of European prototyping are consistent with those outlined in Chapter 1.

4.1 Design Validation: RETALT1

RETALT1 is a two-stage to orbit (TSTO) vertical take-off vertical landing (VTVL) RLV heavy-lift launcher shown in (Figure 4.1) and explained in Chapter 1. In order to reduce costs and risks and to speed up the commercialisation of the technologies to be developed, the reference configuration chosen is based on available propulsion technologies. For this reason, liquid oxygen and hydrogen ('LOX/LH2') engines similar to the Vulcain 2 engine will be selected, with adapted expansion ratios to optimise the thrust of the two stages. The first and second stages use the same type of rocket engines. The first stage is powered by a total of nine engines with an assumed throttling capability for the powered descent phase of 49%. Stabilisation and control is achieved by a novel concept using deployable interstage segments as control surfaces to minimise additional parts and vehicle drag in the ascent phase, thereby increasing efficiency during ascent. Damper legs deploy just before touchdown to cushion the final impact. The second stage is powered by an engine. The concept includes the possibility of either an expendable second stage [4]. In terms of dimensions, the Figures 4.1 and 4.2 will help establish that there are indeed many similarities between the design of the instrument and that of RETALT1. The

Stage Characteristics	1st Stage	2nd Stage	Fairing	Total
Number of engines	9	1	-	10
Height [m]	71.2	19.8	12.0	103.0
Diameter [m]	6.00	6.00	6.00	6.00
Full mass (GLOW) [t]	680.8	204.2	2.5	899.0
Structural coefficient	8.7%	8.3%	-	-
Structural mass [t]	59.3	16.7	-	75.9
Propellant mass (incl. descent) [t]	621.5	187.5	-	809.0
Descent propellant [t]	50.0	0	-	50.0
Residual propellant and residues [t]	7.5	2.5	-	10.0
Engines	RETALT1-LHLOX-E15-FS	RETALT1-LHLOX-E70-FS	-	-
Engine cycle	Gas generator	Gas generator	-	-
Oxidizer/Fuel	LOX/LH2	LOX/LH2	-	-
Expansion ratio	15	70	-	-
Specific impulse SL [s]	372.2	294.4	-	-
Specific impulse Vac [s]	401.6	431.9	-	-
Thrust SL [kN]	$9 \times 1179 = 10614$	$1 \times 930 = 930$	-	-
Thrust Vac [kN]	$9 \times 1273 = 11453$	$1 \times 1364 = 1364$	-	-

Table 4.1: Characteristics of the RETALT1 configuration [4]

arrangement of the engines is also the same, due to the reusability feature adopted by both.

The percentage differences between the case study and RETALT1 are now assessed. In Figure 4.1 and Figure 4.2, the case study is indicated with the colour 'lime green' and the RETALT with 'blue'. In Figure 4.3, the percentage differences are almost all below 10%, confirming the effectiveness of the tool. The fact that all estimated masses are below the threshold value shows how the model manages to provide acceptable results for conceptual design. As anticipated, not all parameters are below this threshold, in particular, it is the thrust in vacuum of the first stage. However, this is a very small difference and below 15%, which allows the design to be validated. The problem with the estimation of the first stage thrust could be related to the formula used to update it, the Equation 2.61. Its link with the mass of the stage may lead to approximations that are not perfectly reliable. This is a point that will be proposed as a future improvement within Chapter 5. Furthermore, this type of graph provides a clear view of the percentage differences between two variables but does not allow weights to be assigned to each. For example, having a difference of 5.5% on the MTOM means having a difference of about $45\,ton$, while, a 9.5% on the $m_{structure}$ of about $7\,ton$. This is to emphasise that sometimes, in the context of conceptual design, it can happen that an excess of one quantity with a higher weight can annihilate the effects of losses of other quantities with a lower weight and still lead to optimistic results.

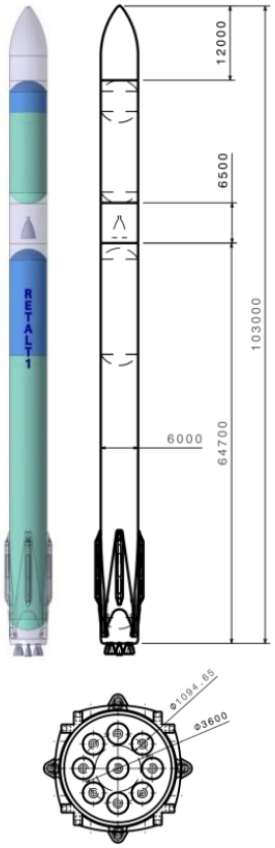

Figure 4.1: RETALT1 [4]

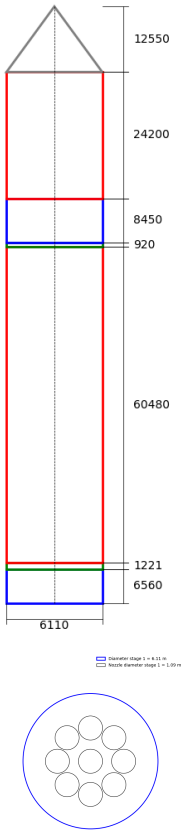

Figure 4.2: Case study

In Figure 4.5, this concept applies somewhat, as the percentage difference of the height of stage two is quite large, but the total height, on the other hand, has a very low percentage difference (3.7%). At the level of conceptual design, one can therefore accept these differences. Analysing the other results, it certainly results: a good approximation of the diameter (1.8%), of the first stage (1.4%) and of the fairing (4.3%). For a visual evaluation of these differences, see the images in Figures 4.3 to 4.6.

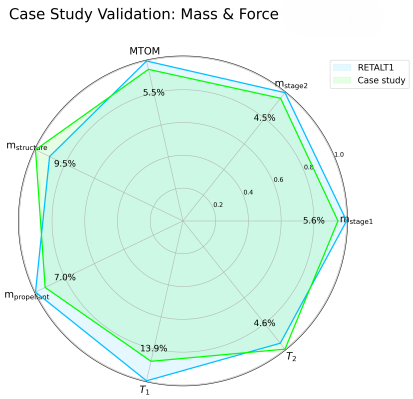

Figure 4.3: Radar graph of design validation: Mass and Thrust

Value Name	<5%	<10%	<15%	>15%
m_{stage1}		5.6%		
m_{stage2}	4.5%			
MTOM		5.5%		
$m_{structure}$		9.5%		
$m_{propellant}$		7.0%		
T_1			13.9%	
T_2	4.6%			

Figure 4.4: Percentage difference table for Mass and Thrust

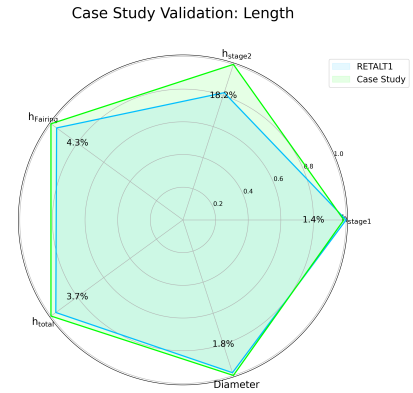

Figure 4.5: Radar graph of design validation: Dimensions

Value Name	<5%	<10%	<15%	>15%
h_{stage1}	1.4%			
h_{stage2}				18.2%
$h_{Fairing}$	4.3%			
h_{total}	3.7%			
Diameter	1.8%			

Figure 4.6: Percentage difference table for Dimensions

4.2 Mission Validation: ASTOS Analysis

This section will discuss the mission analysis of selected launcher to a LTO, following the same mission discussed in Chapter 3. The main objective of this analysis is to estimate the ΔV required for Ascent and Descent, considering drag and gravity losses, with ASTOS [33]. ASTOS is a commercial software used for trajectory simulation and optimization of different spacecraft. The approach is more complex respect the one adopted in Section 2.4.1. In particular, in this case, the model have 3 degrees of freedom while, model in tool, have two.
The analysis performed will consider both the ascent and descent phases, in particular a landing of DL. The inputs used for both do's are now listed:

- **Celestial body**, allows the selection of the planet of interest, in this case the Earth, providing a very accurate gravitational model, including gravitational perturbations ;
- **Atmosphere**, atmospheric model of the planet mentioned above, US Standard 76 was chosen as input, in accordance with Appendix A;
- **Vehicle's Parts & Properties**, in which:
  - *Actuators*, selecting both first and second stage thruster engines. The values of thrust, output section and specific impulse in vacuum are only those of RETALT1 listed in Table 4.1. For further optimization a value between 0 and 1 is considered for the throttle.

	First Stage Engine	Second Stage Engine
Exit Area A_e $[m^2]$	8.5	4.5
Vacuum Thrust $[kN]$	11453	1356
Vacuum I_{sp} $[s]$	401	430
Throttle	[0,1]	[0,1]

Table 4.2: Engine parameters for first and second stage.

  - *Aerodynamics* is the model evaluated taking into account the different contributions for the C_D in Section 2.8. In particular a file with C_D and $Mach$ (derived from Figure 3.2) has read considering the reference diameter of $6\,m$.
  - *Aerothermodynamics* uses the 'convective' model defined by a 'free stream enthalpy'. Thus, no aerothermodynamic constraints are imposed in the tool.

– *Components*: finally, the dimensions and masses (structure and fuel) are defined for each component of the aircraft, namely: stages, fairing and payload. All values are taken from the Table 4.1.

	First Stage	Second Stage	Fairing	Payload
X dimension $[m]$	71.2	19.3	12	8
Y dimension $[m]$	6	6	6	5
Z dimension $[m]$	6	6	6	5
Structural Mass $[ton]$	59.3	16.7	2.5	20
Propellant Mass $[ton]$	621.5	187.5	–	–

Table 4.3: Component dimensions and masses for the launch vehicle.

4.2.1 Ascent phase

In the ascent phase, after defining the main components of the rocket under consideration, a model is generated in the 'Vehicles & POIs Definition' section, assigning the correct position and assignments to the engines and components. For the ascent, the model is shown in figure 4.7. For simplicity's sake, the nine first-stage engines were combined into one with adequate thrust. The mission

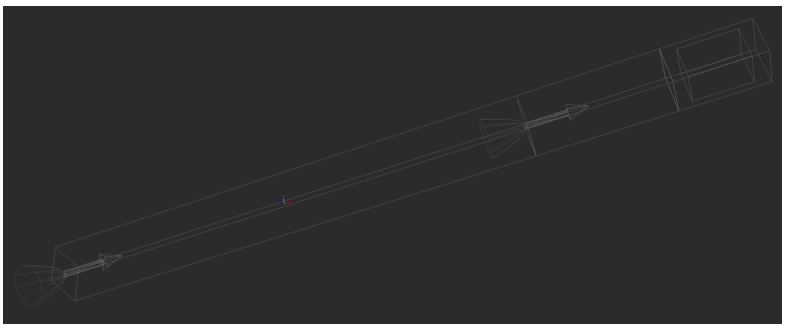

Figure 4.7: Ascent: Assembled Vehicle

phases have been implemented in the model include the initial guess on their duration as input, ASTOS will optimize the duration of each of them subsequently. The sequence of phases is the same use in program guide [21] used for typical vertically launched rocket and mentioned in the 2.4.1. Different Mission phases and guess duration are reported in Table 4.4. One difference from the tool lies in the type of ascent manoeuvre, previously 'Direct', and now with a 'Hohmann'. This choice is justified by the presence of two burns for the second stage, with an intermediate coasting phase. The initial guess choice is given both by the results

Mission Phase [21]	Duration Guess
Lift-Off	15 s
Pitch-Over	1.5 s
Constant Pitch	25 s
First Stage Burn	130 s
Coasting with Fairing	30 s
Second Stage 1st Burn	70 s
Second Coasting	70 s
Second Stage 2nd Burn	100 s

Table 4.4: Estimated durations for each mission phase: Ascent

obtained from Mission Design Module discussed in section 2.4.1. Once the duration has been determined, it is necessary to establish at least the initial conditions for the dynamic study of the mission. In order to establish the initial state of the rocket, the first step is to define the type of reference system, specifically a Planet-centred and Planed-fixed (PCPF), the same one used within the developed tool, but in 2 dimensions. A problem with the latter is that, since it is non-inertial and non-rotating, it does not allow for the speed gained by the rotation of the planet with respect to the launch site in the case of an eastward launch. This simplification will be taken into account in the validation phase. Then the altitude, latitude and longitude of the launch site (*Cape Canaveral*) and the radial, north and eastward velocities are set as the initial state of PCPF reference frame:

$$state_0 = \begin{bmatrix} 0\ [\text{m}] \\ 80.6^\circ \\ 28.6^\circ \\ 0\ [\text{m/s}] \\ 0\ [\text{m/s}] \\ 0\ [\text{m/s}] \end{bmatrix}$$

After selecting the aerodynamic and atmospheric model and defining the type of motion equations to be integrated (*Inertial velocity*), it is time to define the dynamic characteristics of each mission phase. The focus is on the *attitude* with respect to each axis of the reference system under consideration. Defining the correct range of *pitch* and *yaw* angles is essential for successful simulation and optimisation. According to [21]:

- **Lift-Off** with constant yaw pointing in the desired direction (70°) until a certain altitude is reached to avoid collision with the launch pad. For the pitch a control law of *Vertical Take-Off* is set to have an angle of 90° and get out of the denser layers of the atmosphere.

- The **Pitch-Over** maneuver is used to give the rocket a direction.It uses a linear pitch law and a constant yaw law. Pitch rate varies based on launcher type, in this case is set on $1\,\frac{^\circ}{s}$
- An intermediate **Constant Pitch** phase is required to meet gravity turn conditions: flight path angle equal to pitch angle (constant), angle of attack equal to zero and yaw angle remains constant.
- **First Stage Burn: Gravity turn** phase follows until aerodynamic forces are small. Initially, the yaw angle remains constant. Number of *gravity turn* phases and yaw control timing depend on the launcher. At the end of this phase, the release of the first stage is set.
- In **Coasting with fairing** phase the engines are turned off and a constant control law is set for yaw angle and a *gravity turn* for pitch. At the end of the phase the fairing jettison happens.
- With the **Second stage first burn** two constant and optimizable laws are chosen.
- **Second stage coasting** prepares the vehicle to reach desired orbit, for this reason, a linear control law is set for pitch (final value 0°) and for yaw (final value 48°).
- **Second stage second burn** permits to circularize the orbit which *target orbit* $\rightarrow$ *target inclination* $= 50°$ yaw law and *Required velocity* $\rightarrow$ *apo/periapsis* $= 340\,km$ for pitch (set to 0°).

In order for this model to produce correct results, it is important to proceed with optimisation, in particular, the ASTOS software uses the method: CAMTOS (Collocation And Multiple shooting Trajectory Optimization Software) for the MDO. CAMTOS uses advanced optimisation algorithms, such as genetic, stochastic optimization, and nonlinear programming methods [33]. The integration method is Runge-Kutta 4/5, the same of implemented tool in-depth in Appendix C. For optimisation successful, constraints must be introduced:

- **Initial Latitude, Longitude and Altitude** comes from *Cape Canaveral* coordinates and they are set as initial boundary of the first phase.
- **Inital Radial, North an East Velocities** set to null as initial boundary of first phase.
- **Circular Altitude** defines Periapsis and Apoapsis height and circular velocity of selected orbit.

- **Fairing Separation** and **Path heat flux** are constrains related to heat flux. The upper limit is defined for both to 1135 $\frac{W}{m^2}$ and they are respectively assigned as the final boundary of '*Coasting with fairing*' and as the path of the '*Second stage first burn*' and '*Second stage coasting*'.

- **MECO height** is set to 70 km and indicates the maximum height for jettisoning the first stage.

- **Gravity turn** is a constrain set to 0 for constant pitch phase, to avoid the effect of Earth gravitational field on the phase.

A cost function for the maximum transportable payload is also included. The cost function is a mathematical function that maps a set of parameters to a scalar value representing the value that represents a "cost" associated with those parameters. The aim of optimisation is to find the parameters that minimise this cost function. A scaling with a value of 10^{-4} is inserted [21].

Before introducing the results graphically, Table 4.5 reports the results obtained from the optimisation.

Phase	Time [s]	Duration [s]	Initial Mass [kg]	Propellant Consumption [kg]	Jettisoned Mass [kg]
1	0.00–1.00	1.00	815490.8	2913.0	0.0
2	1.00–5.00	4.00	812577.8	11648.3	0.0
3	5.00–31.54	26.54	800929.5	77303.0	0.0
4	31.54–155.40	123.85	723626.5	360714.5	165032.5
5	155.40–177.50	22.10	197879.5	0.0	2268.0
6	177.50–178.00	0.50	195611.5	272.7	0.0
7	178.00–178.50	0.50	195338.8	0.0	0.0
8	178.50–467.90	289.40	195338.8	157847.3	0.0

Table 4.5: ASTOS Optimization Result: Ascent

The values do not coincide precisely with those of RETALT1 because they are optimised by the programme.

Ascent Results

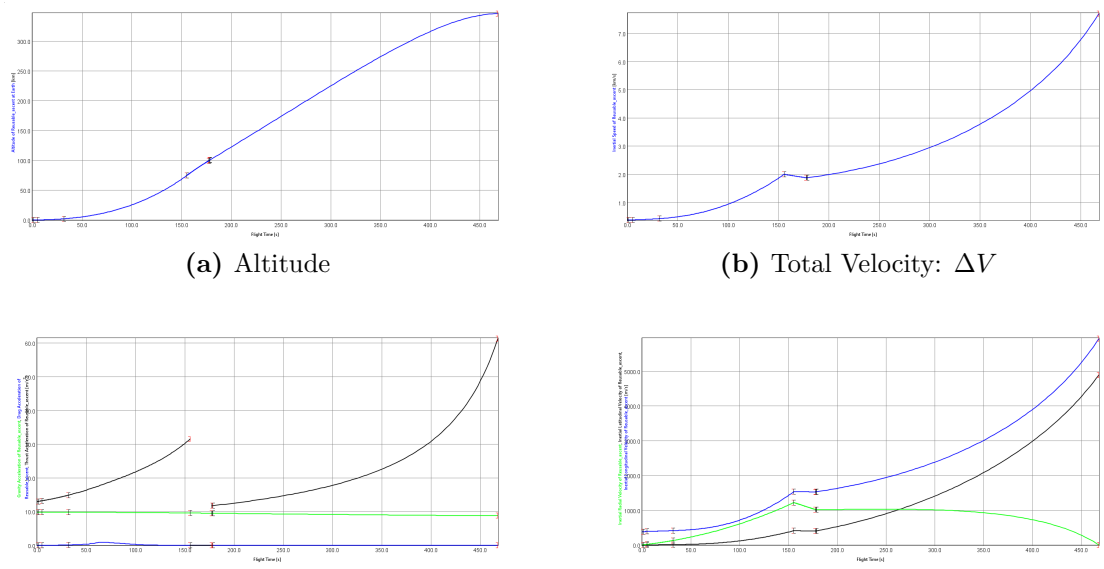

(a) Altitude

(b) Total Velocity: ΔV

(c) Accelerations Contributions

(d) Velocities Contributions

Figure 4.8: ASTOS analysis: Ascent Results I

Results are shown in Figures 4.8 to 4.11. Now have a look at the graphs one at a time.

Figure 4.8a shown the altitude in function of flight time. The vertical lines represent the end of each phase. Note how the first stages are very fast compared to the ignition of the stages and how the height reached corresponds to the radius of the desired orbit. As expected, the initial stages are very fast compared to the main burns. As expected from constrain, the MECO take place at approximately $70\,km$ and at approximately $150\,s$ from the start of the mission.

In Figure 4.8b are shown the velocity required to reach the target orbit. This 'inert velocity' value corresponds to the ΔV needed to accomplish the mission net of losses. It is then the sum in absolute value of all 3 components of the velocity vector, illustrated in Figure 4.8d.

Figures 4.8c and 4.8d show the components of accelerations and velocities according to the chosen losses and reference system.The axial acceleration, along the body 'X' axis, reaches a value of about $3g$ for the first stage and about $6g$ for the second. Losses due to gravity and drag are not visually distinguishable here. They will however be accounted for through numerical integration later on.

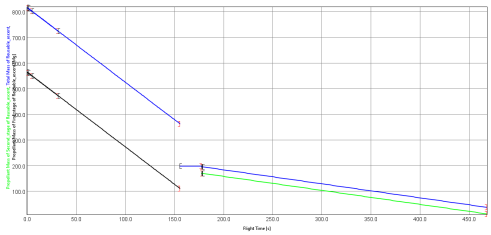

(a) Mass profile

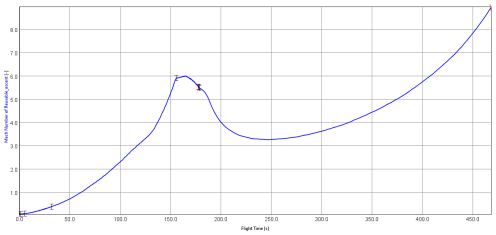

(b) Mach

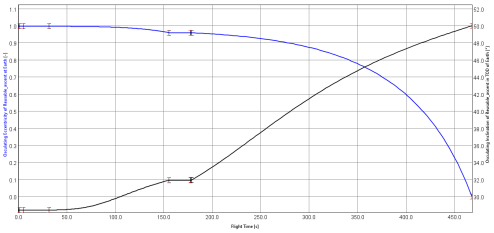

(c) Inclination and Eccentricity Profile

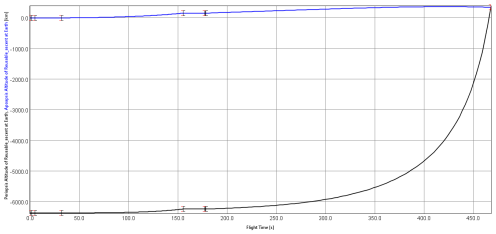

(d) Periapsis and Apoapsis Altitude

Figure 4.9: ASTOS analysis: Ascent Results II

Figure 4.9a shows the mass profile and highlight how the mass of the propellant and stages decreases during the mission. In particular, the black curve indicates the decrease in propellant mass and when MECO is reached, there is a residue of about 100 ton to be used for landing and reserve. The blue curve represents the total mass reaching a minimum value equal to the structural mass of the second stage plus any residual propellant. Finally, the green curve shows the amount of propellant consumed pr the two shots required to reach orbit.

Finally, the Mach versus time profile in figure 4.9b. The first peak coincides as expected with the end of the first stage burn, the second peak with the second stage burn end.

The achievement of the target orbit is confirmed by the image 4.9d, with perigee and apogee heights coinciding at the end of the mission. How the eccentricity varies up to the value 0 (circular) and how the inclination of 50° varies during the mission is shown in Figure 4.9c, respectively with blue curve and black one. Requirements of selected 'LTO' orbit are satisfied.

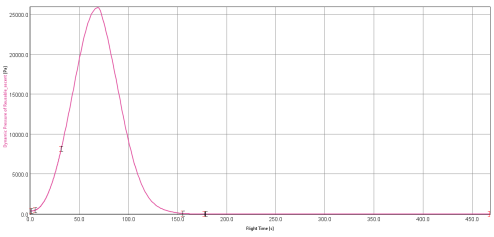

(a) Dynamic Pressure: Q

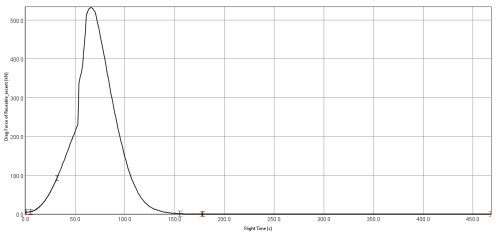

(b) Drag: D

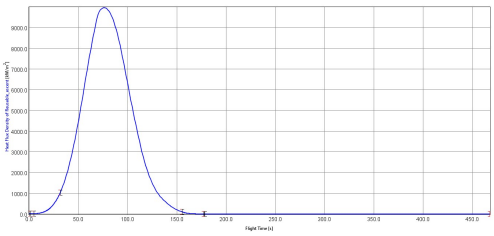

(c) Heat flux: $\dot{q}$

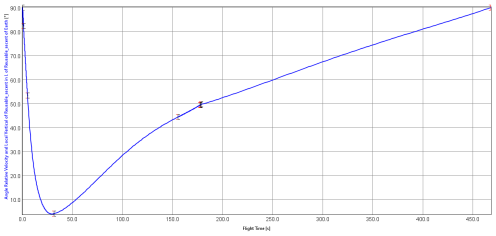

(d) Fligth path Angle: ϕ

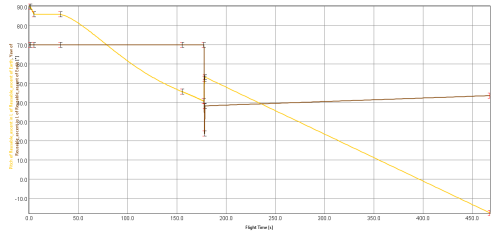

(e) Yaw and Pitch profile

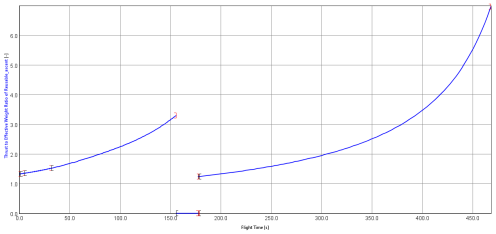

(f) Performance: $\frac{T}{W}$ ratio

Figure 4.10: ASTOS analysis: Ascent Results III

Figure 4.10a gives information about the dynamic pressure that peaks at about $25\,kPa$, consequently, the drag and heat flow profile will follow the same trend (Figure 4.10b and 4.10c).

In Figure 4.10a the profile is instead that of the Fligth Path angle, measured, however, with respect to the local vertical axis. The value of 90° is what is expected for take-off, while for arrival, the classical γ should be 0. However, this is an angle measured with respect to a different reference axis. The value of 90° for arrival is then to be considered correct in this case.

Figure 4.10e wants to show the yaw angle and pitch profile instead. In particular, for yaw, the trend is derived from the optimisation process and the only conditions set are the initial conditions, in order to orient the direction of the launch, and the final conditions in order to reach the target pitch. For the pitch angle, on the other hand, the profile is highly dependent on the phase organisation. In a first section I have a value of 90° for the vertical take-off, a pitch over with a pitch rate of $1\,\frac{°}{s}$

that lasts for a few seconds, a moment in which it is kept constant, the gravity turn, and, finally, a linear descent that brings the value to be null, as one would expect given the insertion in orbit.

Figure 4.10f shows the performance of the rocket, in particular for both the first and second stage, the ratio $\frac{T}{W}$ is about 1.5, a value that tends to increase to 3.5 for the first stage given the mass drop due to fuel consumption. The segments set at 0 identify the coasting stages, while, the growth in performance for the second stage, tends to very high values given the level of thrust relative to the final mass.

The trajectory, a 3D visualisation of the altitude and a satellite view complete the analysis. The trajectory is represented by a gradient representing the Mach number in figures 4.11a, 4.11b and 4.11c. The initial conditions on the yaw, for example, allow the trajectory, given the launch site, to develop over the ocean and not over settlements.

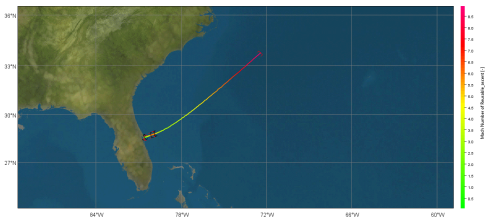

(a) Groundtrack

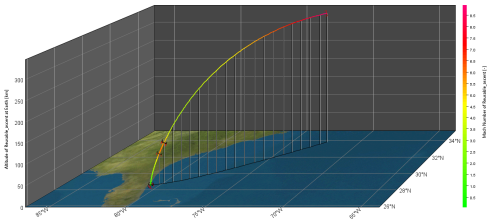

(b) 3D Height Visualization

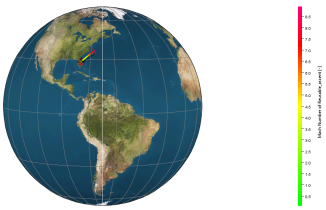

(c) Satellite View

Figure 4.11: ASTOS analysis: Ascent Results IV

4.2.2 Descent phase

For the descent phase, many of the inputs presented in the previous section have been reused.To avoid repetition, only the changes specific to this phase are described. Since it is not possible to define the throttle with any profile, but only with a monotonic increasing or decreasing profile, the following strategy was adopted.3 actuators were created and set with a throttle of 1, the first with a thrust level of 4 motors, the second with a thrust level of 3 motors and the third with a thrust level

of 3 motors. In order to obtain realistic results and not to fix the initial conditions of the test, it was decided to simulate the entire mission of the first stage: ascent and descent. Therefore, I still need the 9 engines activated according to the type of stage. The aim of the subdivision is to simulate the ignition during the descent, as for example foreseen in the RETALT1 mission ([20]). In figure 4.12 you can see the arrangement of the engines which is very similar to the ascent phase, in particular the second stage engine has been inserted to take into account its mass during ascent, it will be jettisoned with the second stage.

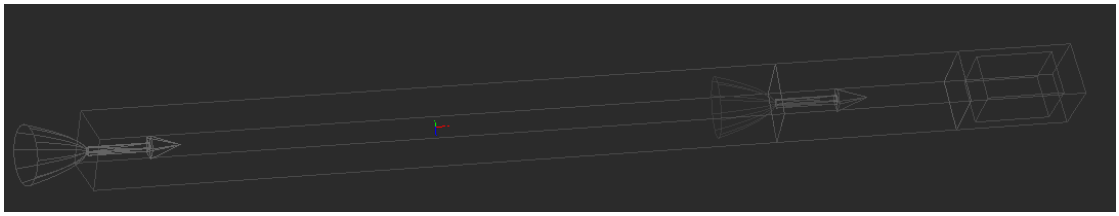

Figure 4.12: Descent Model

The sequence of phases, up to 'First stage burn', is the same. Those inherent to the first stage vertical landing are then inserted, i.e:
Both the initial conditions and the settings for the dynamic mission analysis are

Mission Phase	Duration Guess
Lift-Off	15 s
Pitch-Over	1.5 s
Constant Pitch	25 s
First Stage Burn	130 s
Ascent Coasting	170 s
Flip Over	10 s
Descent Coasting	161 s
Boostback burn	50 s
Aerodynamic glide	110 s
Landing burn	40 s

Table 4.6: Estimated durations for each mission phase: Descent

the same as for the ascent phase, and will therefore be omitted here. Instead, specifically for descent phases:

- In **Ascent Coasting** phase the engines are turned off and a constant control law is set for yaw angle and a *gravity turn* for pitch. This phase lasts until the rocket has reached apogee.

- The **Flip Over** phase rotates the launcher by 180° so that the thrust vector is correctly aligned to decelerate the rocket in the descent phase. This mission phase was simulated by assigning a linear control law that would bring the pitch angle to 180° so that the thrust would be properly aligned for the next burn. For the yaw the control law was set as of tip 'constant law'.This approximation allows the phase to be modelled well. For the flip-over stage, in reality, of all possible systems, only the dedicated ACS or the main engine were considered possible. Other means, such as the use of residual aerodynamics or the effects of upper stage jets were considered as possible opportunities but could not constitute the sole means of stage rotation. The trade-off made between all possible types of ACS and the main engine concluded with the choice of a dedicated gas [34] system.

- In **Descent Coasting** phase the engines are turned off and a constant control law is set for yaw angle and a *gravity turn* for pitch. The phase is structured to reach an ideal altitude for boostbak burn.

- During the **Boostback burn** phase, the rocket is decelerated using the engines for the first time. Specifically, in this phase, according to the RETALT1 mission, the active actuator provides a thrust level equivalent to the use of 3 engines. The control laws for pitch and yaw remain constant.

- Moving on to the **Aerodynamic Glide** phase, where, in reality, devices such as grid fins are used to increase the C_D and decelerate the rocket. This real-world scenario has been simulated by defining a dedicated aerodynamic model for this phase, setting $C_D = 1.6$, as previously introduced in section 2.8. The yaw control law is constant, while the pitch control law is linear, allowing the rocket to reach 90°, a vertical landing condition.

- The sequence concludes with a **Landing Burn** phase, during which the pitch reaches the conditions of 'Vertical take-off,' decelerating the rocket to ensure a soft landing. In this phase has been used one of the nine engines, the central one.

Descent Result

Results are shown in Figures 4.13 to 4.15. Now have a look at the graphs one at a time.

Figure 4.13a shows the altitude as a function of flight time. The graph, as expected, closely resembles the trajectory in Figure 2.17a derived from the DLR database. The lack of perfect longitudinal symmetry with respect to the apogee axis stems from the fact that the final three phases allow the rocket to decelerate and extend the mission duration.

In Figure 4.13b, the inert velocity is shown, providing insights into the ΔV required for landing. The velocity consumption is not computed by simply summing the contributions of the boostback burn and the landing burn. Even in this case, the absolute velocity profile aligns with the database shown in Figure 2.17b, confirming the analysis' accuracy. The reason the velocity starts at 0.45 instead of 0 lies in the absence of optimization analysis. However, the fact that the final velocity is slightly higher than the initial one still validates the model.

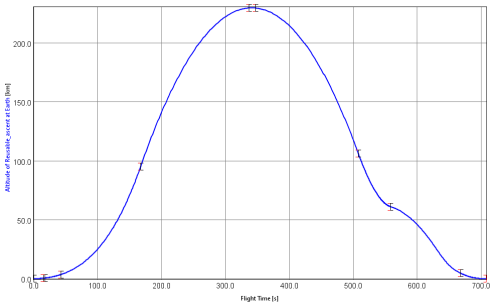

(a) Altitude

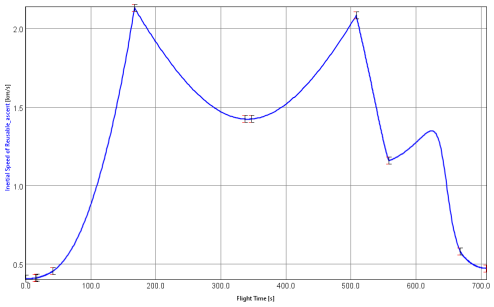

(b) Total Velocity: ΔV

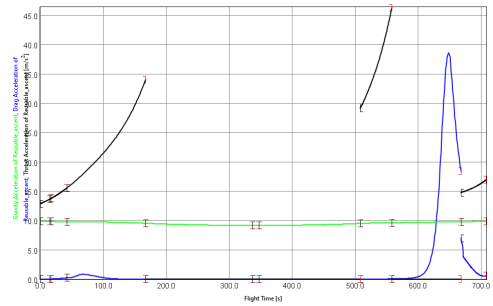

(c) Accelerations Contributions

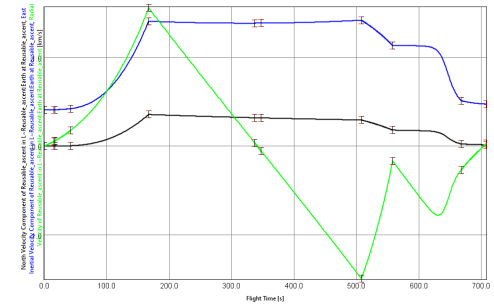

(d) Velocities Contributions

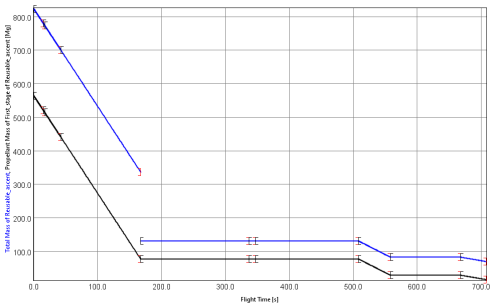

(e) Mass profile

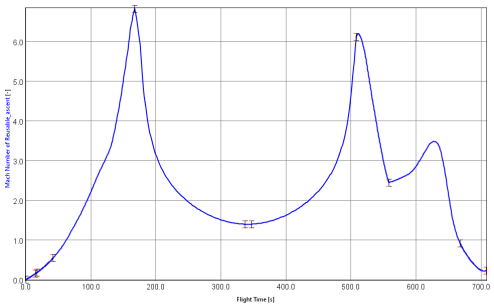

(f) Mach

Figure 4.13: ASTOS analysis: Descent Results I

Figures 4.13c and 4.13d show the components of accelerations and velocities according to the chosen losses and reference system. Axial acceleration, along the body 'X' axis, effectively demonstrates that during the mission, there were three burn events (black curve), while the blue curve shows accelerations due to drag, with a pronounced peak during the glide phase. For the velocity components, it is evident that the radial velocity (green curve) experiences a change in direction due to the flip-over and tends toward zero at the final moment. The only velocity component that does not reach zero is the eastward velocity. However, it returns to a value approximately equal to its initial one. Nevertheless, since this is a DL landing, the landing site differs from the launch site.

Figure 4.13e shows the mass profile, highlighting how the propellant and stage masses decrease during the mission. In particular, the black curve indicates the decrease in propellant mass, with a residue of about 100 ton remaining when MECO is reached, which then decreases to nearly zero to perform the landing phase. The blue curve represents the total mass, reaching a minimum value equal to the structural mass of the first stage plus any residual propellant.

Finally, Figure 4.13f shows the Mach versus time profile. The first peak coincides, as expected, with the end of the first stage burn, and the second peak corresponds to the end of the descent coasting phase. The final peak during the aerodynamic phase is due to the launcher reentering the atmosphere.

Figure 4.14a gives information about the dynamic pressure. In particular, in this case, there are two peaks: one during ascent and the other, with significantly higher values, during the rocket's atmospheric reentry. Consequently, the aerodynamic drag and heat flux profiles will follow a similar trend, as seen in Figures 4.10b and 4.10c. The fact that the graph closely resembles the DLR database results shown in Figure 2.17 further validates the solution.

Figure 4.15a shows the performance of the rocket. The first segment corresponds to the ascent phase, the second to the coasting phases, the third to the boostback burn (characterized by very high $\frac{T}{W}$ ratios), and finally, the landing phase, which exhibits modest values due to the use of only the central engine.

Figure 4.15b illustrates the yaw angle and pitch profile. For the yaw angle, the initial condition matches that of the ascent. However, since there is no need to optimize the first stage, it is assumed to remain constant. For the pitch, the notable feature is the effect of the flip-over phase, which brings the angle to 180° before reducing it back to 90° for vertical landing conditions.

The trajectory, a 3D visualization of altitude, and a satellite view complete the analysis. The trajectory is represented by a gradient showing the Mach number in Figures 4.15b, 4.15c, and 4.15d. The initial yaw conditions, for example, allow the trajectory to land on a barge in the ocean, located 5 degrees east and 2 degrees north of the launch site.

After analysing both types of mission, the validation of the preliminary mission

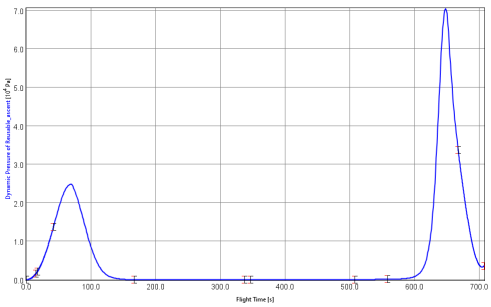

(a) Dynamic Pressure: Q

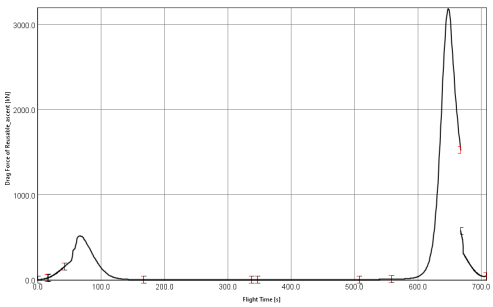

(b) Drag: D

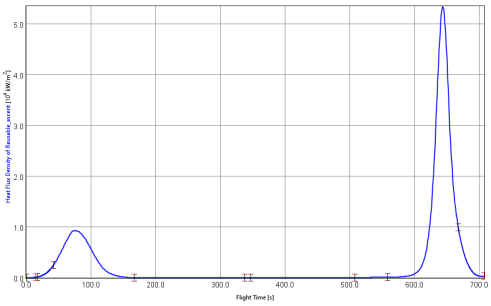

(c) Heat flux: $\dot{q}$

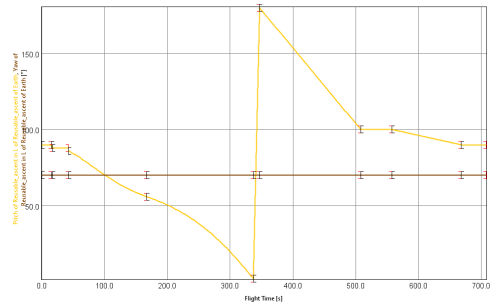

(d) Yaw and Pitch profile

Figure 4.14: ASTOS analysis: Descent Results II

analysis is carried out. Before comparing consumption in terms of ΔV, an additional validation with data from the literature will ensure that the analyses conducted in ASTOS are appropriate.

4.3 Further mission Validation

As mentioned, for further validation, a comparison will be made with the results obtained from the RETALT1 mission. The mission is not entirely equivalent to the one analyzed, as, for example, the target altitude is approximately $250\,km$, which corresponds to the perigee of a GTO orbit [23]. However, it still allows for valid conclusions. The comparison is made by comparing the graphs in Figure 4.16 with those analyzed in the previous two sections.

Figure 4.16a shows how the maximum velocity reached by the first stage is approximately $2\,\frac{km}{s}$ (linear segment), a value that is also found in Figure 4.8b at the end of the first burn phase. The second graph, Figure 4.16b, shows how the Mach peak is higher compared to the one analyzed in ASTOS. The reason for this discrepancy is the difference in the target orbit.

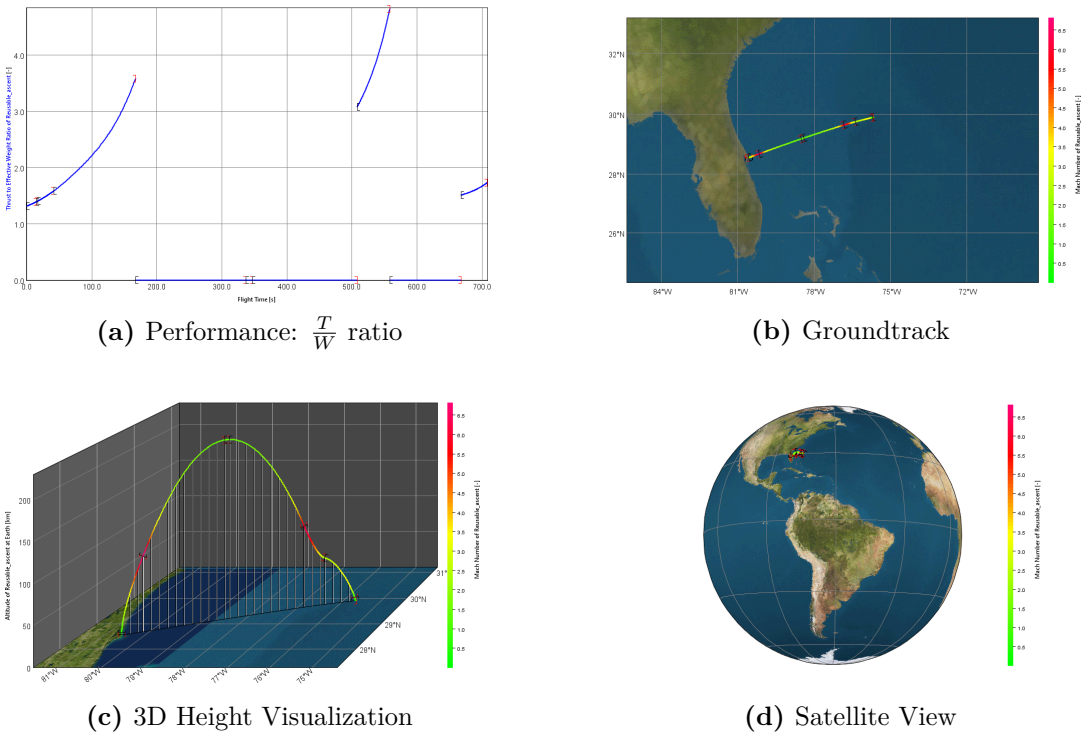

(a) Performance: $\frac{T}{W}$ ratio

(b) Groundtrack

(c) 3D Height Visualization

(d) Satellite View

Figure 4.15: ASTOS analysis: Descent Results III

However, the graphs in Figures 4.16c and 4.16d are very validating, as they show the axial acceleration contributions. The first is certainly comparable to the graph in Figure 4.8c, while the second is similar to the graph in Figure 4.13c.

Finally, the dynamic pressure has a peak of around $20\,kPa$ in Figure 4.16e and about $70\,kPa$ in Figure 4.16f, values very similar to those in Figure 4.14a. The model appears to be very robust, and this assumption will be further confirmed through a numerical comparison.

4.4 Mission Results Numerical Validation

As the final step of this thesis work, a numerical validation of the results was carried out by comparing the ΔV values obtained through the mission module with those derived from the analysis in ASTOS. Figure 4.17 shows that while the percentage differences are significant for losses, they are much smaller when considering the entire mission. The main results obtained are shown in the Table 4.7.

The main objective of this work was to develop a methodology and a tool to perform the conceptual design of a launch vehicle VTVL and TSTO quickly and

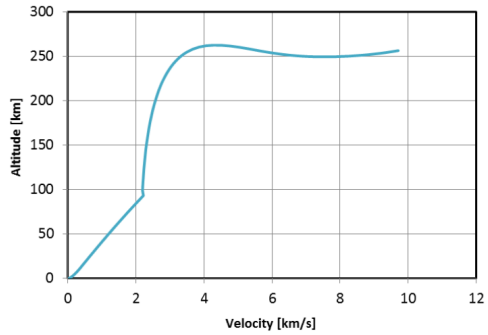

(a) Velocity - Altitude

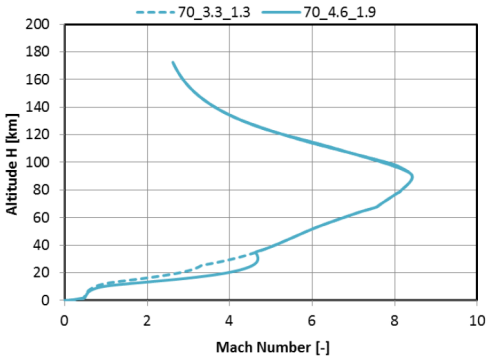

(b) Mach - Altitude

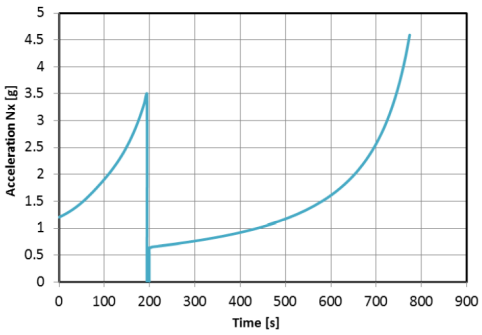

(c) Axial Accelerations: Ascent

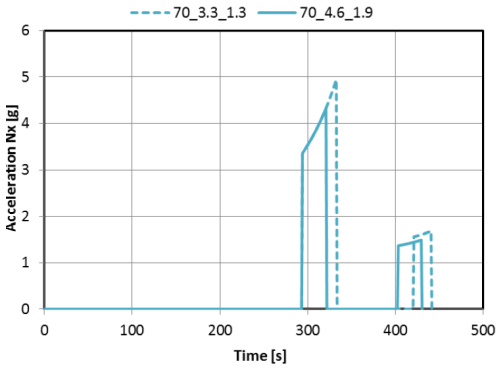

(d) Axial Accelerations: Descent

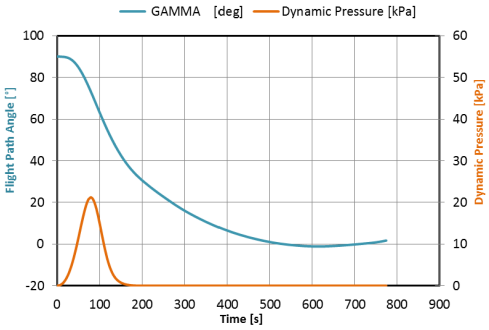

(e) Dynamic Pressure: Ascent

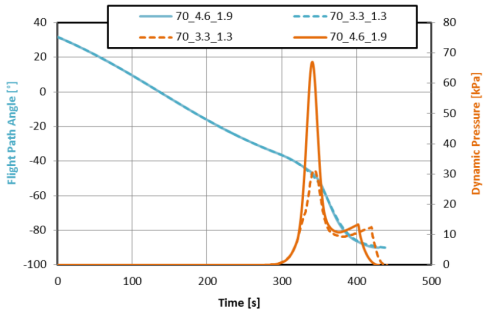

(f) Dynamic Pressure: Descent

Figure 4.16: RETALT1 Mission Analysis [4]

accurately. To ensure consistency of results, the most critical value that must be accurate is the ΔV of the entire mission. This requirement was indeed met. Nevertheless, a detailed mission analysis was carried out, which led to errors in the loss estimate. The question has been raised as to what the reasons might be, and

	ASTOS Results [km/s]	Tool Results [km/s]
Drag Losses	0.396	0.62
Gravity Losses	1.46	1.22
Landing ΔV	1.55	1.65
Mission ΔV	7.70	7.33
Total ΔV	**11.11**	**10.82**

Table 4.7: Mission ΔV Consumption: ASTOS vs tool

the following are possible reasons for these significant percentage variations:

- The ASTOS model uses a 3-DOF approach, while the mission design module works with 2-DOF. In addition, in ASTOS the ascent phase was subjected to an optimisation process that included minimising this type of loss, and in particular resulted in a lower value of ΔV_{drag} than that obtained in the mission module. Another potential problem may arise from the estimation of C_D due to the models used in section 2.8.
- For gravitational losses, the discrepancy could be related to the variation of the trajectory angle during the mission. It should also be noted that the optimisation process changed the duration of each phase, which may have contributed to the observed discrepancies.

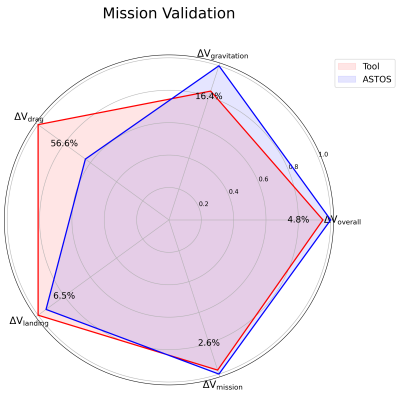

Figure 4.17: Radar graph of mission validation: ΔV consumption

Value Name	<5%	<10%	<15%	>15%
$\Delta V_{overall}$	4.8%			
$\Delta V_{gravitation}$				16.4%
ΔV_{drag}				56.6%
$\Delta V_{landing}$		6.5%		
$\Delta V_{mission}$	2.6%			

Figure 4.18: Percentage difference table for mission validation

Overall, net of the considerations presented above, the tool and methodology were validated. A concluding analysis follows in which the key points and results

achieved during this work are highlighted. The thesis concludes with a list of potential future improvements, as well as suggestions on how to implement them.

Chapter 5

Conclusion and Future works

The intention of this chapter is to report reflections on the results obtained, analysing how the objectives were achieved, what the problems were, how they were dealt with and highlighting what future developments or improvements to this work might be. Chapter 1 not only placed the thesis project in an all-European context, but also focused on a gap: the lack of rapid software for the conceptual design of a rocket. From these needs came the research questions:

Is it possible to develop a methodology on which to base software for the rapid estimation of design parameters and performance of a reusable launch vehicle?

Can this work align with the state-of-the-art European technologies and be easily integrated into ASTRID-H?

Before coming to the final answer to these questions, it is useful to analyse the thesis work in detail for final considerations.

Inputs are find in the Chapter 2 in the first Section 2.1. The number of parameters useful for initialising the analysis has been reduced to a minimum, allowing the user greater flexibility in the choice and reducing the possibility of error due to incorrect selection of initial requirements.

In Section 2.2 the 'Technical Document' module, in which the various pre-set databases are presented, is included. Obviously, a future improvement could be to expand these databases for a more user-friendly experience, but the ability to keyboard initialise one's own dataset for a given category makes this a marginal improvement.

In the Section 2.3 with the 'Statistical Module', it was also possible to accelerate the convergence of the methodology through preliminary validation. However, it is a method that works well for a well-defined class of launchers, liquid propellant RLV or EL that do not use any type of booster.A future improvement might be to categorise the statistical analysis and use one model over another depending on the case being analysed.

The most critical point of the thesis is now discussed, the 'Mission Design Module' presented in Section 2.4. Certainly as a strong point is the fact that a trajectory database validated by the DLR was integrated. Thanks to this integration, it was not necessary to assume a consumption in ΔV for the first iteration, since, having profiles or values of C_D available, it was already possible to analyse the mission from the early stages. The problems identified in the implementation, but above all in the use of the module, were 2: the use of a 2 DOF model leads to an under- or over-estimation of the aerodynamic and gravitational losses respectively; the possibility of only optimising the time of each mission phase. Not having an optimisation on throttle and pitch angle led yes to correct results, but consequently to limitations on their variability. For a better understanding, an example may be useful. As the objective function in the module is to reach a given altitude, then, for each phase, a vector is defined for the pitch angle and one for the throttle, in which a linear trend is usually set. These two quantities are very influential on what the mission is, and for this reason setting them to default may not make the tool as adaptable to a variety of cases. Although the values currently set have provided concrete results for different case studies, two possible improvements are recommended for the future: making the height, pitch angle and throttle optimisable by setting the time; allowing the user to enter mission parameters from the keyboard. There could also be a possible development by allowing the ASTOS environment to become an integral part of the tool, this will be presented later. Looking at the optimisation in more detail, one could impose the following constraints on the iterative duration of each phase ('path'). In addition to initial and final conditions (e.g. height and final landing velocity), it is possible, for example, to impose limits on the dynamic pressure at $30\,kPa$ for ascent and $90\,kPa$ for descent, the axial acceleration at $10g$, the convective heat flux $\dot{q}$ at $1135\,W/m^2$. or limit the angle of attack to 30°. All these values derive from a detailed study of the literature as well as knowledge obtained during the development of this work. The reason why it was not possible to have a graphical representation of the mission also lies in the fact that, for the second stage, the 2BP was used to estimate the ΔV, which does not use integration methods and consequently, by not taking integration steps into account, does not allow data to be collected into vectors to be plotted.

For the 'Optimal Staging Module' in Section 2.5, one could create a theory behind optimal staging for reusable launchers, in order to obtain more accurate results.

The 'Propulsion Module' (Section 2.6) using a validated statistical model for mass estimation allows for very consistent simulations. As an improvement, one could minimise the number of additional inputs for the module and improve the thrust estimation model. A possible solution is presented below.

For the estimation of mass and size (Section 2.7), what has been said for the previous module applies, with only one possible improvement on the type of mass estimation of the 'Landing System', since, to date, there is no statistical model to follow for mass estimation.

The structure is followed by the Aerodynamics module (Section 2.8) which allows very precise estimates of the drag coefficient and, again, a possible future development could be to estimate the contribution of the 'grid fins' on the C_D during the descent phase instead of using a fixed value.

The purpose of the Chapter 3 was to test the actual functionality of the tool through reporting, in addition to the inputs used, the results obtained, also in the form of graphs and sketches of the design as provided by the 'Output window' in Section 2.9. Even without having analysed the validation chapter of the method, it is possible to check whether the requirements for the tool (*REQ-TL*) that were set at the beginning of the work and reported in Chapter 1, have actually been met.

Requirement ID	Description	Validated
REQ-TL-10	The tool shall be developed in Python.	Yes
REQ-TL-20	The tool shall model return-to-launch-site and downrange landing for reusable launch vehicles.	Yes
REQ-TL-30	The tool shall model as well as expendable launch vehicles.	Yes
REQ-TL-40	The tool shall be able to model a reusable launch vehicle in short time.	Yes
REQ-TL-50	The tool shall be able to simulate the ascent and descent of a reusable launch vehicle.	Yes
REQ-TL-60	The tool shall be able to output the physical launch vehicle parameters necessary for analysis and comparison purposes.	Yes
REQ-TL-70	The inputs and outputs of the tool shall be read from Excel files.	Yes
REQ-TL-80	The tool shall be stored databases in user-modifiable files.	Yes

Table 5.1: Tool Requirements with Validation

The table 5.1 how they have all been fully verified, and in support of the thesis, it is also possible to return to Figure 2.1 to confirm that indeed the production of some documents has been planned.

Chapter 4 was used to demonstrate the robustness of the model. From a design

point of view, it was seen that the succeeds in producing good results in terms of size and mass. The only two problems are found in the model's overestimation of the thrust of the first stage and the height of the second stage. Regarding the first problem, it is probably related to the statistical approach used to update T_1. To mitigate the problem, in the future, it is possible to consider integrating a 'Propulsion System Dimensioning Module ' into the tool as seen in Figure 5.1. This will allow, due to the nozzle and feed system design, to minimize user input but more importantly to have a better estimate on the thrust of the stages. On the other hand, the overestimation of the height of stage 2 is related to the optimal staging module, which, not being designed for reusable, distributes the ΔV among the stages without taking this condition into account.

For the validation of the mission module, detailed analyses were conducted in ASTOS, which by taking advantage of the 3-DOF model, implemented in it, resisted much more detailed results. In addition, the ability to perform an optimization allowed to minimize losses and to have much more accurate ΔV estimates. In fact, it was noted how the 'Mission Design Module' in the tool instead returned losses of different magnitudes. As already explained in Chapter 4 the work focused on the design and thus on the final value of ΔV which between tool and ASTOS has a percentage difference of only 2.6%. With ASTOS, however, the ascent and descent phase have been extensively covered, so a future iteration might make one think of integrating the use of the program into the tool. Before discussing how to integrate it, it is good to discuss the validation of mission and trajectory requirements in Table 5.2:

Requirement ID	Description	Validated
REQ-MET-10	The tool shall be able to model the thrust of liquid stages to within 15% accuracy.	Yes
REQ-MET-20	The tool shall be able to model the propellant mass of liquid stages to within 10% accuracy.	Yes
REQ-MET-30	The tool shall be able to model the inert mass of launch vehicle stages to within 10% accuracy.	Yes
REQ-MET-40	The tool shall be able to model the length of launch vehicle to within 10% accuracy.	Yes
REQ-MET-50	The tool shall be able to model the diameters of launch vehicle stages to within 10% accuracy.	Yes
REQ-MET-60	The tool shall be able to model the MTOM of launch vehicles to within 10% accuracy.	Yes
REQ-TR-10	The tool shall be able to evaluate launch mission consumption (ΔV) to within 10% accuracy.	Yes
REQ-TR-20	The tool shall be able to evaluate landing phase consumption (ΔV) to within 10% accuracy.	Yes

Table 5.2: Methodology Requirements with Validation

All requirements were validated, precisely because, as the work was design-centered, there was no requirement on loss accuracy.

Figure 5.1 shows a logic diagram of a future modified methodology, including the new propulsion module and mission analysis module with ASTOS. The intention still remains to use its own mission module, but, at the same time, the robustness of a software such as ASTOS is used to save the final results. Moreover, in this case, the mission outputs, too, are generated by the same program.

Having discussed and compared the results, presented possible improvements, and, most importantly validated the requirements, the answers to the research questions can only be:

Getting a tool to get the conceptual design of a RLV quickly is possible, but more importantly, it provides efficient solutions.

The work is certainly in line with the European state of the art given validation with RETALT1 and is easily integrated into aerospace product design software.

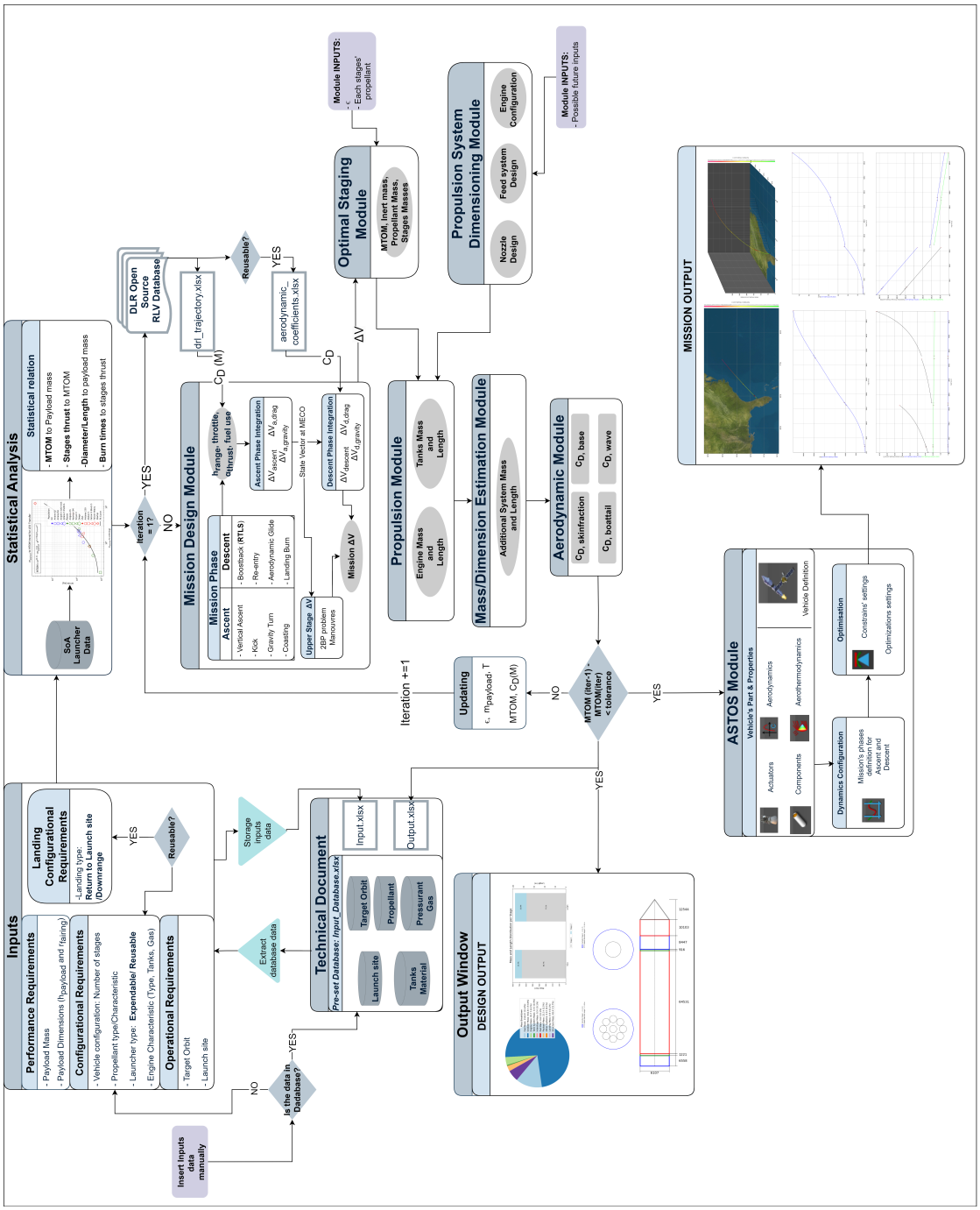

Figure 5.1: Expandable/Reusable Launcher Mission and Design Methodology: Future Logic Scheme

Appendix A

Atmospheric Density

The density of the atmosphere varies with altitude due to changes in temperature, pressure, and composition. The International Standard Atmosphere (ISA) model provides a standard reference for atmospheric conditions as a function of altitude. The atmosphere is divided into several distinct layers, each characterized by different temperature profiles and physical properties:

- **Troposphere** ($0 \leq h \leq 12\,\text{km}$): The temperature decreases linearly with altitude, with an average lapse rate of approximately $6.5\,\text{K/km}$.
- **Stratosphere** ($12 < h \leq 50\,\text{km}$): temperature remains relatively constant around $216.65\,\text{K}$. The density decreases exponentially with altitude due to the lower pressure:

  $$\rho = \rho_0 \cdot e^{-\frac{h-h_0}{H}}$$

  where ρ_0 is the density at the lower boundary, h_0 is the height of that boundary, and H is the scale height.
- **Mesosphere** ($50 < h \leq 85\,\text{km}$):The temperature begins to decrease again, reaching approximately $200.0\,\text{K}$.The density continues to drop significantly, and can also be modeled using the exponential decay formula similar to the stratosphere.
- **Thermosphere** ($85 < h \leq 600\,\text{km}$): The thermosphere features high temperatures (up to $500.0\,\text{K}$) due to solar radiation absorption. The density is extremely low, approximately $1e-4\,\text{kg/m}^3$.
- **Exosphere** ($h > 600\,\text{km}$): temperatures can reach up to $1500.0\,\text{K}$, but the density is extremely low (around $1e-6\,\text{kg/m}^3$).This layer transitions into outer space, where atmospheric properties are negligible.

Appendix B

Propulsion Model: Thrust Evaluation

For the propulsion system model, the ideal thrust it should provide is the same regardless of the type of launcher:

$$T = \dot{m}c + A_e(P_e - P_0) \tag{B.1}$$

where $\dot{m}$ is propellant mass fow rate, A_e exit area, P_e and P_0 is nozzle exit pressure and atmospheric. Ehaust velocity c is linked to specific impulse with following correlation $I_{sp} = \frac{c}{g_0}$. The inputs required for performance evaluation are as follows:

Table B.1: Propulsion Design Parameters

Inputs	Description	Units
P_c	Combustion chamber pressure	[Pa]
T_c	Combustion chamber temperature	[K]
γ	Specific heat	[-]
P_e	Nozzle exit pressure	[Pa]
d_s	Stage diameter	[m]
d_e	Nozzle exit diameter	[m]
t_b	Burn time	[s]
t_c	Coast time	[s]
MR	Mixture ratio	[-]
N_{engines}	Number of engines	[-]

The steps required to obtain the thrust value are as follows (where ϵ is expansion

ratio, c^* characteristic velocity and C_F thrust coefficient):

$$\Gamma = \sqrt{\gamma}\left(\frac{2}{\gamma+1}\right)^{\frac{\gamma+1}{2(\gamma-1)}} \tag{B.2}$$

$$\epsilon = \frac{A_e}{A_t} = \frac{\Gamma}{\sqrt{\frac{2\gamma}{\gamma-1}\left(\frac{P_e}{P_c}\right)^{\frac{2}{\gamma}}\left(1-\left(\frac{P_e}{P_c}\right)^{\frac{\gamma-1}{\gamma}}\right)}} \tag{B.3}$$

$$\dot{m} = \frac{P_c A_t \Gamma}{\sqrt{RT_c}} \tag{B.4}$$

$$c^* = \frac{1}{\Gamma}\sqrt{RT_c} \tag{B.5}$$

$$C_F = \Gamma\sqrt{\frac{2\gamma}{\gamma-1}\left(1-\left(\frac{P_e}{P_c}\right)^{\frac{\gamma-1}{\gamma}}\right)} \tag{B.6}$$

$$c = c^* C_F \tag{B.7}$$

Now, starting with burning, we can use B.1 to find out the thrust produced.

Appendix C

Runge-Kutta integration Method

The Runge-Kutta method, particularly the fourth-order variant (RK4), is a widely used numerical integration technique for solving ordinary differential equations (ODEs) of the form:

$$\frac{dy}{dt} = f(t, y), \quad y(t_0) = y_0$$

In this method, the next value of y at $t_{n+1} = t_n + h$ is approximated using a weighted average of slopes calculated at several points within each step h. This approach reduces the error significantly compared to simpler methods like Euler's method. The RK4 method is defined as follows:

1. Compute intermediate slopes:

$$k_1 = hf(t_n, y_n) \tag{C.1}$$

$$k_2 = hf\left(t_n + \frac{h}{2}, y_n + \frac{k_1}{2}\right) \tag{C.2}$$

$$k_3 = hf\left(t_n + \frac{h}{2}, y_n + \frac{k_2}{2}\right) \tag{C.3}$$

$$k_4 = hf(t_n + h, y_n + k_3) \tag{C.4}$$

2. Update y using a weighted sum of the slopes:

$$y_{n+1} = y_n + \frac{1}{6}(k_1 + 2k_2 + 2k_3 + k_4) \tag{C.5}$$

This method has an error of $O(h^5)$ per step and $O(h^4)$ for the entire integration, making it both accurate and efficient for many applications.

Bibliography

[1] Valeria Vercella. «Cost-effective and sustainable scenarios for future reusable space transportation and re-entry systems». Doctoral Program in Aerospace Engineering (34th Cycle). Doctoral Dissertation. Politecnico di Torino, 2023. URL: https://hdl.handle.net/11583/2981465 (cit. on p. 3).

[2] Stephane Contant. «Design and Optimization of a Small Reusable Launch Vehicle Using Vertical Landing Techniques». Master thesis. Delft University of Technology, 2019. URL: https://resolver.tudelft.nl/uuid:58cb0a6e-e9ac-4ce5-9051-5ddd863e98a8 (cit. on pp. 3, 7, 11, 32, 37, 41).

[3] Sven Stappert Jascha Wilken. «Comparative analysis of European vertical landing reusable first stage concepts». In: *CEAS Space Journal* (2024). URL: https://doi.org/10.1007/s12567-024-00549-9 (cit. on pp. 4–7, 59, 60, 66, 72, 74).

[4] Ansgar Marwege et al. «Retro Propulsion Assisted Landing Technologies (RETALT): Current Status and Outlook of the EU Funded Project on Reusable Launch Vehicles». In: (Oct. 21–25, 2019). Ed. by United States 70th International Astronautical Congress (IAC) Washington D.C. URL: https://elib.dlr.de/132566/ (cit. on pp. 4, 19, 73, 81–83, 100).

[5] Sven Stappert, Ingrid Dietlein, Jascha Wilken, et al. «Options for Future European Reusable Booster Stages: Evaluation and Comparison of VTHL and VTVL Return Methods». In: *CEAS Space Journal* (Feb. 21, 2024). URL: https://doi.org/10.21203/rs.3.rs-3972618/v1 (cit. on p. 5).

[6] Michel Illig, Shinji Ishimoto, and Etienne Dumont. «CALLISTO, a demonstrator for reusable launchers». In: *9th European Conference for Aeronautics and Space Sciences (EUCASS)* (2021). Presented by CNES, JAXA, and DLR representatives. DOI: 10.13009/EUCASS2019-956. URL: https://www.eucass.eu (cit. on p. 6).

[7] Jerome Vila and Jeremie Hassin. «Technology acceleration process for the THEMIS low cost and reusable prototype». In: *8th European Conference for Aeronautics and Space Sciences (EUCASS)*. ArianeWorks / CNES. Madrid,

Spain, 2019. DOI: 10.13009/EUCASS2019-97. URL: https://www.eucass.eu (cit. on p. 6).

[8] Michel Illig, Shinji Ishimoto, and Etienne Dumont. «Concept of Operations - CALLISTO demonstrator». In: *8th European Conference for Aeronautics and Space Sciences (EUCASS)* (2019). DOI: 10.13009/EUCASS2019-956. URL: https://www.eucass.eu (cit. on p. 6).

[9] European Space Agency. *Themis*. 2024. URL: https://www.esa.int/Enabling_Support/Space_Transportation/Themis (cit. on p. 6).

[10] Francesco Castellini. «Multidisciplinary Design Optimization For Expendable Launch Vehicles». Doctoral Dissertation. Politecnico di Milano, 2012. URL: https://hdl.handle.net/10589/56841 (cit. on pp. 7, 36, 51–53, 56, 58).

[11] Simon Jentzsch. «Optimization of a Reusable Launch Vehicle using Genetic Algorithms». Master Thesis. RWTH Aachen University, Institute of Jet Propulsion and Turbomachinery, 2020. URL: https://elib.dlr.de/137799/ (cit. on pp. 7, 46, 49, 50).

[12] Loic Brevault, Mathieu Balesdent, and Ali Hebbal. «Multi-Objective Multidisciplinary Design Optimization Approach for Partially Reusable Launch Vehicle Design». In: *Journal of Spacecraft and Rockets* 57.2 (2020). DOI: 10.2514/1.A34601. URL: https://hal.archives-ouvertes.fr/hal-03046307 (cit. on p. 7).

[13] Mathieu Balesdent. «Optimisation Multidisciplinaire de Lanceurs». Spécialité : Génie Mécanique. Doctoral Thesis. Nantes, France: École Centrale de Nantes, 2011. URL: https://www.researchgate.net/publication/256292310_Multidisciplinary_Design_Optimization_of_Launch_Vehicles (cit. on pp. 7–9).

[14] Nicole Viola Davide Ferretto Roberta Fusaro. «A conceptual design tool to support high-speed vehicle design». In: *AIAA* (2020). URL: https://doi.org/10.2514/6.2020-2647 (cit. on p. 9).

[15] Wikipedia. *List of rocket launch sites*. URL: https://en.wikipedia.org/wiki/List_of_rocket_launch_sites (cit. on p. 17).

[16] G. Janin. «Lifetime of Objects in Geostationary Transfer Orbit». In: *Mission Analysis Section ESOC, 6100 Darmstadt, FRG* (). URL: https://conference.sdo.esoc.esa.int/proceedings/isdrw02/paper/10/ISDRW02-paper10.pdf (cit. on pp. 19, 26, 27).

[17] George P. Sutton and Oscar Biblarz. *Rocket Propulsion Elements*. 2017 (cit. on pp. 20, 36, 37, 50).

[18] FAA Office of Commercial Space Transportation. «The Annual Compendium of Commercial Space Transportation: 2018». In: (Jan. 2018). URL: https://www.faa.gov/about/office_org/headquarters_offices/ast/media/2018_ast_compendium.pdf (cit. on p. 23).

[19] DLR. *Open Source Model for Reusable Launch Vehicles*. URL: https://www.dlr.de/en/as/research-and-transfer/projects/open-source-model-for-reusable-launch-vehicles (cit. on p. 29).

[20] Ansgar Marwege et al. «RETALT: review of technologies and overview of design changes». In: *CEAS Space Journal* (2022). URL: https://doi.org/10.1007/s12567-022-00458-9 (cit. on pp. 30, 94).

[21] ASTOS solutions. *Conventional Launcher Tutorial*. 2021 (cit. on pp. 30, 73, 86, 87, 89).

[22] SpaceX. *Starship | First Orbital Flight Test*. https://www.youtube.com/watch?v=Z4TXCZG_NEY. Accessed: 2024-11-21. 2023 (cit. on p. 31).

[23] Gabriele De Zaiacomo, Guillermo Blanco Arnao, Roland Bunt, and et al. «Mission engineering for the RETALT VTVL launcher». In: *CEAS Space Journal* 14.4 (2022), pp. 533–549. DOI: 10.1007/s12567-021-00415-y. URL: https://doi.org/10.1007/s12567-021-00415-y (cit. on pp. 32, 33, 98).

[24] Tamas Bykerk. «A standard model for the investigation of aerodynamic and aerothermal loads on a re-usable launch vehicle». In: *Aerospace Europe Conference 2023 - 10th EUCASS - 9th CEAS* (2023). URL: https://elib.dlr.de/194475/2/AEC2023_rfz.pdf (cit. on pp. 34–36).

[25] Space Exploration Technologies (SpaceX). *Falcon User's Guide*. 2020. URL: https://www.spacex.com/media/falcon-users-guide-2021-09.pdf (cit. on p. 41).

[26] Lorenzo Casalino. «Space Propulsion Lectures». 2024 (cit. on pp. 45–48).

[27] Politecnico di Torino. «iASTRID-H - Description Document, Technical Note 2, iDREAM (TN2)». 2022 (cit. on pp. 45, 49, 52–54, 56, 58).

[28] Ulrich Walter. «Rocket Staging». In: *Astronautics: The Physics of Space Flight*. Cham: Springer International Publishing, 2018, pp. 47–65. ISBN: 978-3-319-74373-8. DOI: 10.1007/978-3-319-74373-8_3. URL: https://doi.org/10.1007/978-3-319-74373-8_3 (cit. on p. 46).

[29] R. A. Braeunig. *Rocket and Space Technology: Rocket Propulsion*. http://www.braeunig.us/space/index.htm. Accessed: 2024-11-21. n.d. (Cit. on p. 50).

[30] Alexandru-Iulian Onel, Tudorel-Petronel Afilipoae, Ana-Maria Neculaescu, and Mihai-Victor Pricop. «Drag coefficient modelling in the context of small launcher optimisation». In: *INCAS BULLETIN* (2018) (cit. on pp. 61, 65).

[31] P. Sharma. «Drag Coefficient Prediction». In: *Journal of Aerodynamics* (2015). URL: https://www.academia.edu/6825134/Drag_Coefficient_Prediction_Chapter_1 (cit. on pp. 61–64).

[32] S.R. Vukelich, S.L. Stoy, K.A. Burns, and et al. «Missile DATCOM, volume I-final report». In: *McDonnell Douglas, Technical report AFWAL-TR-86-3091* (1988) (cit. on p. 61).

[33] ASTOS solutions. *User Manual*. 2021 (cit. on pp. 85, 88).

[34] Antoine Patureau de Mirand, Jean-Marc Bahu, and Eric Louaas. «Ariane Next, a vision for a reusable cost efficient European rocket». In: *8th European Conference for Aeronautics and Space Sciences (EUCASS)*. Centre National d'Etudes Spatiales (CNES). Paris, France, 2019. DOI: 10.13009/EUCASS2019-949. URL: https://doi.org/10.13009/EUCASS2019-949 (cit. on p. 95).